



Aerospace Regenerative Fuel Cell Fluidic Component Design Challenges

Phillip J. Smith
Glenn Research Center, Cleveland, Ohio

Zhimin Zhong
HX5, LLC, Brook Park, Ohio

Kerrigan P. Cain, Jessica L. Cashman, Bryan W. Debelak, and Ryan P. Gilligan
Glenn Research Center, Cleveland, Ohio

David S. Hervol
HX5, LLC, Brook Park, Ohio

Cody A. O'Meara, Robert D. Green, Erik J. Stalcup, and Ian J. Jakupca
Glenn Research Center, Cleveland, Ohio

NASA STI Program . . . in Profile

Since its founding, NASA has been dedicated to the advancement of aeronautics and space science. The NASA Scientific and Technical Information (STI) Program plays a key part in helping NASA maintain this important role.

The NASA STI Program operates under the auspices of the Agency Chief Information Officer. It collects, organizes, provides for archiving, and disseminates NASA's STI. The NASA STI Program provides access to the NASA Technical Report Server—Registered (NTRS Reg) and NASA Technical Report Server—Public (NTRS) thus providing one of the largest collections of aeronautical and space science STI in the world. Results are published in both non-NASA channels and by NASA in the NASA STI Report Series, which includes the following report types:

- TECHNICAL PUBLICATION. Reports of completed research or a major significant phase of research that present the results of NASA programs and include extensive data or theoretical analysis. Includes compilations of significant scientific and technical data and information deemed to be of continuing reference value. NASA counter-part of peer-reviewed formal professional papers, but has less stringent limitations on manuscript length and extent of graphic presentations.
- TECHNICAL MEMORANDUM. Scientific and technical findings that are preliminary or of specialized interest, e.g., “quick-release” reports, working papers, and bibliographies that contain minimal annotation. Does not contain extensive analysis.
- CONTRACTOR REPORT. Scientific and technical findings by NASA-sponsored contractors and grantees.
- CONFERENCE PUBLICATION. Collected papers from scientific and technical conferences, symposia, seminars, or other meetings sponsored or co-sponsored by NASA.
- SPECIAL PUBLICATION. Scientific, technical, or historical information from NASA programs, projects, and missions, often concerned with subjects having substantial public interest.
- TECHNICAL TRANSLATION. English-language translations of foreign scientific and technical material pertinent to NASA's mission.

For more information about the NASA STI program, see the following:

- Access the NASA STI program home page at <http://www.sti.nasa.gov>
- E-mail your question to help@sti.nasa.gov
- Fax your question to the NASA STI Information Desk at 757-864-6500
- Telephone the NASA STI Information Desk at 757-864-9658
- Write to:
NASA STI Program
Mail Stop 148
NASA Langley Research Center
Hampton, VA 23681-2199



Aerospace Regenerative Fuel Cell Fluidic Component Design Challenges

Phillip J. Smith
Glenn Research Center, Cleveland, Ohio

Zhimin Zhong
HX5, LLC, Brook Park, Ohio

Kerrigan P. Cain, Jessica L. Cashman, Bryan W. Debelak, and Ryan P. Gilligan
Glenn Research Center, Cleveland, Ohio

David S. Hervol
HX5, LLC, Brook Park, Ohio

Cody A. O'Meara, Robert D. Green, Erik J. Stalcup, and Ian J. Jakupca
Glenn Research Center, Cleveland, Ohio

National Aeronautics and
Space Administration

Glenn Research Center
Cleveland, Ohio 44135

Trade names and trademarks are used in this report for identification only. Their usage does not constitute an official endorsement, either expressed or implied, by the National Aeronautics and Space Administration.

Level of Review: This material has been technically reviewed by technical management.

Aerospace Regenerative Fuel Cell Fluidic Component Design Challenges

Phillip J. Smith

National Aeronautics and Space Administration
Glenn Research Center
Cleveland, Ohio 44135

Zhimin Zhong

HX5, LLC
Brook Park, Ohio 44142

Kerrigan P. Cain, Jessica L. Cashman, Bryan W. Debelak, and Ryan P. Gilligan

National Aeronautics and Space Administration
Glenn Research Center
Cleveland, Ohio 44135

David S. Hervol

HX5, LLC
Brook Park, Ohio 44142

Cody A. O'Meara, Robert D. Green, Erik J. Stalcup, and Ian J. Jakupca

National Aeronautics and Space Administration
Glenn Research Center
Cleveland, Ohio 44135

Summary

A discrete regenerative fuel cell (RFC) system is currently under development at the NASA Glenn Research Center and Johnson Space Center. The objective of this activity is to produce an energy storage system with a higher specific energy than the state-of-the-art battery technologies. The system will then be tested within an environment simulating the temperatures and pressures expected over a full lunar day cycle on the lunar surface. This RFC is designed to be as flight-like as possible given project resource and commercially available technology limitations. In addition to the software required for automatic operation, the RFC system consists of the following subsystems: avionics, fuel cell, high-pressure electrolysis, fluidic and electronic balance of plant, and power management and distribution. This technical memorandum discusses components and subsystems that present challenges in developing flight-ready RFCs. To remedy identified issues, functional application test plans are presented for components and subsystems primarily constructed with commercially available options due to the budget and schedule constraints of this ground technology demonstration project.

1.0 Introduction

A regenerative fuel cell (RFC) system is currently under development at the NASA Glenn Research Center and Johnson Space Center, funded by the Game Changing Development Program Office in the Space Technology Mission Directorate. The objective of this activity is to produce an energy storage

system with a higher specific energy than the state-of-the-art battery technologies, then test that system within an environment simulating the temperatures and pressures expected over a full day and night cycle on the lunar equator surface. The system is designed to be as flight-like as possible given resource and commercially available technology limitations. Though this RFC is nominally a 100-W system, which is a low power level for a practical lunar RFC, an additional project objective is to study and remove obstacles to development of a flight RFC system of up to 10 kW.

RFCs are desired for applications with substantial energy storage requirements where batteries are not practical. This includes missions on the lunar surface where long charge and discharge periods are a driving requirement for significant energy storage capacities, specifically the lunar equator where the lunar night lasts up to 2 weeks. One such scenario could be lunar habitat energy storage in which solar energy is captured by photovoltaic (PV) arrays during the lunar day and converted to chemical energy by electrolysis of H₂O into H₂ and O₂ gases, which are stored in high-pressure vessels. Throughout the lunar night, the fuel cell (FC) converts the stored H₂ and O₂ into electrical energy that is supplied to a customer as well as H₂O and heat. Relative to existing batteries, RFCs may offer a more energy dense solution, with potential to exceed a specific energy of 550 Wh/kg (1.98 MJ/kg) (Refs. 1 and 2).

While proton exchange membrane (PEM) FCs and electrolyzers (EZs) are mature terrestrial technologies, with detailed discussions of fundamental RFC electrochemical technologies, operational theory, concept of operations, and scaling that can be found in the literature (Refs. 3 to 7), both remain in development for aerospace applications. The FC technology is at a technology readiness level (TRL) of 5, while balanced, high-pressure EZs have a TRL of 3. Flight-qualified primary FCs have been previously used as electrical energy sources by NASA missions, with PEM FCs powering Gemini vehicles and alkaline FCs powering Space Shuttle Orbiters (Refs. 8 to 11). Both FC technologies were retired along with the corresponding space vehicles. Low, unbalanced pressure EZs are currently operational aboard the International Space Station (ISS). Since 2007, NASA has used a PEM EZ in the ISS within the Oxygen Generation Assembly (OGA) to supply O₂ for crew respiration (Refs. 12 to 15). The Russian space agency Roscosmos supplied Elektron-VM alkaline EZs to generate O₂ within the Russian section of the ISS.

In a discrete PEM RFC system, a FC is paired with an EZ to convert and store energy. Integrating FC and EZ technologies into a viable RFC system requires multiple mechanical, electrical, and thermal subsystems, making RFCs relatively complex systems of hundreds of independent components. These balance of plant (BOP) components and subsystems all serve important roles in effective performance. For example, to achieve a high specific energy, the system design must emphasize low-mass and low-power-draw components that maximize the RFC system round-trip efficiency (RTE) and specific energy.

In this report, existing BOP technologies are analyzed for ground demonstration and lunar flight mission suitability. The topic areas include liquid-gas phase separation; high-pressure gas storage; safety devices such as gas sensing and flammability prevention, pressure relief, and flow monitoring; general reliability and materials compatibility issues; mechanical components such as pumps and solenoid valves; electrical components such as heaters and remote actuators; and passive variable heat transfer devices. Requirements and desired features for each are discussed along with commercially available technologies. The feasibility of application for RFC are to be addressed by subsystem testing that is planned to evaluate components and process designs. The primary intent of this report is to inform on the most significant BOP issues limiting RFC development, what improvements are needed, and the initial steps that NASA is performing to solve or at least better define the challenges.

1.1 Regenerative Fuel Cell Operation

The operation of RFC utilizes H₂O electrolysis to store chemical energy (similar to the charge operation of a rechargeable battery) and a FC to produce electrical energy (like the discharge operation of

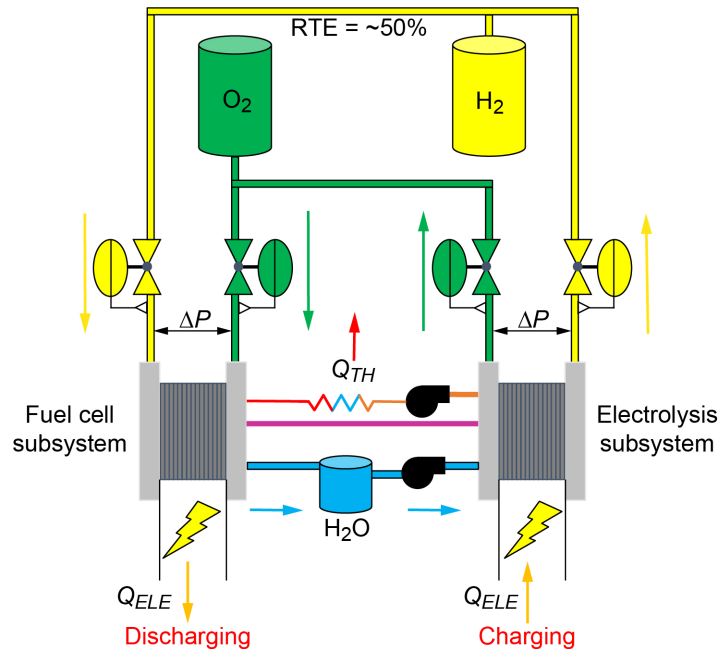


Figure 1.—Discrete regenerative fuel cell. Thermal flow (Q_{TH}). Electrical flow (Q_{ELE}). Pressure change (ΔP). Round-trip efficiency (RTE).

the battery). Whereas in batteries, the components of specific energy and specific power are directly coupled, in RFCs the two elements are dissociated and physically separated, with specific energy primarily resulting from reactant (H_2 and O_2) storage and specific power a function of electrochemical stack design and sizing. In a RFC system, FC and EZ hardware are often two different (i.e., discrete) stacks with each optimized for the specific electrochemical reaction.

Figure 1 is a diagram of a discrete RFC with a FC, an EZ, gas and H_2O storage, and heat and fluid management. This schematic shows how RFCs differ from primary FCs in that product H_2O formed during the discharge reaction is stored rather than discharged overboard so that H_2O can be supplied to the EZ stack and electrolyzed back into H_2 and O_2 during the charge operation. While there remains current research into unitized PEM designs where one unit can sustainably and efficiently support both reactions, no viable design has yet been produced for energy storage applications at this time.

Though the advancement of aerospace FC technology parallels terrestrial FCs in developing durable membrane materials, active electrode catalysts, and modern membrane electrode assembly (MEA) designs (Ref. 16), aerospace FC designs are distinct from terrestrial FCs in that stored pure O_2 must be used as the oxidant instead of air. This complicates removal of product H_2O from the stack, even before consideration of microgravity conditions.

During charging, the gaseous products of electrolysis (H_2 and O_2) are stored in gas storage tanks. The amount of gas that can be stored in a given vessel increases proportionally with the pressure, therefore, high-pressure storage is generally preferred. This is essential to achieve high specific energy and energy density because reactant storage dominates RFC total mass and volume for all but the smallest scale systems. If a low-pressure EZ (like the ISS OGA designed for supplying O_2 to the ISS cabin atmosphere) is adopted, a high-pressure pump will be required to compress H_2 and O_2 to a targeted pressure of at least 12 MPa (1,800 psi) for storage within an acceptable volume for launch packaging. There are significant recent terrestrial EZ developments for renewable energy storage based on both PEM and alkaline anion exchange membranes (AEM) technologies (Refs. 17 to 19). From a 1-MW system in 2015 to 10 MW in

2018, multiple 3.5-MPa output pressure PEM EZs have been successfully operated for energy storage demonstration as well as commercial H₂ production in Germany, Australia, and the United Kingdom (Ref. 20). AEM technologies remain relatively new and have not yet demonstrated the mechanical durability required for aerospace application, however, AEM EZs have the advantage of not requiring precious metal catalysts for H₂O electrolysis.

1.2 Known Technical Challenges

There are several challenges that are consistently present for multiple categories of BOP components. TRLs for many individual RFC components are low since most commercial-off-the-shelf (COTS) components are not designed for and have never been evaluated in vacuum, let alone a lunar surface environment. Further common difficulties include commercial availability, cost, thermal management, materials compatibility with fluids, and long-term reliability. The following subsections discuss these general challenges.

1.2.1 Component Availability and Cost

The current RFC project scope consists of research and ground demonstration only with a corresponding budget not scaled for the development or procurement of customized spaceflight-rated components. For example, flight-rated solenoid valves cost in excess of \$50,000 each and a dozen of them are needed for a single RFC. When prioritizing low mass, low power consumption, and rating for vacuum environment operation with the identified process fluids and operational conditions, few existing commercial products meet all the required specifications. In some cases, there are products close to the specifications, but for others, no COTS options satisfy every item.

RFC components, such as valves, pumps, gas storage vessels, high-power direct current (DC) heaters, relief devices, and flow switches, will be operated in the lunar equator simulating vacuum environment for long durations and over a wider temperature range than is typical even for low Earth orbit (LEO). Component, subsystem, and integrated system-level testing are required to verify acceptable performance in the intended environment. Given the unique requirements of the RFC, COTS BOP components may not exist for certain functions and will have to be custom designed and made for eventual flight systems.

The RFC demonstration units in development for this project must operate in both laboratory and vacuum environments. For safety reasons, NASA complies with the National Fire Protection Association (NFPA) 70 (National Electric Code (NEC)) Article 500.5, which states that components used in an environment with a plausible release of a flammable gas (e.g., H₂) must meet Class I Division 2 Group B (CI/DivII/GB) hazardous location requirements (Ref. 21). This imposes a challenge for all electrically powered components as the CI/DivII/GB requirements are frequently mutually exclusive to the requirements for operating in a vacuum environment (e.g., the lunar surface or a vacuum chamber). In a vacuum environment, CI/DivII/GB compliant components may overheat or leak purge gases into the vacuum chamber thereby compromising the facility vacuum pumps and the ultimate vacuum level achieved during demonstration. Electrical components designed for use in vacuum environments rarely are evaluated for CI/DivII/GB classified spaces.

1.2.2 Thermal Management

Because PEM FCs and EZs produce and utilize liquid H₂O, system temperatures throughout most of the RFC must be maintained such that H₂O does not change state during operation. Additionally, PEM stacks have a relatively narrow optimum operational temperature range of ~60 to 70 °C for best reaction kinetics and internal humidification while not degrading the MEA. Supporting electronic and fluidic BOP components also present operating temperature requirements, especially if the component manages H₂O.

Surface temperatures at the lunar equator range from -177 to 118 °C (Ref. 22), far exceeding the limits for liquid H_2O .

Solar flux at this location can also vary from 0 to $1,420$ W/m^2 . Thus, maintaining RFC components within allowable temperature ranges presents both a priority and a challenge for system optimization. It is advantageous to package and insulate as many components as practical from the harsh lunar environment. RFC RTE, a key performance metric, is directly influenced and reduced by parasitic electrical loads; these are any electrical loads not delivered to the “customer” (presumed to be a lunar lander or similar application) and that instead are used by the RFC internally for operation. Thus, wherever possible, passive thermal control techniques (i.e., those that do not require power from the RFC) should be utilized versus active thermal control techniques when the mass and overall complexity between options are similar.

Figure 2 provides an overall schematic of the RFC thermal design implementing both passive and active thermal methods. The RFC thermal enclosure uses multilayer insulation (MLI) to thermally isolate the RFC from the lunar environment. The PEM stacks, electronic BOP, and fluidic BOP components, excluding the reactant tanks, are located within the thermal enclosure. Components within the thermal enclosure will have view factors to the innermost layer of MLI, which per RFC project requirements is to remain between 4 and 85 °C. The temperature differences between components inside the enclosure and the inner layer MLI are not likely to be sufficient heat sources or sinks for significant heat transfer. The H_2 and O_2 tank volumes are too large to include inside the enclosure without adding complications, mass, and volume. These issues increase in impact for scaled up RFC flight systems. The tanks and dry reactant gases are slightly more tolerant to environmental temperature extremes. O_2 condensation is a concern, but heaters can be installed on the tanks to keep temperatures above that threshold. These tanks are also insulated with MLI, which has an outer layer selected to minimize heat loss during the lunar night while limiting high tank temperatures due to solar flux and lunar surface infrared radiation (IR) during the lunar day.

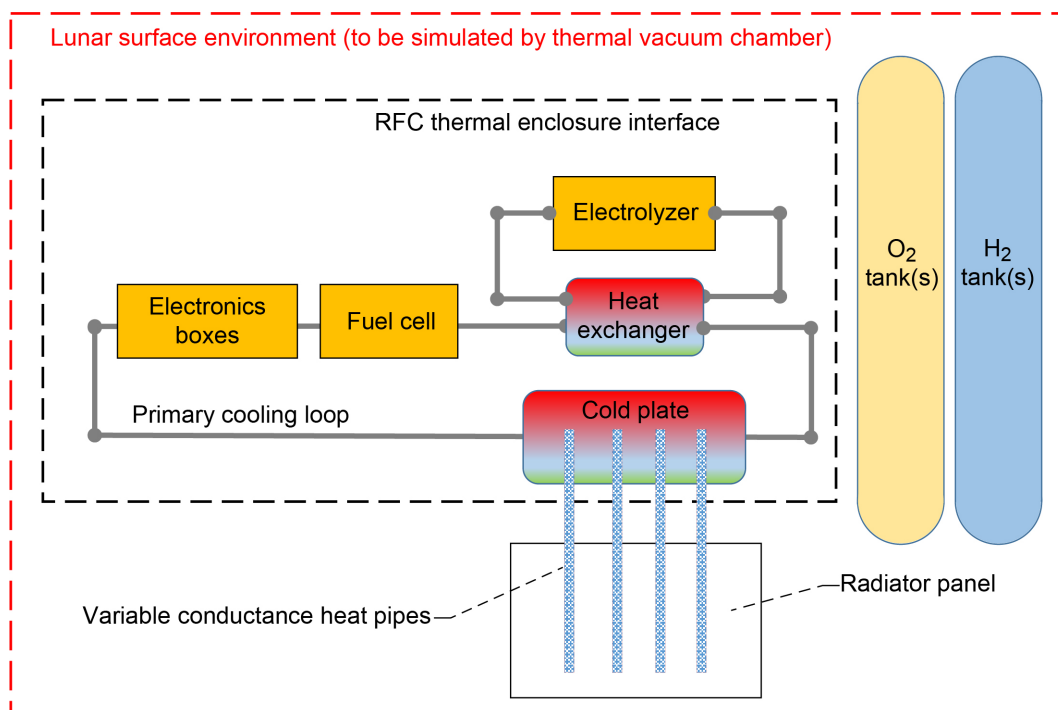


Figure 2.—Regenerative fuel cell (RFC) thermal design showing RFC thermal enclosure interface, primary cooling loop, and radiator coupling.

The operating temperatures of modules in the RFC system are moderated by using heat exchangers, cold plates, coolant loops, thermal switches, and heaters. In normal operation, the FC, EZ, avionics, power management and distribution (PMAD), and BOP components all produce heat. This heat flow must be managed to prevent overheating during the lunar day or freezing during the lunar night. During the lunar day, the primary heat sources are the EZ, PMAD box, and avionics box. The maximum RFC heat generation coincides with the highest environmental temperature since the electrolysis rate is preferentially highest when the most solar power is available. This heat must be transferred from within the enclosure to the radiator, which is external to the enclosure. During the lunar night, the primary heat sources are the FC, PMAD box, and avionics box. Most of the heat generated by the RFC during lunar night must be conserved internally or shared with the power customer in order to keep components above the low-temperature limits.

A coolant loop internal to the thermal enclosure, called the primary cooling loop (PCL) is thermally coupled with heat sources inside this enclosure. The PCL receives waste heat and rejects it into a cold plate. A radiator coupling thermally connects the cold plate to a radiator allowing heat dissipation to deep space. RFC operation on the lunar surface under vacuum limits the heat rejection mechanism to radiation alone. The coupling between the RFC thermal enclosure and radiator must be able to “engage” for maximum heat rejection during the lunar day, and “disengage” during the lunar night to minimize heat loss to the external environment. The thermal interface between the PCL and radiator is further discussed in Section 2.1.

The radiative sink temperature of the two-sided radiator at the lunar equator (parallel and normal orientations to the equatorial plane) depends on the specifics of the lunar landing site, local lunar geography, radiator optical properties, and the radiative environment. The effective maximum daytime sink temperature may be as high as 48 °C, which approaches the operational temperature of a PEM EZ. Additionally, lunar dust accumulation on radiator surface and radiator orientation may adversely affect the sink temperature. Thermal vacuum chamber (TVAC) testing will not expose the RFC to a thermal environment that properly simulates all severe lunar surface environment conditions without a solar flux simulator, lunar surface IR, or simulated lunar dust. Further details are provided in Appendix B on the thermal modeling effort, including the radiator design.

1.2.3 Material Compatibility

H₂, O₂, and H₂O systems introduce many material compatibilities issues. Care must be taken in selecting metals and soft goods that minimize or eliminate risks associated with issues such as hydrogen environment embrittlement (HEE) and high-pressure pure oxygen environments. Additionally, corrosion may occur in many places with continued exposure to conductive and acidic FC product H₂O within the overall system including the PEM stacks and components throughout the reactant and coolant systems. The product H₂O may need to be treated to limit the potential corrosion problem. Ideally, there would be an inert treatment option to reduce or prevent corrosion.

1.2.4 Reliability

The RFC is a system comprising hundreds of components. Without redundancy, failure of any single component, including individual cells in the electrochemical stacks, may disable the entire RFC system. Although there has been work done to make PEM stacks more passive and eliminate required auxiliary components, that can only go so far. For COTS components, selection of more durable products with certifications or known lifetimes is a priority. The issue is that there is very limited existing information on the mean time between failures (MTBFs) for all components. A system designer needs to know such values for the exact components in the system, otherwise, having unknowns greatly increases what must be assumed for the random failure rate.

Terrestrial RFC systems are expected to have a reasonable operational life (5,000 h min.) and be reliable. The ultimate goal of flight RFCs is to support bases that could last 10 years (~100,000 h) with a 50,000-h maintenance interval. This is a known challenge due to the quantity of independent components that requires additional testing to determine both component and system MTBFs. It is not possible to test every component and subsystem for that timespan within the current project. Component, subsystem, and complete RFC system life testing are planned as one beginning step to remedy this lack of knowledge. Accelerated life testing processes can be developed to discover faults and potential modes of failure in a reduced amount of time using testing conditions more severe than normal service parameters. Then, the module can be redesigned, rebuilt, and retested to increase service life. For a single component or subsystem, simultaneous multiple and/or repeated testing is necessary to statistically determine failure rates.

Component life and maintenance cycle also affects its reliability. TVAC testing can enable forecasting the effect of temperature and vacuum on RFC operation. The effects of microgravity and solar radiation on component life and system reliability are more difficult to predict. Once the component and subsystem testing are completed, MTBF of alternatives can be compared. Although low mass and power components are preferred, MTBF is also an important factor for selection of components and subsystem design. The improvement of reliability at component and/or subsystem levels should be identified and implemented to contribute to a robust and reliable system. Aside from testing, reliability simulation and analysis software can be used for weak link analysis and reliability calculation.

2.0 Fluid Management and Storage

There are numerous individual RFC components that require significant research to identify, select, develop, and procure for full system integration. This section is to cover relevant technological aspects of active thermal management, reactant gas drying, fluidic flow control and generation, and reactant storage for a RFC design targeted at a lunar-equator-like environment demonstration.

2.1 Fluid and Thermal Management

Section 1.2.2 introduced the overall RFC thermal design consisting of various passive and active thermal features. In this section, a more detailed description of the active thermal management is provided including the internal pumped loop and the coupling to a radiator for heat rejection. Since this radiator interface is a major design challenge, a number of radiator coupling technologies were considered and are described along with the chosen technology.

2.1.1 Primary Cooling Loop

As shown in Figure 2, the PCL captures waste heat from key RFC components including the FC, EZ, PMAD system, and avionics box then actively transports the heat to a radiator interface via a convective cooling fluid. The PCL consists of a flow loop with pump; fluid lines; cold plates for the PMAD and avionics; FC stack; and thermal fluid. The EZ is cooled separately by a H₂O loop (with the H₂O flow through the stack serving both as reactant feed and cooling fluid) that interfaces to the PCL via liquid-to-liquid heat exchanger. The interface of the PCL to the radiator is a cold plate attached to the variable conductance heat pipe (VCHP) evaporator sections. The chosen thermal fluid for the PCL is a H₂O-glycol mix with the exact ratio to be determined. More glycol depresses the freezing point and better lubricates the pump head at the cost of reduced heat capacity and increased pump power. The PCL includes a bypass loop and flow control valve to bypass the radiator coupling and maintain temperature control of the cooling loop under varying total heat load conditions.

2.1.2 Radiator Coupling Overview

The PCL is thermally coupled to the radiator allowing heat dissipation to the lunar environment. The RFC presents a thermal challenge in that the maximum heat load occurs during the lunar day when surface temperatures are the highest. During the lunar night, the heat load is moderate and thermal energy needs to be conserved to maintain temperatures inside the thermal enclosure when surface temperatures are low. The radiator and the associated coupling technology must be able to adjust to these contrasting heat rejection needs, and ideally, be able to effectively disconnect during the lunar night to minimize heat loss. The following sections describe the radiator coupling technology options considered along with the advantages, disadvantages, and maturity of each technology.

2.1.3 Coupling Requirements

The method used to thermally connect the PCL to the radiator is a critical consideration and must

- Maintain the PCL within a narrow temperature range
- Accommodate thermal rejection power from a variable PCL temperature and to a variable environmental sink temperature
- Maintain a minimum fluid temperature during the long lunar night; ideally, the heat rejection system ceases operation (i.e., becomes adiabatic) during the lunar night to minimize heat rejection from the RFC
- Minimize parasitic losses from the fluid system to the environment during the lunar night
- Avoid interference with the geometry, orientation, and placement of the radiator
- Function in a vacuum environment of <1 mPa (10^{-5} torr)
- Be freeze-tolerant or nonfreezing to a minimum of 120 freeze and thaw cycles

Furthermore, it is desirable but not required to use nontoxic fluids.

2.1.4 Candidate Technologies

The following technologies were evaluated for performance, TRL, complexity, mass, and commercial availability.

- External pumped loop (EPL) system using regenerative heat exchanger and single-phase freeze-tolerant thermal fluid
- Freeze-tolerant external pumped loop (FT-EPL) system using two-phase thermal fluid (freeze-tolerant radiator)
- Passive thermal louvers (PTLs)
- Conventional heat pipes (CHPs)
- Variable conductance heat pipes (VCHPs)
- Thermal switches
- Shape memory alloy technologies

The various merits and disadvantages of each are described in the following sections.

2.1.4.1 External Pumped Loop System Using Regenerative Heat Exchanger and Single-Phase Freeze-Tolerant Thermal Fluid

A single-phase freeze-tolerant thermal fluid EPL system is a mature and flight-demonstrated active thermal control technology. In particular, single-phase pumped loop technology, with an internal single-

phase loop utilizing a nontoxic thermal fluid (either H₂O or H₂O-glycol mix) inside the pressurized volumes, is utilized in all three of the most recent NASA manned flight programs: the Space Shuttle Orbiter (retired in July 2011 (Space Transportation System (STS)–135)), the ISS (operational), and the Orion/European Service Module (ESM, in development).

Conceptually, a single-phase pumped loop radiator would be implemented in the RFC system as an external thermal control loop as shown in Figure 3. The EPL system consists of a fluid loop connected to the PCL via a heat exchanger, a radiator panel, a pump, and an accumulator. A radiator bypass line in the loop plus a thermostatic valve (not shown) controls the thermal fluid return temperature to the RFC internal loop heat exchanger. The RFC internal active thermal control loop is insulated by the RFC thermal enclosure to limit temperature extremes, in particular, exposure to temperatures below the freezing point of the H₂O-glycol thermal fluid.

The choice of thermal fluid for this external thermal control loop is highly dependent on the mission thermal environment. The thermal control system, in particular the radiator, is sized for the maximum heat load in the warmest thermal environment but must also operate at reduced heat loads in the worst-case cold environment. This can make freeze tolerance a key design challenge for single-phase pumped loop systems. The NASA applications listed earlier, the STS Orbiter and the ISS, operating primarily in LEO conditions, utilize Freon™ 21 (Chemours Company) and NH₃, respectively. The Orion/ESM, which is designed for several severe thermal environments (LEO, trans-lunar orbit, and lunar orbit), utilizes a hydrofluoroether.

In the case of the STS Orbiter and ISS, worst-case LEO thermal environment temperatures are slightly below the freezing points of the thermal fluids. As a further risk reduction, the ISS uses a “designed-to-freeze” radiator design, which incorporates tubes sleeved with high-strength material to handle the extra stress from a frozen plug of NH₃, along with variable tube spacing to avoid all tubes freezing at once (Ref. 23). The

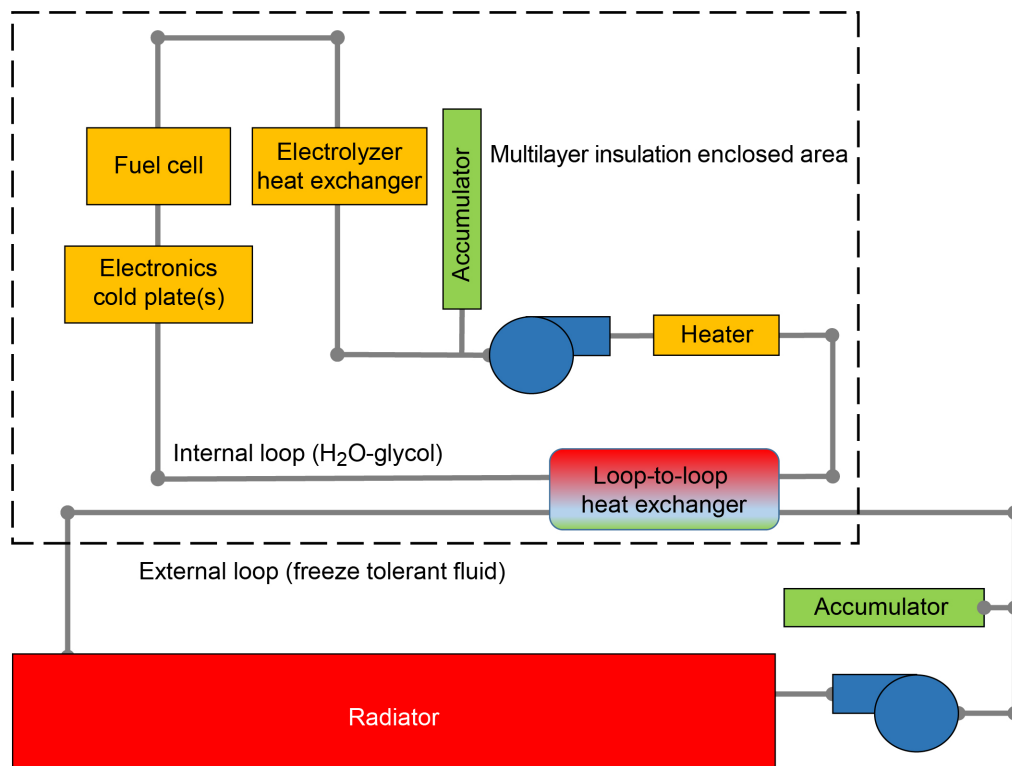


Figure 3.—Key components in single-phase pumped loop heat rejection system (labeled as external loop) along with its interface to regenerative fuel cell internal thermal control loop. Multilayer insulation (MLI).

Orion/ESM radiator will see worst-case thermal environments with temperatures significantly below the freezing point of the thermal fluid, but the parasitic loads are such that it is not ever necessary to fully bypass the radiator, allowing some flow there to maintain temperatures above the freezing point. The Orion/ESM radiator also employs heating elements embedded in the radiator to protect the tubes from freezing in the event of abnormally low heat loads from the vehicle.

For the RFC radiator application, the freezing potential is a key concern and disadvantage of the technology. Table I lists a number of commercially available candidate thermal control fluids under generic identifiers. Note that Freon™ 21, the thermal fluid used in the STS Orbiter thermal control system, is no longer manufactured and therefore not listed in this table. The worst-case lunar night effective sink temperature is $-194\text{ }^{\circ}\text{C}$ for a lunar equatorial location and most of these potential fluid candidates have freezing points above this temperature. The refrigerant R-124 does have a freezing point of $-199\text{ }^{\circ}\text{C}$ but also has a boiling point of $-12\text{ }^{\circ}\text{C}$, which is below the operating temperature range of the RFC stacks.

TABLE I.—THERMAL PROPERTY DATA FOR SEVERAL SINGLE-PHASE HEAT TRANSFER FLUIDS
[Sources for all physical property data are listed separately (Refs. 24 to 31).]

Fluid name or identifier	Chemical name(s)	Temperature, $^{\circ}\text{C}$				Kinematic viscosity, cSt	Toxicity
		Operating		Boiling	Freezing		
		Low	High				
NH ₃	Ammonia, trihydridonitrogen, nitrogen trihydride	-----	-----	-33.3	-77.7	0.276 mPa·s (-40 $^{\circ}\text{C}$)	High
A	Organosilicate ester blend	-101.0	149.0	232.0	N/D	44 mm ² /s (-65 $^{\circ}\text{C}$)	Low
B	-----	-90.0	45.0	55.0			Low
C	-----	-75.0	60.0	70.0			Moderate
D	-----	-80.0	70.0	80.0			Moderate
E	Aromatic hydrocarbon blend	-112.0	163.0	176.0	-129.0	218 cP (-112 $^{\circ}\text{C}$) 4.92 cP (-62 $^{\circ}\text{C}$)	Low
F	1-methoxyheptafluoropropane	-120.0	25.0	34.0	-122.5	2 (-80 $^{\circ}\text{C}$), 17 (-120 $^{\circ}\text{C}$)	Low
G	Methoxy-nonafluorobutane (C ₄ F ₉ OCH ₃)	-105.0	50.0	61.0	-135.0		Low
H	Ethoxy-nonafluorobutane (C ₄ F ₉ OC ₂ H ₅)	-105.0	65.0	76.0	-138.0		Low
I	-----	-30.0	85.0	98.0	-38.0	3.51 (-30 $^{\circ}\text{C}$)	Low
Propylene	Propylene, propene	-----	-----	-47.6	-185.2		Low
R-124	1-Chloro-1,2,2,2-tetrafluoroethane	-----	-----	-12.0	-199.2		Moderate
J	1,1,1,3,3-Pentafluoropropane	-----	-----	15.1	-102.1	401 mPa·s (25 $^{\circ}\text{C}$)	Low
K	-----	-----	-----	176.0	-129.0	1 (25 $^{\circ}\text{C}$), 10 (-78 $^{\circ}\text{C}$)	Low

The lunar equator RFC will generate reduced peak heat loads during the lunar night operations. It is also anticipated that the RFC customer will have a requirement for using some or all of the excess heat load from the RFC to maintain temperatures in other systems, such that either a full bypass or thermal switch be implemented in a RFC single-phase pumped loop design in order to minimize waste heat losses. As an estimate, Ungar (Ref. 23) calculates that a 30-percent bypass of the design heat load flow would be necessary to maintain nonfreeze conditions in an NH₃ fluid radiator under similar lunar conditions but proposes this could be somewhat reduced using a regenerator bypass system. Another key disadvantage of the single-phase pumped loop is the increased parasitic loads, mainly the pump and associated actuators and electronics for the additional thermal loop. The total pump power may actually increase under reduced heat loads during the lunar night due to increased viscosity of the thermal fluid at lower operating temperatures.

Besides freeze tolerance, other key considerations in the selection of a thermal fluid for a pumped loop system include high sensible heat, low pressure drop, low pump power, and small accumulator size. For example, van Gerner, van Benthem, and van Es (Ref. 32) provide a figure of merit methodology incorporating the fluid physical properties to select a thermal fluid for single-phase pumped loop systems and several other thermal control technologies. A single-phase thermal fluid continues to be of research interest to meet lunar thermal environment requirements for operating temperature range along with high-performance thermal properties (Ref. 33).

In summary, the single-phase pumped loop radiator system is a technologically mature and flight-demonstrated spacecraft heat rejection system. Due to the added complexity of an external loop, increased parasitic loads, and the freeze-tolerance concern coupled with the requirement of the RFC to provide a keep-alive heat load to the customer, it was not selected as the radiator system technology for the RFC project.

2.1.4.2 Passive Thermal Louvers

PTLs are an active thermal control technology capable of increasing or decreasing the view factor from a radiator panel to the surroundings by mechanical means. The amount of heat transfer between the radiator and the deep space environment is governed via pivoting blades or vane louvers mounted within a frame. These louvers open and close to control temperature through the use of bimetallic actuator springs that are thermally connected to the radiator. As the radiator temperature reaches a predetermined value, the louvers are fully opened for maximum thermal radiation transfer. Effective emissivity of the louver is defined in terms of the effective combined thermal emissivity of the mounting surface and louver. A louver will provide an effective emissivity of 0.14 or less when all blades are closed and 0.74 or greater when all blades are open. These values assume a radiator mounting surface with emissivity of 0.85 in the IR spectrum. In general, the achievable turndown ratio (defined as heat rejected during open state divided by heat rejected in closed state) is ~6 for vane-type louvers (Ref. 34).

This technology can potentially be incorporated with most types of radiator panels, independent of the radiator coupling technology, that is, single-phase pumped loop, two-phase freeze-tolerant, heat pipe, etc. As an aside, thermal louvers can also be used to control heat transfer between internal surfaces of a spacecraft, or amount of heat from spacecraft internal surfaces directly to space (Ref. 34). Because the COTS options for louvers are primarily for a lower heat rejection size capability than what is needed for the RFC, this technology has not yet been implemented in the RFC project design. There remains potential to design a custom solution (dependent on funding) and, in particular, this technology could be considered for a flight configuration if additional turndown ratio capability is warranted, and the mass penalty is not too great.

2.1.4.3 Conventional Heat Pipe

A CHP consists of a metal tube containing an entrained two-phase working fluid (WF). Heat transfer is dominated by liquid-vapor phase change in an evaporator at one end and a condenser at the other. Although there is some conduction along the metal tube, this heat transfer effect is much smaller and is considered a second-order effect. The WF at the evaporator end is initially in a liquid state and the evaporator is thermally linked to the PCL via a heat exchanger. The condenser end is thermally embedded into the radiator. In between the evaporator and condenser, there is a length of pipe referred to as the “adiabatic section” where the heat exchange with the surrounding environment is essentially zero.

During normal operation, the PCL provides sufficient heat flux into the evaporator to generate liquid-to-vapor phase change. The vapor flows towards the condenser where heat is removed by vapor-liquid phase change. The dominant mechanism for returning liquid WF to the evaporator is capillary action along the perimeter of the tube wall, though gravity can be used to assist the liquid return flow (Ref. 35). Grooves or wire mesh are usually placed inside the tube to assist with the capillary action. This process forms a closed loop with a very high effective thermal conductivity due to the high heat transfer coefficients associated with liquid-to-gas phase change. The effective conductivity is several orders of magnitude greater than thermal conduction through metal.

There are multiple design considerations for a heat pipe. One is to ensure that there is enough fluid mass to maintain a two-phase system over the desired operating temperature range. If too much heat is applied, all of the fluid can convert to vapor; at this point, the heat pipe is considered to be “dried out,” and the effective heat transfer coefficient plummets. The upper temperature is mainly limited by the required thickness of the tube wall to safely contain the two-phase fluid pressure at the highest temperature while being thin enough to minimize resistance to radial heat transfer in the evaporator and condenser sections. Different fluids can be selected to tailor the working temperature and heat transfer capability of the heat pipe.

In summary, CHP technology is a mature and flight-demonstrated spacecraft heat rejection system. Unfortunately, CHPs do not have a lower limit shutoff temperature without sustaining damage when the WF freezes. This presents issues similar to those of a single-phase pumped loop system, requiring parasitic keep-alive electrical heating loads and a freeze-tolerant fluid. For these reasons, it was not selected as the radiator coupling technology for the RFC project.

2.1.4.4 Freeze-Tolerant External Pumped Loop

The FT-EPL technology is a fairly recent development in thermal control. It utilizes a two-phase WF that allows gas (vapor) flow into the radiator under low heat load conditions. There are at least two designs in development by different vendors. One incorporates vapor and liquid flows in separate parallel radiator tubes, allowing freezing of the liquid tubes under low heat load conditions with the vapor laden tubes handling the reduced heat load. In the other design, freeze-tolerant condensers, in parallel tubes similar to heat pipes, are fed vapor from a membrane evaporator (coupled to the primary cooling loop), and the condensers self-regulate the thermal conductivity by condensing the WF (e.g., H₂O) (Ref. 36). This technology has the potential to achieve turndown ratios >10.

Although this technology is promising, it does add a number of extra components, increasing complexity compared to single-phase pumped loop or heat pipe technology. Furthermore, the technical maturity is low. As of this writing, two Phase I Small Business Innovation Research (SBIR) contracts have been completed and one of the vendors was awarded a Phase II. The earliest date that the Phase II work would have a system for procurement is not compatible with the RFC project schedule, but it merits consideration for a later flight system.

2.1.4.5 Variable Conductance Heat Pipes

Like a standard heat pipe, a VCHP has an evaporator, an adiabatic section, and a wick used to return the condensate back to the evaporator. It also relies on two-phase heat transfer in combination with a comparatively small amount of simple conduction through the thin-walled tubing of the adiabatic section. However, a VCHP adds a noncondensable gas (NCG) to the two-phase WF and a NCG reservoir. The pressure in the NCG reservoir determines the VCHP working pressure, and therefore, the temperature of the phase change. The NCG reservoir is usually located at the condenser end and is actively heated (usually with a parasitic electric heater). However, parasitic loads need to be minimized for RFC application. In order to eliminate this loss, the reservoir may instead be located adjacent to and in thermal contact with the evaporator. A small tube connects the NCG reservoir to the condenser end as shown in Figure 4.

During operation, WF flow sweeps a high concentration of NCG into the reservoir. This results in the evaporator WF vapor pressure being much higher than the condenser WF partial pressure and creates a boundary known as the gas-front location within the pipe. This is where the sum of the condenser end WF partial pressure and NCG pressure equal the evaporator end WF vapor pressure.

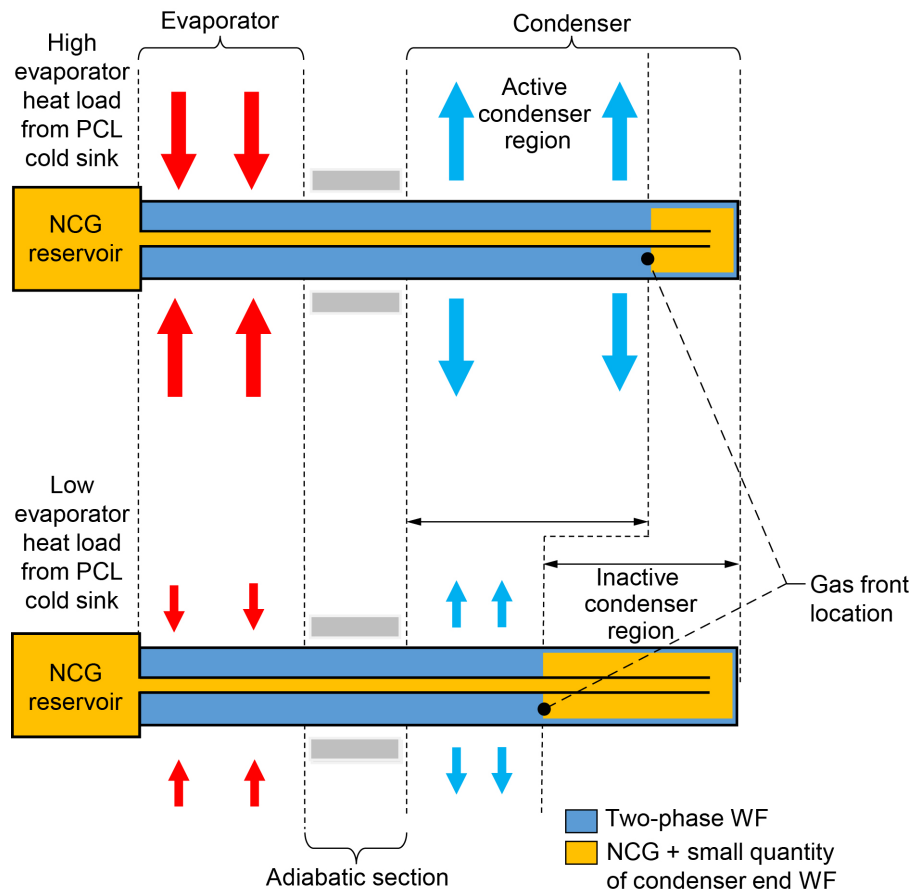


Figure 4.—Operation of variable conductance heat pipe. Noncondensable gas (NCG). Primary cooling loop (PCL). Working fluid (WF).

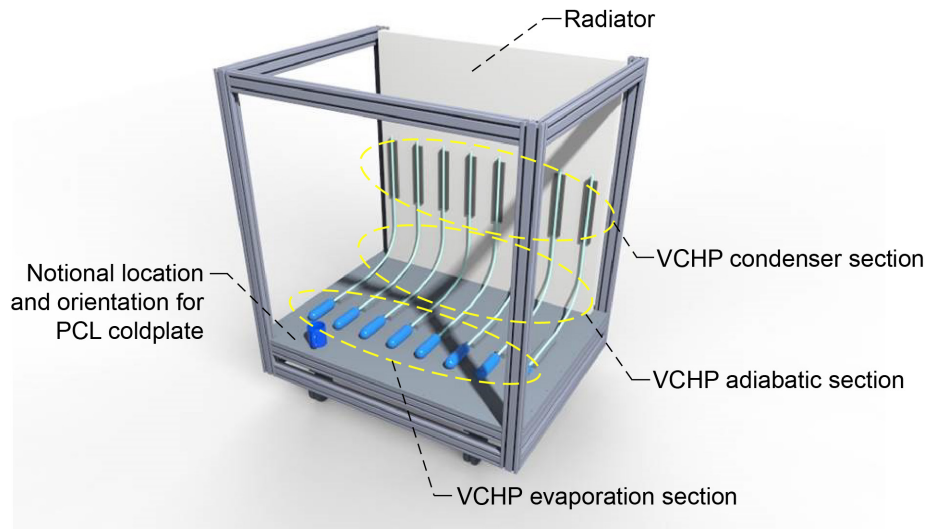


Figure 5.—Variable conductance heat pipe (VCHP) integration with regenerative fuel cell system. Primary cooling loop (PCL).

Therefore, NCG quantity in the reservoir is proportional to the evaporator WF vapor pressure. At full design thermal power, the majority of the NCG is driven into the gas reservoir allowing the entire condenser region to be active. At lower thermal power, the evaporator WF vapor pressure drops allowing the WF and NCG boundary to move into the condenser region, reducing the active heat transfer area until a new equilibrium is achieved. The WF and VCHP charge pressure combination is chosen to minimize evaporator WF saturation temperature change versus pressure. This maintains a small evaporator temperature band. Furthermore, if the power level is low enough, there will be no convective heat transfer in the VCHP as the NCG will occupy the entire condenser section. There will be a small amount of heat transfer via gas and thin-walled tubing conduction, but this will be orders of magnitude less than the WF two-phase heat transfer. This ability allows the VCHP to function as a “thermal switch” (see Section 2.1.4.6) between the PCL and radiator by having a high effective conductance during the lunar day and a low effective conductance during the lunar night. Resultant turndown ratios can exceed 5:1 (Ref. 37).

The VCHP evaporators are rigidly mounted to the PCL cold sink using methods to thermally optimize the conductive heat transfer. The VCHP condenser is thermally mounted to heat spreaders mounted to the radiator surface. A preliminary configuration for the RFC project is shown in Figure 5. The fixed configuration is required due to the orientation sensitivity of this technology. There is a strict tolerance for maximum inclination angle of installation with respect to gravity.

2.1.4.6 Thermal Switches

Thermal switches, incorporated at the interface between internal and external thermal loops, are an attractive option for increasing turndown ratio. Two passive heat switch models were evaluated as a potential thermal bridge between the RFC PCL and radiator. Both operate on the principle of a paraffin-based actuator that contracts and expands with temperature such that thermal contact varies between a heat source and heat sink at a set temperature. One commercially available passive thermal control heat switch is a 2.5-cm-diameter by 3.8-cm-long cylinder that costs ~\$10,000, weighs 110 g, and is capable of rejecting 6 W maximum heat (Ref. 38). These individual units are better suited for low-power electronics boxes than for a RFC, which requires hundreds of watts total heat rejection.

For higher power applications, a thin-plate heat switch is more practical. These units integrate 2.5- by 2.5-cm cells, each capable of rejecting 12 W, into a larger plate for interfacing with the radiator. Thin-plate heat switches operate over a wide temperature regime from –130 to 100 °C with actuation set points from –10 to 50 °C. While these offer high turndown ratios around 78:1, the large number of cells required for RFC heat rejection loads made the cost of these units impractical for RFC. Still, if packaging requirements are particularly restrictive for a given RFC application, this class of devices could remain desirable.

2.1.4.7 Shape Memory Alloy Technologies

Another radiator technology considered is a particular novel one: the Shape Memory Alloys for Regulating Thermal Control Systems in Space (SMARTS). The SMARTS technology is an innovative use of shape memory alloys to passively control heat transfer that is somewhat analogous to louvers, but the technology is at a low TRL, and the particular hardware geometry being pursued by SMARTS is for lower heat load applications and may not scale efficiently for the RFC application.

2.1.4.8 Summary Comparison

Table II provides a summary of discussion on the relevant thermal coupling and management technologies.

2.1.5 High Power Density Electric Heaters

Heaters are required in the coolant loop and EZ recirculation loop to heat the process fluids that will in turn preheat the FC stack and the EZ stack, respectively. Assuming worst-case conditions, the process fluid will initially be at 4 °C, and the heater will need to help raise the temperature to near 60 °C. In order to moderate the heater power, the fluids will be heated over the course of 90 min.

An ideal heater for the RFC system would be a 24 to 28 Vdc high power density heat trace for vacuum chamber operation. It should also be lightweight, have a long operational lifetime that does not require maintenance, and be installed using a pressure-sensitive adhesive that is vacuum compatible with limited or no off-gassing. An immersion heater was also considered to improve heat transfer efficiency, but those require tubing enclosure too massive for RFC integration in high-pressure sections. Many COTS heat traces that are certified for vacuum operation either are not designed to operate on 24 Vdc or have a low power density, resulting in the need for a lot of applied surface area. There are vendors making custom heaters to accommodate these requirements, with concordant cost increases. Due to the presence of H₂ in the RFC system, it would be ideal if the heater was rated for hazardous location operation, which is a location where ignitable concentrations are possible but would only exist in the event of accidental rupture or breakdown. Although this is not an issue for the TVAC environment, the RFC must also safely operate in atmospheric pressure laboratory environments as described in Section 1.2.1.

Compared to more specialized RFC components, high-power DC heater integration is much less complex. For a flight test, vibration and reliability testing should still be completed, but only minor verification testing is necessary for the RFC. Therefore, no subsystem test plan is detailed in this section. The following sections will address the specific heater requirements of each loop.

TABLE II.—SUMMARY OF ADVANTAGES AND TECHNICAL MATURITY RATINGS FOR IDENTIFIED THERMAL TECHNOLOGIES

Advantages	Disadvantages	Relative maturity
External pumped loop (EPL)		
Simple; flight demonstrated	External loop may contain hazardous fluids. It requires an extra heat exchanger and second loop with associated controls, pumps, and support hardware that increases complexity, parasitic electrical power, and possibility of mechanical failure.	High technology readiness level (TRL)
Freeze-tolerant external pumped loop (FT-EPL)		
Simpler and lighter than external loop pumped system; high thermal turndown ratio; lower parasitic power requirements than external loop pumped system; can use H ₂ O working fluid (WF)	It adds complexity in terms of additional components to system.	Low TRL
Passive thermal louver (PTL)		
Simple design; high solar irradiance capability; spaceflight heritage; fully passive thermal control; fairly wide range of operational temperature band and setpoints	Limited turndown ratio. Published performance data is advertised as 0.74/0.14 or ~5.3. This value does not allow for both maximum heat transfer and prevention of loop freezing without adding parasitic heating. There are mounting location limitations. The regenerative fuel cell (RFC) fluid system primary cooling loop (PCL) would, by necessity, be mounted to the radiating surface. Commercial-off-the-shelf sizes are small, requiring multiple louver systems or a custom-designed system. Limited to single source vendor.	High TRL
Conventional heat pipe (CHP)		
Lightweight; passive, no parasitic pumping load loss; flight demonstrated	It has limited ability to regulate the PCL temperature within a narrow range. The rate of vapor formation is a function of temperature (which follows the WF saturation curve) and heat flux. Heat flux is determined by radiative heat transfer. It has limited ability to limit heat transfer below a desired temperature. This creates large thermal loss, which becomes an issue during the lunar night requiring large parasitic heating requirements to maintain minimum temperatures for RFC system health.	High TRL
Variable conductance heat pipe (VCHP)		
Lightweight; passive, no parasitic pumping load loss; maintains near constant PCL temperature; can effectively shut off at a desired temperature; parasitic heating requirements are very small	There are specialized design considerations. Careful coordination with VCHP supplier is required to ensure adequate performance.	Moderate TRL
Thermal switches		
Lightweight; passive; modular, easy to package	It is small scale relative to RFC thermal loads. Cost is a factor.	Moderate TRL

2.1.5.1 Coolant Loop

Since there is no vacuum-compatible 24-Vdc COTS heat trace with a high enough power density, immersion heaters were investigated. An immersion heater will minimize the heat loss from the heating element to the coolant since it is directly in contact with the fluid. It does not depend on available surface area from tubing and equipment, like heat trace, since it can be installed inside the tubing or the coolant reservoir. An important design guideline to note is that if the heater is installed in a pipe, the pipe diameter must be at least 4 times the diameter of the heater and always remain fully submerged in the coolant while operating to prevent overheating and burnout. Both the mass of the heater and the additional mass increase from the increased diameter pipe must be considered when selecting the heater type. Still, the decision was made to specify an immersion heater with a circular geometry for the coolant tank reservoir. To increase operational life, the maximum designed heater power is somewhat larger than the minimum required power to ensure the heater is not constantly running at maximum power.

2.1.5.2 Electrolyzer Recirculation Loop

Immersion heaters were also investigated for the EZ recirculation loop, with the additional requirement that the heater must operate in a fluid with a pressure of 17.2 MPa. Immersion heater vendors cannot meet the pressure requirements without significant redesign and customization. Additionally, the heater would need to be installed in a pipe with a diameter at least 4 times greater than the diameter of the heater, which results in a significant mass penalty. Therefore, custom heat trace was investigated since COTS heat trace does not meet the RFC requirements. Several vendors can meet the design requirements but at an increased price due to customization and vacuum-compatible materials.

2.2 Gas Drying

In an aerospace PEM RFC application, gas drying is required due to closed-loop operation of H₂O-based processes. The following sections describe the RFC requirements and applicable technologies.

2.2.1 Gas Drying Requirements

The gas drying process must be highly efficient, reliable (>10 years of operation without servicing desired for a lunar lander application), and compatible with the product gases. However, aerospace RFCs present additional unique challenges that must be overcome for the gas drying process to be effective (Refs. 3 and 39). Traditional regenerative drying systems vent the captured H₂O to the environment, which for closed-loop systems, would deplete the available stock of H₂O to electrolyze and therefore reduce the maximum potential RFC system energy storage capacity. Furthermore, since parasitic power directly reduces RTE, the dryers must consume little to no power. The dryers must also have low mass and volume and be able to operate in a vacuum environment (<0.001 Pa). Lastly, any gas drying equipment would be required to operate at the temperatures inside the RFC thermal enclosure (4 to 85 °C). This is a much narrower range than the lunar surface temperatures.

Figure 6 shows the ambient temperature and RFC reactant tank pressure over the course of a lunar day and night cycle at the lunar equator (Murchison crater rim) for a 100-W nominal net output RFC. Time 0 corresponds to the beginning of a lunar day where the surface temperature rises quickly and EZ operation begins, increasing the reactant tank pressure. Near the end of a lunar day, there is a short transition period where neither the EZ nor FC stack is operational, causing pressure to remain constant. During the lunar night, the FC operates at an assumed constant power output, resulting in a constant reactant consumption rate.

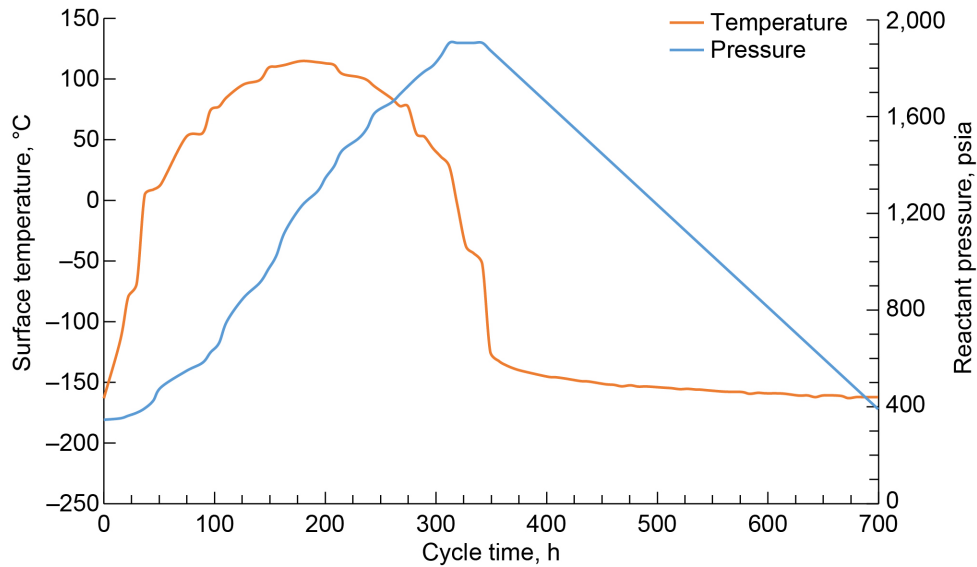


Figure 6.—Lunar equatorial surface temperature and reactant tank pressure in 1 lunar day (710 h).

Figure 6 demonstrates that a RFC at the lunar equator will experience extreme temperature conditions. More importantly, without H₂O removal, reactants produced by the EZ will enter the storage tanks with H₂O. The tanks are outside the thermal enclosure and will need to be heated to avoid the H₂O freezing, adding a significant parasitic load and reducing RTE. For example, in this lunar equator scenario, the storage tanks must be heated to above 0 °C to ensure H₂O does not freeze and the heating requires considerable amounts of power (>80 percent of the nominal net power output of a 100-W RFC (Ref. 1)). However, the storage tanks could be kept at much lower temperatures if there was minimal H₂O present in the stored gases. By reducing H₂O concentration so the tanks only have to be heated to -50 °C (i.e., above the frost point), the RFC system power requirement decreases to less than 40 percent of the nominal net power output of a 100-W RFC, and the RTE increases by over 19 percent (Ref. 1). In addition, H₂O not converted into reactants results in reduced energy storage capacity. Therefore, the goal of the gas drying subsystem is to completely remove all H₂O from the reactants and recycle it back to the EZ.

2.2.2 Gas Drying Techniques

As described in the previous section, removing H₂O from the EZ product streams is essential for creating the most efficient RFC system. H₂O removal can be achieved, depending on the desired final H₂O content of the gas stream, through a process with one or multiple stages. The use of additional stages will remove more H₂O (assuming the process is designed properly) but add more mass, so a cost-benefit analysis should be completed to determine the necessity of additional stages.

The gas drying process depends on the type of EZ used in the RFC. For liquid anode or cathode feed EZs, liquid H₂O will be present in at least one of the outlet streams and the first (or possibly only) stage is a vapor-liquid phase separator (VLPS). Once the liquid H₂O is separated from the EZ outlet stream, several different gas drying techniques—the most common being absorption, adsorption, coalescence, deliquescence, membrane, and refrigeration—are available if H₂O vapor concentration is unacceptable after the VLPS. For vapor feed EZs, liquid H₂O will not be present in the outlet streams at the same concentrations, so a VLPS is not required, but any of the other previously mentioned gas dryers are applicable. The remainder of this section discusses the different technologies available to dry a gas stream and the viability of each in aerospace RFC applications.

2.2.2.1 Vapor-Liquid Phase Separators

VLPSs are used in the outlet streams of liquid anode or cathode feed EZs in order to separate liquid H₂O from entrained H₂ or O₂ gas. VLPSs can either be active (i.e., require power to achieve separation like a centrifuge) or passive (i.e., no power is required for separation). Active VLPSs are not feasible for aerospace RFCs due to the power requirements, but passive VLPSs are acceptable. One important consideration for the selection of a VLPS is the environment. In locations with a constant gravity direction (e.g., the lunar surface), VLPSs can rely on buoyancy forces for separation. Gravity forces the denser liquid phase to the bottom of the VLPS while the less dense vapor phase exits at the top of the VLPS. However, if a RFC in an aerospace application would be in an environment where the gravitational vector changes (during flight) or a microgravity environment where buoyancy is very limited or nonexistent, gravity can no longer be used for the separation. Typically, capillary and centrifugal forces are used to overcome the lack of gravity to separate the two phases, but it is common for these VLPSs to require power (Refs. 40 and 41). However, there has been considerable research designing and testing passive VLPSs that can be used in situations where gravitational forces vary (Refs. 41 to 47).

2.2.2.2 Absorption Dryers

Absorption dryers flow a liquid absorbent countercurrent to a wet gas stream in a column. The liquid absorbent, usually a glycol-based or ionic liquid, absorbs H₂O from the gas stream, producing dry gas and H₂O-rich absorbent in the column outlet streams (Refs. 48 to 52). While absorption dryers are a common gas drying technique, they are not feasible for an aerospace RFC because (1) the absorbent needs an energy-intensive regeneration process for reuse (Refs. 48 and 52 to 54) that requires additional equipment, adding mass and (2) additional power and equipment are required to generate the absorbent flow.

2.2.2.3 Adsorption Dryers

Adsorption dryers operate similarly to an absorption dryer, but these instead use a solid desiccant with high H₂O affinity (Refs. 53 and 55 to 57). H₂O flows through a packed column, and the desiccant physically adsorbs H₂O until reaching the saturation point where it can no longer adsorb H₂O. Typically, adsorption dryers are deployed in pairs to allow one dryer to be regenerated while the other continues to dry the gas (Ref. 55). Unfortunately, a dual dryer design with regeneration is not feasible for an aerospace RFC for reasons similar to the absorption dryer (i.e., size and mass constraints). Adsorption dryers can be deployed as a single unit in an aerospace RFC, but this introduces a maximum lifetime when desiccant needs replaced once becoming saturated. Furthermore, any H₂O removed by the desiccant cannot be recovered, resulting in a decrease of energy storage capability and RTE. If used, single adsorption dryers should be designed as the final stage of a drying process for an aerospace RFC to remove the least amount of H₂O, but the designer needs to ensure that the benefit of reduced storage tank heating outweighs the lost H₂O.

A RFC-specific use for a dryer of this type would be to place the desiccant in the gas storage tank ports to dry the gases upon entry and humidify the gases upon exit. Morishige and Iwasaki (Ref. 58) showed that the freezing point of H₂O adsorbed by silica gel was considerably lower than 0 °C, but it depended on the fraction of filled silica gel pores. More filling (i.e., more H₂O removed from the gas) resulted in a higher freezing point, but still less than 0 °C. The melting point was always measured at -17 °C, regardless of pore filling. Using this approach would result in needing to heat the storage tanks less, and the gases could be humidified before reaching the FC with proper thermal management of the storage tanks.

2.2.2.4 Coalescing Filters

Coalescing filters flow wet gas from the inside of a filter element to the outside in order to collect H₂O on the filter fibers. H₂O droplets on the fibers grow as they move outward and meet other droplets,

eventually dropping off the element and into a collection area while the dry gas exits the filter. Any contamination such as oil or particulate matter significantly reduces the lifetime of these filters by restricting flow (Refs. 59 and 60). Coalescing filters are a viable option in an aerospace RFC because they allow any H₂O removed from the gas to be recycled back to the EZ. However, currently available commercial coalescing filters are not compatible with high-pressure (>7 MPa) O₂ due to static charge buildup concerns.

2.2.2.5 Deliquescent Dryers

Deliquescent dryers use a hygroscopic material (usually a salt) that is dissolved (i.e., deliquesced) when it encounters H₂O (Ref. 61). Similar to a single adsorption dryer, the hygroscopic material must be replenished when all of it has dissolved. While these dryers do not require power, the hygroscopic media is dissolved in the recovered H₂O, so H₂O must be purified before being fed to an EZ again. For these reasons, deliquescent dryers are not viable for aerospace RFCs.

2.2.2.6 Membrane Dryers

Membrane dryers use a hydrophilic membrane that is selectively permeable to H₂O (Refs. 62 to 65). When wet gas flows through this dryer, H₂O vapor diffuses through the membrane and is removed by a sweep gas, which is usually a small fraction of the dry outlet gas (Ref. 62) or another purge gas (Ref. 63). Membrane dryers are a passive drying technique, but, currently, there are no commercial membrane dryers that operate at high pressure and are compatible with H₂ or O₂.

2.2.2.7 Refrigeration Dryers

In most cases, refrigeration dryers require power to cool a wet gas stream below its dewpoint to condense and collect H₂O. The resulting dewpoint of the gas stream is slightly above 0 °C due to the freezing point of H₂O (Refs. 66 to 68). Since this method requires power in order to cool the gas stream, it is not preferable for an aerospace RFC. Furthermore, the elevated temperature of the product streams from the EZ would require significant power and a large refrigeration system, adding extra mass.

In some cases, parasitic power is not required for a refrigeration dryer. At locations where the daytime temperature is consistently below the freezing point of H₂O (e.g., Mars), the gas streams could be cooled passively to freeze H₂O. Burke and Jakupca (Ref. 69) demonstrated that no parasitic power was required to dry H₂ and O₂ from a unitized reversible fuel cell (URFC) by using the gas storage tanks for thermal control. The URFC system wrapped heat pipes around the gas storage tanks to dissipate heat generated during operation. While the URFC was in electrolysis mode, the storage tanks were at or below a temperature of -30 °C. The tubing for the product gases wrapped around the storage tanks before entering the vessels, allowing any H₂O in the gas stream to freeze before the gases were stored. Then, in FC mode, the tanks were at a temperature greater than 25 °C, so the gases were humidified as the H₂O ice melted.

2.2.3 Planned Testing

NASA Glenn Research Center is planning to test certain gas drying techniques listed earlier to determine the optimal drying processes for both outlet streams from a liquid anode feed EZ at a near-side lunar equatorial surface location. These tests will attempt to simulate conditions expected during EZ operation. As discussed in the previous sections, not all gas drying techniques are viable in an aerospace RFC, so the testing is focused on applicable drying techniques. The results from these tests will provide information crucial to designing the most effective and efficient gas drying process for an aerospace RFC.

Since the anode outlet of the EZ will be mostly liquid H₂O entrained with O₂ gas, the O₂ stream drying process first stage will be a VLPS to remove the liquid H₂O. The testing is planned around a passive VLPS that utilizes gravitational, buoyancy, and centrifugal forces for the separation. Testing will

be conducted with H₂O and an inert gas (N₂) at various flow rates, pressures, and temperatures to determine the maximum H₂O concentration of the gas stream exiting the VLPS. H₂O concentration of the gas exiting the VLPS is crucial for knowing if a second stage is necessary depending on design factors.

Due to the possibility of liquid H₂O at the cathode outlet of the EZ, the first stage of the drying process for the H₂ stream will be a coalescing filter. Testing is planned to evaluate the performance of several different coalescing filters. They will be tested with inert gas (He) at various flow rates, pressures, and temperatures to evaluate each filter's effectiveness. Additional testing is planned to determine the benefit of having several filters in series. Similar to the VLPS, determining the H₂O concentration at the exit of the chosen coalescing filter is essential to knowing if a second stage is necessary.

Testing is also planned for two adsorption dryers, one for the O₂ stream and one for the H₂ stream, should a second stage be required for either gas. A molecular sieve was chosen as the desiccant for the O₂ stream because it provides excellent high-temperature capabilities along with pure O₂ compatibility. Silica gel was chosen as the desiccant for the H₂ stream due to its simplicity and availability. This testing is aimed at determining the capacity of each dryer to uptake H₂O per unit mass of the dry desiccant. This can be accomplished by testing the dryer to breakthrough (i.e., the point where the desiccant is saturated with H₂O) with an inert humidified gas (N₂ or He). Knowing the flow rate and H₂O content at the inlet and outlet of the dryer along with the test time and original mass of the desiccant would allow for this calculation. Further testing will be done at different flow rates, pressures, and temperatures in order to determine the effectiveness under different conditions. The main downside of this dryer, as mentioned previously, is that any H₂O removed cannot be recovered, which is why it is crucial to determine the maximum H₂O content of any upstream drying processes (i.e., VLPS or coalescing filter).

2.3 H₂O Purification

In RFCs, H₂O is the FC reaction product as well as the only reactant for EZ supply. Contamination of H₂O can cause damage to both the FC and EZ, therefore, H₂O purification is an important part of the RFC BOP. In this section, potentially applicable pure H₂O standards are discussed. However, it is a unique challenge to achieve the pure H₂O requirements for RFC due to limited energy availability, the desire for system simplicity, and mass limitations. The relevant H₂O purification technologies are discussed for various types of impurities that may be present in the system.

2.3.1 Pure H₂O Standards and NASA International Space Station H₂O

Electrochemical conversion of H₂ and O₂ to and from H₂O are the only desired chemical reactions in RFC. In principle, the FC reaction produces pure H₂O, and the EZ consumes pure H₂O, however, there are side reactions generating byproducts. Pure H₂O can leach ions from wetted surfaces and the large, wetted surface areas within a RFC make it prone to contamination, causing various problems for long-term operation. Therefore, the H₂O in RFC must be treated to maintain purity. There are several indicators for purity of H₂O with the first being a very low electrical conductivity. There is an equilibration between H⁺ and OH⁻ concentrations in H₂O, and the equilibrium point depends on temperature. Because of the temperature dependence, it is standard practice to measure and report the conductivity at 25 °C (Ref. 70). High-purity H₂O is free from other conducting ions, and the conductivity is determined by mobilities and concentrations of H⁺ and OH⁻. An increase of H₂O conductivity indicates contamination by ionic impurities.

Nonionic soluble organics, solids, and bacteria concentrations are also important indications of H₂O purity. For terrestrial applications, H₂O is often processed by complicated and energy-consuming procedures to meet high-purity standards for semiconductor and pharmaceutical industries. Guidelines have also been established for ISS H₂O (Refs. 71 to 74). In ISS, H₂O is processed and managed for crew consumption, OGA electrolysis for O₂ production, and scientific experiments. The standards of semiconductor, pharmaceutical, and NASA

ISS H₂O are listed in Table III for comparison to desired RFC EZ feedwater specifications. It is worthwhile to note that the H₂O standard specifications for the Russian ISS module are much less restrictive than those of the United States due to the different electrolyte chemistries (Ref. 72). For RFC H₂O, it may be difficult to reach the semiconductor purity standard, but that is the closest existing analogue. Pharmaceutical H₂O or NASA ISS H₂O standards are more relaxed. Existing PEM RFC H₂O specifications are incomplete, but it is known that neutral pH and very low conductivity are desirable.

There is considerably more organic carbon allowed in the NASA ISS H₂O compared to the semiconductor standard. Much of these organic compounds can become nutrition sources for microorganisms such as bacteria. To suppress the bacterial growth, 1.0 to 4.0 mg/L of I₂ biocide is added in the ISS H₂O (Ref. 71). When H₂O is used for the OGA, H₂O passes through a deionizing (DI) bed to remove I₂ (Refs. 12 to 15 and 75 to 78). As H₂O is continuously converted to H₂ and O₂ by the OGA EZ, the total organic carbon (TOC) concentration increases in the OGA H₂O recirculation loop. After I₂ biocide is removed from H₂O, no disinfection measure is implemented for the loop, and bacteria growth has been observed (Refs. 14, 77, and 78).

In addition, HF and H₂SO₄ are released by the EZ PEMs (see Section 3.4.1 for additional detail) during normal electrolysis operation (Refs. 12 to 15 and 75). Dissolution of inorganic and organic compounds from FC, EZ, metal tubing, fittings, valves, etc., has been observed in previous closed-loop RFC systems (Ref. 76). Solid particulates in H₂O may accumulate from internal actuator parts (valve seats, pump impellers, etc.) or electrolysis cells shedding catalyst material or fluoropolymer particulates releasing from membranes or sealing elastomer, etc. Consequently, OGA recirculation loop H₂O samples are periodically returned to the ground for chemical, particulate, and microbial analysis (Refs. 12 to 15 and 75 to 78). For H₂O samples collected in 2018, analytical results revealed an average pH of 5.5 and average conductivity of 1.9 μS/cm. The TOC was between 9,000 and 21,000 μg/L. Microbial enumerations, given in colony forming units per milliliter (CFU/mL), ranged from 6.15×10³ to 3.45×10⁵ (Ref. 14). All values are outside of what would likely be acceptable for RFC.

In the evaluation of a 100-W PEM RFC in 2015, the pH of FC product H₂O was between 4.0 to 4.8 with conductivity between 11 to 43 μS/cm during five cycles (Ref. 79). The product H₂O was treated with a DI bed prior to feeding to the EZ stack. After DI treatment, the pH was between 5.5 to 5.7 with conductivity between 1.2 to 1.5 μS/cm. These values are more acidic and conductive than desired for long-term RFC operation.

TABLE III.—SPECIFICATIONS FOR HIGH-PURITY H₂O

Parameter	Standard				
	Pharmaceutical	Semiconductor	NASA International Space Station (ISS)	Roscosmos ISS	Regenerative fuel cell
Conductivity (μS/cm) at 25 °C	<1.3	0.055	<1	<150	<0.3
pH at 25 °C	-----	7.0	6.0 to 8.5	5.0 to 9.0	7
Total organic carbon (TOC in μg/l)	<500	<10	<3,000	<20,000	No spec
Bacteria (CFU/ml) ^a	<100	<0.01	<50	<10,000	No spec

^aColony forming unit (CFU).

A future design upgrade of the ISS OGA may include periodically purging and flushing the recirculation loop H₂O to limit contamination (Ref. 15). While RFC requirements are different from the OGA (particularly regarding operational pressures), H₂O treatment is still likely to include DI to remove ionic impurities, activated carbon absorption of nonionic organic chemicals and other soluble impurities, filtration to screen out solid particulates, and microbe control.

2.3.2 H₂O Deionization

DI technologies through ion exchange (IX) remove unwanted ions dissolved in H₂O. The most common means of IX are an IX resin or an electro-DI device. In order to reduce parasitic loads for the RFC project, IX resins are of interest as a passive means to remove inorganic and organic ionic impurities from H₂O.

Industrial H₂O treatment resins are classified into four basic categories: strong acid cation (SAC), weak acid cation (WAC), strong base anion (SBA), and weak base anion (WBA). SAC resins neutralize strong bases and convert neutral salts into corresponding acids. SBA resins neutralize strong acids and convert neutral salts into corresponding bases (Ref. 80). SAC and SBA are utilized in most softening and full demineralization applications. WAC and WBA resins neutralize strong bases and acids, and these resins are for dealkalization and partial demineralization. Due to the need for full demineralization, this work will focus on the SAC and SBA resins for producing DI H₂O.

SAC resins have a negative functional group that attracts positively charged ions. In demineralization applications, SAC resins remove raw cations in H₂O, replacing them with H⁺. SBA resins have a positive functional group that attracts negatively charged ions. In demineralization applications, SBA resins remove raw anions in H₂O, replacing them with OH⁻. The H⁺ released from the SAC, and the OH⁻ released from the SBA combine, forming pure H₂O.

Most resin manufacturers recommend that SBA IX should not be operated in the OH⁻ form above 60 °C (Refs. 81 and 82). This 60 °C recommendation is not a step function that defines a fine line between success and failure of the resin bead, but SBA resins are more affected by elevated temperature than SAC types. The decline of exchange capacity of SBA IX with temperature has been observed. Moreover, strong base resins suffer irreversible chemical damage and lose most of the capacity when the temperature goes much beyond 60 °C. Under pure thermal degradation, the loss of the exchange site is the predominant and most serious degradation mechanism. Although this was discovered in 2006, the copolymer and functional groups of most IX resin remain the same. The suggested operating temperature range of many resins is 5 to 60 °C (Ref. 82).

Combining SAC and SBA resins together is very common for DI applications and is known as a mixed-bed resin. Several companies have developed high-temperature mixed-bed resins for DI applications. These are specifically designed for sustained high-temperature operation up to 80 to 93 °C (Refs. 83 and 84). These high-temperature resins will be investigated for use in the RFC project, which has a nominal operating temperature of 65 °C, with operation up to 85 °C possible.

A preliminary DI H₂O test stand was developed, as illustrated in Figure 7. The test stand is connected to an incoming H₂O source, which may be real or simulated FC product H₂O for corrosion testing (see the description in Section 3.4.1). The conductivity of that H₂O is measured before and after it passes through the DI filter. A flow meter measures the volume of H₂O that passes through the filter. This data is used to calculate the total dissolved solids that were removed by the filter during operation. Future iterations of the test stand will be able to vary the temperature of the incoming H₂O to examine the performance of the DI filters at various temperatures, particularly elevated temperatures.

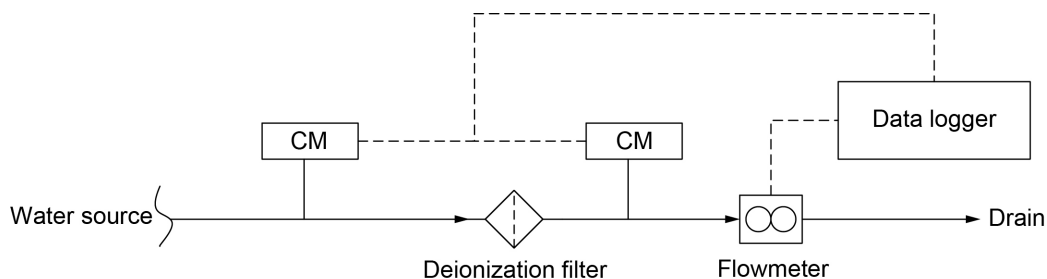


Figure 7.—Deionized H₂O test stand. Conductivity meter (CM).

The DI process eliminates ionic impurities from H₂O. A good DI bed should reduce the conductivity of H₂O and keep the pH value close to 7. High H₂O conductivity can increase shunt currents and induce electrochemical corrosion of metallic components in both the PEM stacks and BOP hardware. Low pH also makes H₂O corrosive to metals. In 2010, H₂O with a pH of 4.19 and conductivity of 34.5 μS/cm was observed in the recirculation loop of the OGA (Ref. 75). The corrosive nature of that H₂O resulted in significant levels of metals in solution both as ionic species and as particulate. High concentration of metal ions triggered increases in membrane resistivity and the premature failure of EZ cells. Besides, transitional metal ions, such as iron contaminants, are responsible for accelerated membrane degradation that reduces service life of PEM stacks.

It has been concluded that the mixed-bed resin is necessary in the OGA to remove HF from H₂O in the recirculation loop and keep it close to neutral (Refs. 12 to 15 and 75 to 78). In RFC, cell membranes of both the FC and EZ are expected to release HF during normal electrochemical operations. When the cells are operating at high temperature, the rate of HF release increases. High temperature also reduces the capacity of IX resin bed, so evaluation of the elevated temperature performance of DI filters is very relevant to RFC.

2.3.3 Absorption of Nonionic Organic Chemicals

The detrimental effect of ionic impurities is well established. While both inorganic and organic ionic impurities can be removed by a DI bed, the IX resin of the DI bed may not be effective in absorbing nonionic organic impurities. Dimethylsilanediol (DMSD, molecular formula C₂H₈O₂Si) and dimethyl sulfone (DMSO₂, molecular formula (CH₃)₂SO₂) are two organic impurities identified in the recirculation loop of the OGA. It has been found that IX resin absorbs DMSD and then releases it again as other ions are taken up by IX resin, and the resin shows poor absorption toward DMSO₂ (Ref. 77). DMSD and DMSO₂ in the OGA recirculation loop have traced their sources to feedwater in portable H₂O bus in ISS. While these specific contaminants are not likely present in RFC, other less chemically active contaminants may be found and, in general, IX resins exhibit poor absorption for nonpolar or weakly polar organic chemicals. On the other side, activated carbon demonstrates excellent capacity and strong binding of nonionic organic impurities.

TOCs potentially impair EZ MEAs as the organic chemicals are likely to participate in electrochemical reactions and may poison catalyst active sites of electrodes (Refs. 12, 75, and 77). Film buildup due to high TOC concentration can take place on PEM, and it effectively reduces protonic conductivity of PEM. Also, the TOC can promote bacteria growth. Besides DMSD and DMSO₂, other organic impurities associated with large molecules (possibly releasing from IX resin, membrane, or sealing elastomer) have been observed but are difficult to characterize (Refs. 77, 85, and 86). While TOC (including both ionic and nonionic) can be readily measured by a TOC analyzer, it is far from trivial to identify individual organic impurities. To identify and characterize the organic chemicals in RFC will be an important step for effectively removing them from RFC to prevent component damage (Refs. 77, 85, and 86). For example,

various chemical and biological contaminants and byproducts were found to have fouled a magnetically coupled pump in an ISS spacesuit (Ref. 85). Several activated carbons have been evaluated for absorption of TOC in ISS H₂O for an extravehicular mobility unit (Refs. 85 and 86). Beds of mixed IX resin and activated carbon with 50:50 or 70:30 volume ratio can remove ionic impurities and TOC altogether and any solid particulate in RFC H₂O can be removed by a screen filter, like the 200- μ m-size filter in the ISS OGA (Refs. 12 to 15 and 75 to 78).

2.3.4 Bacterial Growth Control

Mitigation of bacteria growth in H₂O is especially important for aerospace missions when the H₂O is supplied for crew consumption in food and drink packages. The need for further development of human-safe and long-term effective biocides has been noted (Ref. 87). Any risk of bacteria influencing crew health or electrochemical stack performance should be avoided. Sulfonated tetrafluoroethylene-based fluoropolymer-copolymer PEMs, the membrane for both the RFC FC and EZ, inhibits growth of some types of bacteria through acidity and preventing transmission. While that material selection aids bacterial growth suppression, additional control methods may be necessary. The acceptable sterilization methods include heat, chemical, filtration, and radiation. For heat to kill all microbes in water, H₂O is heated to 130 °C for 10 min (Ref. 88). This takes a lot of energy. The chemical antimicrobials for H₂O systems in manned spaceflight include Cl₂, I₂, silver ion (Ag⁺), and ortho-phthalaldehyde (molecular formula C₆H₄(CHO)₂) (Ref. 88). All these chemicals are reactive in EZs; therefore, the chemical disinfectants cannot be used in the H₂O system of RFC without removal before H₂O entry to the EZ stack. Additionally, Ag⁺ increases H₂O conductivity, hence the less restrictive Roscosmos ISS Elektron-VM standard for the alkaline electrolyte compared to the PEM-based NASA ISS OGA standard, and Ag⁺ can bridge electrochemical cell internal gaps, causing electrical shorting (Ref. 88). To suppress bacteria activity, continuously maintaining some concentration of Ag⁺ in H₂O is required. However, Ag⁺ tends to react with stainless steel (SS) (bulk of RFC BOP) and is difficult to maintain at the desired concentration. This is another reason that a Ag⁺ biocide does not work for RFC.

Filtration is a simple disinfection technique. When H₂O passes through a 0.2- μ m-size filter (usually disposable or single use), microorganisms, such as bacteria, are blocked and cannot travel along with H₂O. Therefore, the downstream H₂O is free of microorganisms, but the method does not kill bacteria. Undesirable bacteria growth and biofilm formation may continue upstream of the filter and the continued presence of solid particulates and biofilm growth would require frequent replacement of the submicron filter. Since RFC maintenance is to be minimized, filtration alone does not appear to be a satisfactory option.

Nevertheless, bacteria growth in RFC H₂O system should be controlled. *Ralstonia pickettii* is a bacterium found in ISS OGA H₂O recirculation loop. It can survive and thrive in low-nutrient conditions. In ultrapure H₂O systems, *Ralstonia pickettii* may be able to scavenge energy from the polymers in plastic piping (Ref. 14). The microbial infallibility hypothesis predicts that if there is energy to be gained from a compound, a microorganism will figure out how to extract it and create a niche for itself. Some microbes even find a way to use tough compounds like per- and polyfluoroalkyl substances (PFAS) (Ref. 89) by utilizing peroxide radicals to attack C-F bonds in PFAS, just like the mechanism of releasing HF by FC and EZ cell membrane during normal RFC operation. The PEM is a PFAS, and the potential degradation of PEM by bacteria can accelerate the failure of cells in both the FC and EZ. Microbiologically influenced corrosion (Ref. 88) is also a concern for cell stacks and BOP components.

Ultraviolet (UV) radiation, especially short-wavelength UV-C radiation, is a viable option for a RFC bacteria control strategy. UV has been used for over 100 years for disinfecting drinking H₂O and wastewater treatment, has a quick startup time, is made to be continuously submerged in H₂O, works against many organisms resistant to other treatments, involves no chemicals, generally operates independently of H₂O

temperature and pH, and can be easily integrated into a flowthrough tube design (Ref. 90). UV-C radiation functions by damaging bacteria DNA. This requires some minimum UV radiation dosage, a function of time (tenths of a second to several seconds) and intensity (Ref. 90). The UV light should be able to reach the DNA (i.e., line of sight) to be effective. Suspended particles can serve as umbrellas for bacteria to evade UV radiation, and therefore, nullify the UV disinfection. Some germicidal UV disinfection systems require the total suspended solids in H₂O to be <10 mg/L (Ref. 91). Another investigation sets similar limits (Ref. 92). Due to the line-of-sight limitation, bacteria residing on the walls of tubing, valves, and DI beds can escape from UV radiation. It has been suggested that UV disinfection would likely require constant flowthrough of potable H₂O systems to limit bacterial counts (Ref. 71). TOC in H₂O is nutrition for bacteria, providing carbon that is indispensable for bacteria growth and metabolism. If the TOC is kept low, hopefully, bacteria growth can be minimized through use of UV-C radiation.

In 2006, the U.S. Environmental Protection Agency (EPA) issued UV disinfection guidance for H₂O treatment (Ref. 90). Commercial UV lamps have been recently developed for low-pressure applications (Ref. 93). These may meet RFC H₂O disinfection needs, however, the commercially available systems powered by 100 to 240 Vac power are not compatible with RFC DC power and may not be available for high-pressure operation (Refs. 90 and 91). A NASA project attempted to develop a high-pressure UV lamp as part of a RFC system in 2004 (Ref. 76). Unfortunately, the transparent quartz tube used in that demonstration failed repeatedly as it was very delicate, prone to surface imperfections, and sensitive to system vibrations during any pressure changes. The incandescent bulbs available at the time exhibited poor life and frequently created debris during failures. Additional challenges include the potential for required maintenance (such as bulb replacement before 12,000 h, which is less than some mission concepts), and the need for a high-quality power supply, which should be possible with appropriate RFC PMAD design. Light-emitting diode lamps could provide adequate life and reduce power consumption but would require some custom development in order to be integrated into the current RFC development project.

2.4 Solenoid Valves

Solenoid valves are one of the most numerous BOP components by type. Since these are powered devices and control fluid movement throughout the RFC system, the valve selections are critical for achieving RFC key performance parameters and safe and reliable operation. Pneumatically or hydraulic actuated valves do not meet the RFC system requirements for operating in a vacuum. In particular, these actuation mechanisms require additional process fluids, and the commercially available valves are not designed to operate in a vacuum environment. The following defines valve requirements, known operational issues, and planned risk reduction activities.

2.4.1 Solenoid Valve Requirements

By powering on or off electromagnetic coils, solenoid valves are used to control the flow of fluids in the RFC. The general requirements for solenoid valves include reasonable cost, material compatibility with H₂ and O₂ service, high reliability, minimal maintenance needs, low power consumption, safe operation in a hazardous environment, vacuum environment compatibility, low internal and overboard leakage rates, low mass, and relatively high temperature rating.

Due to the quantity of solenoid valves in the RFC system, there is a significant total steady-state parasitic power consumption. During RFC operation, solenoid valve state changes are infrequent, usually occurring during operational mode changes between charge and discharge cycles. As such, it may seem desirable to use a latching solenoid valve that is designed to allow the valve to stay either open or closed without continuous power, reducing parasitic power consumption. Through the usage of a permanent

magnet, the latching valve is bistable in either shifted state. This imposes additional electrical control strategies to safe-state a valve during off-nominal events removing actuator power.

In general, a latching solenoid valve requires an established and consistent set of operating conditions. Inlet and outlet pressures must be within a relatively narrow range compared to expected RFC conditions. Small deviations will likely cause the valve to not operate properly, and typical latching valves are not designed for high-pressure operations. Since the H₂ and O₂ storage tank pressures vary between 0.3 to 17 MPa during charge and discharge phases of operation, most latching valves are not likely to meet RFC requirements. Only one vendor was identified as producing latching valves meeting all requirements including high-pressure applications. Unfortunately, each valve costs ~\$50,000, which is ~25 times the cost of a comparable nonlatching valve. While such latching valves may be an option for a flight program, this RFC project demands alternatives due to the high cost.

Excluding latching valves, solenoid valves can be further classified as direct-acting and pilot-operated solenoid valves. Direct-acting solenoid valves have a direct connection with the opening and closing armature, whereas pilot-operated valves employ the use of the process fluid to assist in piloting the operation of the valve. The advantage of using the process fluid for operation is to reduce electrical power consumption. However, pilot-operated valves are more complicated, cost more, and require some minimum pressure differential between inlet and outlet (0.05 to 0.34 MPa) to open pilot-operated valves. Conversely, direct-acting valves can open without any pressure difference or even with a negative pressure difference.

There are multiple solenoid valves for each H₂, O₂, and H₂O flow line. Based on preliminary research, at least eight different manufacturers supply potential options to fit various parts of the RFC system. High-pressure valves are summarized in Table IV and named A to I. Table V lists potential valves, identified as J to O, for lower pressure sections of the RFC system. Previous experience with J and K models revealed shortcomings in reliability and corrosion resistance, as well as insufficient pressure ratings for some RFC use cases. Similarly, L valves are limited by the low-pressure rating (0.7 MPa for this proportional valve), however, low-pressure proportional valves can have a niche for the H₂ FC stack vent valve, opening a little for normal venting or wide for evacuation of the H₂ cavity during the FC stack startup and shutdown sequences.

TABLE IV.—SUMMARY OF SPECIFICATIONS RELATED TO IDENTIFIED HIGH-PRESSURE SOLENOID VALVES

Valve	Price, USD	Weight, lb	Body material ^a	Rated pressure, MPaG	Nominal power, W	Working temperature, °C	Type
A	174	1.5	SS	20.68	9.5	-18 to 65	Direct acting
B	1,920	0.23	15-5 SS	20.68	9.8	-54 to 141	Pilot operated
C	1,950	2.0	303 SS	20.68	9.5	-54 to 74	Direct acting
D	627	1.72	SS	25	16	-40 to 80	Direct acting
E	1,131	4.57	SS	25	10	-40 to 80	Pilot operated
F	694	2.90	316 SS	43.44	22	Cryo to 204	Direct acting
G	835	2.85	316 SS	24.13	10	-18 to 204	Pilot operated
H	50,000	0.22	304L SS	17.24	8	0 to 80	Latching
I	50,000	0.39	SS	31	12.6 (open) 1.6 (hold)	0 to 80	Direct acting

^aStainless steel (SS).

TABLE V.—SUMMARY OF SPECIFICATIONS RELATED TO IDENTIFIED LOW-PRESSURE SOLENOID VALVES

Make and model	Price, USD	Weight, lb	Body material ^a	Rated pressure, MPaG	Nominal power, W	Working temperature, °C	Type
J	38	0.12	316 SS	0.34	2	−40 to 100	Direct acting
K	88	0.07	316 SS	1.55	10	−40 to 100	Direct acting
L	84	0.15	304 SS	0.69	1.8	−40 to 93	Direct acting
M	5,000	1.2	Al alloy	>0.69	4	−54 to 60	Direct acting
N	10,000	0.5	SS	>0.69	4	−58 to 71	Direct acting
O	108	1.38	SS	0.69	9.5	−18 to 65	Direct acting

^aStainless steel (SS).

Initial testing shows the baseline valves are from vendor A. These valves draw lower than rated power and have not failed during initial vacuum compatibility testing even without a specific rating for that environment. High-pressure valves from vendors D, E, F, and G are rated for vacuum applications. The acceptable media for vendor A valves are listed as air, noncorrosive gases (including O₂ for select applications), H₂O, and oil. Not all valves are specifically rated for O₂ compatibility. Vendors F and G valves are marketed for H₂ service, O₂ service, and FC applications. Valves from vendors D and E are already used for terrestrial FC applications. Some valves from the listed suppliers potentially fit in every position in the RFC system.

2.4.2 Solenoid Valve Failure Mechanisms

Many potential valve failure mechanisms exist including compromised material initial strength, obstructed fluid flow, component misalignment, coil burnout related to voltage and frequency perturbations, variable spring force, frequency of operation, fluid temperature, and aging of insulation (Ref. 94). These solenoid valve failures can occur suddenly or gradually due to wear.

The primary factors related to solenoid valve failure are the maximum temperature reached during testing, the number of actuation cycles, the change in resistance compared to initial state, and the peak current observed prior to failure (Ref. 95). Higher values in all cases led to more likely failure. Temperature impacts coil resistance over time, but number of cycles, even in the millions, may not lead to failure (Ref. 95). Higher temperature leads to higher peak currents and reduces cycle life (Ref. 95). Life approximately doubles with every 10 °C decrease in operating temperature (Ref. 96).

Direct-acting poppet-style valves are more reliable than spool styles or pilot valves (Ref. 97). Spool valves require more maintenance, are not preferred for variable operating conditions, and could require lubrication incompatible with RFC fluids. Pilot styles can be impacted by internal moisture, contamination, and corrosion (Ref. 97). Valve design should prevent media from reaching valve coil to maintain highest reliability as moisture and other impurities can cause valves to stick in position. Lower nominal power valves are desired to reduce RFC parasitic power consumption, but there are also potential downsides. Smaller valve body orifices increase the chances of failure due to foreign particles entering the valve and 5- to 10- μ m filtration is recommended (Ref. 96).

Repeated valve failures have been noted in existing NASA FC test systems. One concern is internal corrosion and residue noted on valves that are supposed to be clean enough for H₂ or O₂ service. An example of a used H₂ vent valve is shown in Figure 8. This vent valve is downstream of the FC stack and is thus potentially exposed to humidified reactant in a reducing fluid media. Valves used in O₂ and product H₂O service appeared in a similarly degraded state. These miniature, low-power valves frequently operate erratically, potentially requiring replacement long before reaching the expected cycle life.



Figure 8.—Corrosion and residue on surface of 316 SS (stainless steel) solenoid valve used in H₂ vent service for fuel cell system.

While operating FC test systems, it was also noted that valve installation orientation may affect operation. In a system with the valves manifold mounted into FC endplates and the stack oriented vertically, three out of four valves mounted to the bottom endplate (with the valve body above the solenoid coil) failed to open following long-term storage. Of the four valves installed in the top endplate (with the valve body below the solenoid coil), only one of the four failed over the same period. Once removed from the manifold and stored openly in air, some valves regained functionality. This suggests that H₂O might be passing internal seals to reach and damage the coil. While potentially a different issue entirely, the corrosion is a persistent concern, even with materials selected for corrosion resistance and media compatibility.

“Stiction” may present an even greater problem. It is caused by corrosion, metal-metal adhesion, lack of lubrication, deposit buildup, foreign material contamination, adverse chemical reactions, or valve seal breakdown (Ref. 98). Valve sticking and the resultant failure to function is one of the primary valve failure modes (Ref. 98), and it may be responsible for component failures observed in existing NASA FC test systems. O-ring stiction increases over time, reaching a maximum after 1 week to 1 month without a state change (Refs. 98 to 100). For many valves, the maximum level of stiction is reached around 275 to 300 h (Ref. 99). This greatly increases the force required to actuate a valve.

Low-power valves are designed with less actuation force margin, making them more susceptible to stiction. Although a high spring force can offset this additional friction force (Ref. 97), in low-power applications, manufacturers reduce spring force to allow valve actuation with minimal power. This can result in force-to-friction ratios (FFR) as low as 6, which is below the accepted minimum FFR of 10 for safety (Ref. 97). When encountering stuck solenoids in FC systems, tapping on the valve body occasionally frees up the movement, a remedy that is impractical for automated or remote operations. Rather than drying out the coils of the previously discussed failed FC valves, it is possible that stiction was the true problem and physical manipulation of the valves reduced stiction.

If a low-power valve must be used to achieve desirable RFC efficiency levels, there may be a procedural mitigation to stiction. Operating a valve at least once per week, or once per shift, not only periodically demonstrates the intended function but reduces the built-up stiction, hopefully maintaining it to an acceptably low level (Ref. 99). Called stroke testing, the valve state command is changed, and operators try to observe flow or pressure changes that indicate actual state change (Refs. 94 and 99). Such a procedure can prevent failure rather than just detect it (Ref. 98). Testing once a week compared to once per 6 months

can reduce failure rate by 100 times (Ref. 98). This may be preferred over increased valve power or force because high power increases temperature and risk of coil burnout. If weekly testing frequently finds valves stuck, more frequent testing, or at least partial stroke testing, is recommended (Refs. 98 and 99). In long-term storage or steady-state operation of a RFC system, it may be necessary to introduce periodic valve actuation to ensure continued valve functionality. The valve actuation would not be simultaneous so as to avoid alteration of the desired fluid flow or isolation in either the FC or EZ mode.

2.4.3 Planned Testing and Preliminary Results

To address concerns related to RFC solenoid valves, there are several evaluations available to reduce operational risk. The plan is to test valves in vacuum, long-term operation, and spike-and-hold operation to evaluate if any leaders appear when it comes to reliability, low power consumption, and low operational temperature. There are other planned subsystem tests related to corrosion and orientation sensitivity.

When a solenoid valve is actuated, the ohmic resistance of the coil causes self-heating and raises the temperature of the solenoid valve. Most solenoid valves are designed to operate in terrestrial atmosphere where natural air convection alleviates the effect of self-heating. In contrast, the RFC is designed to operate in a simulated lunar environment that includes vacuum. Operating solenoid valves in vacuum eliminates the primary cooling mechanism, which results in increased self-heating. Preliminary solenoid valve testing under vacuum confirms the effect, as shown in Figure 9. Long-term overheating of the coil can cause coil burnout so all solenoid valves are designed to operate under some rated temperature to avoid coil burnout. The preliminary results demonstrate that manipulating operational voltage (i.e., below the rated voltage) can reduce parasitic loads and operational temperatures.

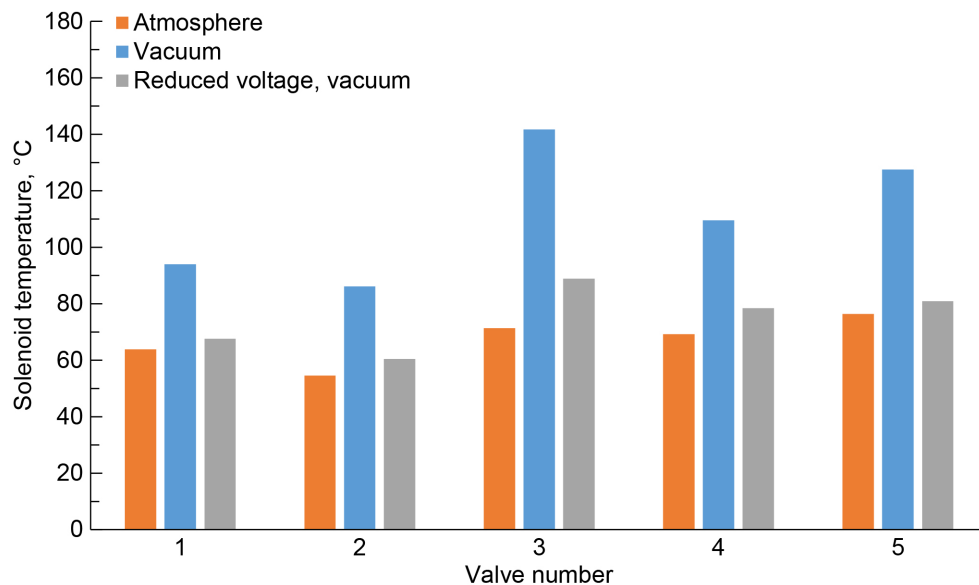


Figure 9.—Solenoid valve external body temperatures at nominal rated voltage in atmospheric air compared to nominal rated voltage and reduced 2/3 nominal rated voltage in $<10^{-3}$ torr vacuum.

The component testing of the solenoid valve utilizes an adjustable DC power supply. In the RFC, the operation of the solenoid valve is controlled by the PMAD circuit boards with a valve driver that uses pulse width modulation (PWM) power to improve energy efficiency. PWM is the reduction of the effective voltage at the valve by setting a duty cycle percentage and cycle time to decrease the equivalent average voltage but still hold the valve in the actuated state. The PWM power contains an alternating current (AC) power component, which may generate some small amount of counteracting heating. The performance of solenoid valves with PWM control is an important part of prototype testing to reduce the overall parasitic power required by these components.

Solenoid valves will be evaluated by steady-state life testing. Throughout testing, valve operation will be checked periodically by dropping voltage to zero and audibly verifying operation. New valves make a distinct sound when actuating, but the sound level may become quieter as valves wear in (Ref. 95). A significant increase in valve temperature and reduction in electrical resistance is anticipated when the solenoid valves fail from wires in the coils shorting (Ref. 95). In a past study, valves kept under 185 °C, just under the coil insulation breakdown temperature, tended to last much longer (Ref. 95).

Some valve vendors recommend reducing valve voltage post actuation to reduce self-heating and power consumption (Ref. 101). Spike and hold tests are designed to mimic PWM operation and evaluate the reduction in parasitic power usage by operating the valves below rated voltages. The primary purpose of the test is to determine the minimum voltage required to maintain solenoid valves in the actuated state. The secondary benefit of running the valves at low power is to minimize the heating effects, therefore, reducing operating temperature. It may enhance the service life of valves and improve the reliability of the RFC system, especially during vacuum environment evaluation.

For example, with a direct-acting valve I, there are rated voltages for actuation and holding open in steady-state conditions. The nominal power consumption for opening is 12.6 W at 28±6 V. The power usage for holding (at 10±2 V) decreases to 1.6 W. However, other valve manufacturers do not provide data for reduced hold voltages. The spike and hold testing will directly measure the power usage for maintaining the valve open over a range of RFC conditions, providing data for hold open voltages for each valve model that will be used for RFC PMAD design. Negative reliability effects of reduced voltages are not expected.

2.5 High-Pressure H₂O Pumps

High-pressure H₂O pumps are critical devices for supplying the EZ stack at the pressure level required for satisfactory reactant gas storage. The following sections detail the challenging requirements for this component and the identified best-fit COTS candidates.

2.5.1 Pump Requirements

The fundamental requirements for a high-pressure EZ feed pump for the 100-W RFC system include

- Operation in vacuum environment, pressure at 10⁻⁵ torr or lower
- Ambient temperature between 4 and 85 °C
- Motor operation on 24- to 28-Vdc power bus
- DI H₂O pumped fluid with a resistivity from 16.5 to 18 MΩ-cm as measured at 25 °C and process fluid temperatures between 4 and 70 °C
- Duty cycle of 15 days powered on and 15 days powered off for at least a total of 12 cycles
- High reliability with lifetime exceeding 5,000 h
- Minimal routine maintenance, even after long periods of nonuse

- Low mass, less than 5 kg
- High efficiency to minimize input power required
- Variable flow rate from 1 to 1,000 mL/min
- Capability of generating outlet pressures of at least 17 MPa
- Metallic gasket face seal fittings, such as vacuum coupling radiation (VCR) type, for the pump assembly fluidic interface
- No contamination of the DI H₂O by the pump assembly

2.5.2 Identified Vendors

No pump meets all of the desired specifications, and there are several requirements met by no commercial pumps. These include vacuum environment operation, ambient temperature up to 85 °C, continuous duty cycle performance for at least 5,000 h, variable flow rate over the full desired range, low mass, and factory option for metallic gasket face seal fittings, hence, the low confidence in the availability of this component for integration into the RFC system.

Few pumps are available with DC motors (let alone CI/DivII/GB compliant ones) as standard equipment, and few vendors are willing to help identify suitable motors for available pump heads. Often, seemingly suitable high-pressure pumps are designed for hydraulic fluid only and will wear exceptionally quickly if used to pump pure H₂O. Many available options are much too heavy for this 100-W-class application and would be more suitable for 1-kW-class RFC or larger, if the mass did not scale up with rated flow rate. Additionally, an oversized pump, designed to flow more H₂O than is needed, will negatively affect overall efficiency by requiring more input power than is necessary to move the smaller fluid flow needed by the EZ. Nine pump manufacturers have been identified that sell pumps similar to the specifications detailed previously. The following list summarizes interactions with contacted vendors about their potentially applicable products:

1. Pump 1: While inexpensive, these pumps are high mass and are designed to flow more H₂O than is needed. The maximum generated pressure is lower than desired.
2. Pump 2: These are relatively inexpensive and designed for continuous operation pumping high-purity H₂O. Flow rate is adjustable, and they use DC motors, but the flow rate scale might be too low for the final RFC design.
3. Pump 3: This company offers many pumps for high-pressure H₂O applications but all of them are for higher flow rates than needed here. The higher pressure offerings produce minimum flow rates much too high for RFC consideration. Mass is also a negative, but reliability would likely be better than most all other options.
4. Pump 4: This metering pump requires a modified motor and gear set from standard. Maximum flow rate might be too low for RFC application, but it is a readily available option.
5. Pump 5: Significant mass penalty with this brand but this is a unique design that is able to operate at relatively low revolutions. It must be paired with a high-torque motor that adds to the total mass.
6. Pump 6: This is a solid-state drive pump that is very unproven. It appears to fit many of the desired specifications, but it cannot be operated with a continuous duty cycle. The recommended operation is 30 s on, followed by a 5-min cooldown period in an ambient air environment and in a vacuum environment this cooldown period will almost certainly increase.
7. Pump 7: This pump has high mass and cannot meet the high ambient temperature requirement of 85 °C. It is one of the more expensive pumps identified and has a 3-month lead time. It is an established commercial product with a wide range of motor and pump head options.

8. Pump 8: A compact gear pump that has two primary limitations: reliability and differential pressure. In a pure H₂O system, gear pump heads are likely to wear out in less than 1,000 h, which is only adequate for three to four lunar cycles. This design is also only able to generate a differential pressure of 0.52 MPa, so it is not capable of generating EZ operating pressure in one pass.
9. Pump 9: Though this company offers a wide variety of high-pressure hydraulic and aerospace pumps, none are designed for pure H₂O, and they would not operate very long without any lubrication from the fluid media.

This list is not to identify all considered or contacted vendors but those that appear to meet a significant number of the RFC requirements. Many well-known pump manufacturers offer nothing remotely compatible. Six different pump models have been purchased for further evaluation, though one vendor was unable to actually produce the advertised product. Utilization of these pumps may require multiple pumps in series or parallel to meet the RFC flow and pressure requirements. Some of these potential configurations are described in other review-supporting documentation and will be evaluated in planned subsystem tests. Further pump specifications are provided in Table VI.

The procured pumps will be installed in a laboratory test system to evaluate performance, power consumption, and reliability. From there, the most promising candidate will be installed into the final RFC system builds.

2.6 Storage Vessel and Heating

For RFC systems at almost any scale, the majority of total system mass and volume is from the high-pressure reactant storage vessels and the stored reactant. This makes the vessels among the most impactful components on critical RFC system metrics. To produce a safe energy storage system with a reasonable mass and volume and high specific energy, the reactant storage must be well defined and optimized. The following sections detail the critical requirements for the vessels, the applicable vessel configurations, and market research results.

TABLE VI.—SUMMARY OF DETAILS RELATED TO IDENTIFIED PUMP OPTIONS

Pump	Cost, USD	Mass, kg	Flow, ml/min	Pressure, MPa	H ₂ O rated	Purchased
1	2,000	16	1,900	8.3	Yes	No
2	3,100	4	10	13.8	Yes	Yes
3	10,000	15	2,000	10.0	Yes	No
4	11,200	14	160	34.5	Yes	Yes
5	7,000	30	700	17	Yes	Yes
6	31,500	4	1,000	18.6	Yes	Yes ^a
7	17,300	74	683	17	Yes	Yes
8	5,300	2	500	34.5	Yes	Yes
9	-----	2+	100+	6.9+	No	No

^aVendor unable to deliver pump

The procured pumps will be installed in a laboratory test system to evaluate performance, power consumption, and reliability. From there, the most promising candidate will be installed into the final RFC system builds.

2.7 Storage Vessel and Heating

For RFC systems at almost any scale, the majority of total system mass and volume is from the high-pressure reactant storage vessels and the stored reactant. This makes the vessels among the most impactful components on critical RFC system metrics. To produce a safe energy storage system with a reasonable mass and volume and high specific energy, the reactant storage must be well defined and optimized. The following sections detail the critical requirements for the vessels, the applicable vessel configurations, and market research results.

2.7.1 Storage Vessel Requirements

The RFC supplies electric power during the lunar night, lasting about 2 weeks, depending on the location. The electric power comes from conversion of chemical energy, which is stored as H₂ and O₂. The amount of H₂ and O₂ in the RFC system determines the amount of energy it can supply. Therefore, the system must hold enough H₂ and O₂ to meet project or mission requirements for at least the 2-week period. While cryogenic storage of liquid H₂ and O₂ has been previously used in primary FC systems for a NASA aerospace mission, it takes too much energy (~13 kWh/kg H₂ for small plant (Ref. 102)) for a RFC and requires a complicated cooling and compressing system to liquefy H₂. The only established storage technology for both H₂ and O₂ is compressed gas storage. As the amount of gas that can be stored in a vessel is approximately proportional to the pressure, high-pressure storage is usually preferred. Excluding PV system mass, RFC system mass and volume are likely to be mostly composed of H₂ and O₂ storage (Ref. 103).

RFC storage tank pressure is rated to match the output pressure of the EZ. A flight RFC system and tank will be operated on the lunar surface and exposed to environmental conditions such as vacuum, extreme temperature (-177 to ~118 °C), and reduced gravity. It is ideal to select tanks that are the most similar to those that will be used in actual future lunar missions. While the tanks do not need to be flight rated for demonstration, whatever is used should approximate the thermal response of such a tank while containing the reactant gases. Two technical facets of the research and development include

1. Thermal performance: A key technical parameter is to understand the thermal dynamics of the RFC system, particularly in relation to H₂O management for a flight configuration.
2. Physical size: The majority of the available TVACs suitable for RFC testing lack the volume to contain the experiment, and any required structural modifications necessary to support the tanks would be unfeasible.

The primary requirements for the RFC high-pressure storage tanks are shown in Table VII.

TABLE VII.—STORAGE VESSEL PRIMARY REQUIREMENTS

Category	Property	Requirement	Justification
Ambient environment	Pressure	The reactant tanks shall operate in ambient pressures from vacuum ($<10^{-5}$ torr) to atmospheric pressure.	The system will be tested in a thermal vacuum chamber to simulate the lunar conditions.
Pressure	Maximum expected operating pressure range	The reactant tanks shall contain reactants within the pressure range of 0.10 to 17.24 MPa.	The reactant tanks are required to store the pressurized gas produced by the electrolyzer (EZ) stack. The EZ stack is being designed to operate within the pressure range of 0.10 to 17.24 MPa.
Temperature	Nominal environmental temperature range	The nominal environmental temperature of the reactant tanks shall be from -177 to 118 °C.	In order to simulate the wide temperature range at the lunar surface, heaters may be installed with the vessels to increase the minimum operating temperature to some point above -177 °C.
Life	Cycles	The tanks shall be designed for a minimum of 50 cycles.	The tanks will be subjected to a number of thermal-pressure cycles to simulate the lunar day and night operations.
Materials compatibility	-----	It shall be capable of withstanding “wet” H_2 and O_2 .	If the tanks were to corrode due to the presence of H_2O , this could compromise the vessels, and thus, safety of the mission (Ref. 104).
Fluidic interfaces	-----	The reactant tank fluidic connections shall have metallic gasket face seal fittings such as vacuum coupling radiation.	Zero or low leakage is preferred to conserve reactants and increase system safety.
External heating	Power	The reactant tanks should have the capability to integrate with external heaters.	The reactant tanks are outside the regenerative fuel cell main system thermal enclosure boundary. Depending on the effectiveness of the gas drying design, external heating may be required to prevent liquid H_2O from freezing inside the vessels.
Design standard	-----	The applicable standards are ISO 11119-2/3 or AIAA S-081B. ^a	This is per industry and NASA standards.
Availability	-----	The product is readily available, or an existing design is established.	This is in order to reduce the risk of project schedule slip and reduce custom design costs.
Reactant tank mass	Mass	It should have the lowest weight with the highest value.	All components are desired to be low mass in order to simulate flight-like conditions, and the lower the component mass, the higher the packaged system specific energy.
Leakage	Gas leakage rate	It should be the minimal overboard leakage.	Low leak rates are desired to conserve reactants and extend the useable lifetime of the system.

^aInternational Organization for Standardization (ISO). American Institute of Aeronautics and Astronautics (AIAA).

2.7.2 Pressure Vessel Design Standard

Permanent ground-based pressure vessel systems are required to be American Society of Mechanical Engineers (ASME) code stamped per NASA Policy Directive and NASA Technical Standards (STD). If the system is a portable skid, cylinders certified by the Department of Transportation (DOT) are permitted. There are provisions for using DOT cylinders in permanent ground-based systems in NASA STD 8719.17, but this involves derating the DOT cylinders in order to have equivalent maximum allowable working pressures to ASME code. Composite overwrap pressure vessel (COPV) vendors do not supply ASME code stamped vessels because the code does not apply to how those types of vessels are designed and constructed. Off-the-shelf COPVs are DOT rated for primary use cases such as H₂ storage tanks in the automobile industry or as O₂ storage tanks for first responders or commercial aircraft emergency oxygen systems. When custom COPVs are fabricated for aerospace applications, vendors typically do not provide any certification and standards due to the low production quantity. Instead, vendors ensure tanks will perform to the design specifications through a rigorous design process and validation and verification of system-level requirements. The primary reason for this is that not all tanks will operate in the same fashion or at the same pressures, and all tests may not be necessary. If a specific standard is desired for the design (e.g., ASME, American National Standards Institute Natural Gas Vehicle 2, International Organization for Standardization (ISO), DOT, etc.), vendors will work to that standard for qualifying the tanks without formally obtaining the certification, as it is typically a costly process that most end users deem unnecessary for low-level production.

When vessels are required to be flight qualified, and/or are test article specific, the vessels are designed to AIAA S-080 or S-081. It is understood that DOT cylinders could be accommodated by AIAA standards with some provisions as flight vessels. This direction is a result of NASA STD 8719.17, NASA Requirements for Ground-Based Pressure Vessels and Pressurized Systems (PVS) (Ref. 105). The document generally states that PVS should be designed to ASME standards; however, Section 4.2.4 gives an assessed hazard exclusion to that requirement. The Pressure Safety Manager (PSM) has the authority to exclude other PVS including Test Article and Test Specific PVS from the Center's certification program if the following conditions are met (Ref. 105):

- A risk and hazard assessment is performed, and any risk to personnel is accepted.
- Acceptance of all mission risks and facility damage potential.
- All applicable NASA and other regulatory safety requirements are met.
- Any exclusion taken is documented.

2.7.3 Storage Vessel Types

High-pressure vessels are classified in five construction types (Ref. 106):

1. Type I: fully metallic tank
2. Type II: metallic tank hoop wrapped with composite shell
3. Type III: metallic liner fully overwrapped with composite shell
4. Type IV: polymer-lined composite vessel
5. Type V: linerless composite pressure vessel

The following sections discuss specific considerations for each vessel type.

2.7.3.1 Types I and II Vessels

Type I vessels are constructed entirely out of metal and contain no composite material. Advantages of Type I vessels include being the simplest design and having well-defined codes and standards. This makes Type I vessels readily available and highly reliable. There are numerous vendors available who can construct these vessels to ASME code standards. Other advantages include being the least expensive as the metalworking skills and equipment needed to produce these vessels are widely available. There are no gas permeation concerns with the all-metal construction and thicker walls (Ref. 107).

The main disadvantage for Type I vessels for a RFC is that these are not a realistic flight vehicle component. Since the vessels are one of the largest components by mass and volume of a RFC, it would be ideal to be as light as possible. However, Type I vessels are the heaviest of all types (Ref. 107), with a density near $1,360 \text{ kg/m}^3$. The first proposal received for a Type I tank was from a metal fabricator able to provide tanks meeting our design requirements with the exception of weight. The H_2 vessel was 1,814 kg (to contain $\sim 6 \text{ kg H}_2$), and the O_2 was 1,089 kg (to contain $\sim 42 \text{ kg O}_2$). For comparison, the composite vessel proposals received were on the order of 91 to 227 kg per vessel (in some cases the smaller O_2 vessel weighed more than H_2 because the vendor quoted a metal-lined vessel for O_2 and an all composite for H_2).

Type II vessels are mostly steel with a glass-fiber composite overwrap in the hoop direction. For an equivalent pressure rating, the Type II design is able to reduce the metal wall thickness since the composite overwrap takes some of the load. The metal vessel and composite materials share about equal structural loads. This allows for a lighter vessel than a Type I, typically 30 to 40 percent less (Ref. 107). Similar to Type I vessels, Type II are readily available, are designed to ASME standards, and present no permeation concern.

The main disadvantages are that Type II vessels cost about 50 percent more to manufacture than Type I vessels and more design and analysis are needed to balance the structural loads taken by the two different materials. These types of vessels were not considered during the vendor search because of the same issues of not being a realistic flight vehicle component due to greater mass than the Type III, IV, or V vessels.

2.7.3.2 Types III, IV, and V Vessels

Type III and IV vessels take weight savings even further than the Type II, at 340 to 454 kg/m^3 densities. The cost of Type III and IV vessels, however, is roughly 2 times greater than Type II vessels and 3.5 times greater than the all-metal Type I tanks (Ref. 107). Type I and II vessels were deemed infeasible options early in the design phase; therefore, the following discussion shall only compare the composite Type III, IV, and V vessels.

Type III vessels have a metal liner, generally aluminum or SS, with full composite overwrap like a carbon fiber composite. The composite materials carry the structural loads (Ref. 107). When compared to Type V vessels, Type III are a more proven and frequently implemented technology, thus more vendors can build this type, even if the vessels are custom. Since Type III and Type IV are used in the automobile and aerospace industry, there are defined design standards including DOT and AIAA. Type III also have lower permeation rates than Type IV or V due to the metal liner.

A disadvantage of a Type III vessel includes being 2 to 2.5 times heavier than a Type V. There are known safety concerns associated with Type III vessels including liner failure caused by corrosion, debonding, or collapse. A common liner failure cause is accumulation of gas between the liner and composite overwrap in a void or buckle (Ref. 108). The magnitude of temperature variations can be problematic as there is a significant difference of coefficient of thermal expansion (CTE) between aluminum and carbon-fiber composite (aluminum CTE is $23.6 \times 10^{-6} (\text{°C})^{-1}$ between 20 to 100 °C, carbon composite transverse CTE varies from 5×10^{-6} to $10 \times 10^{-6} (\text{°C})^{-1}$ and longitudinal CTE from 1.6×10^{-6} to $2.1 \times 10^{-6} (\text{°C})^{-1}$ (Ref. 109)). Cyclic temperature swings can induce stress between the aluminum liner and

the carbon-fiber composite structural layer of the vessel. The low temperature during lunar night also makes heating the storage vessels necessary for FC operation.

Type IV vessels have an all-composite construction featuring a polymer (typically high-density polyethylene) liner with carbon fiber or hybrid carbon and glass fiber composite. The composite materials carry all of the structural loads (Ref. 107). Compared to Type III, Type IV vessels do eliminate corrosion concerns and are lighter overall due to the plastic liner instead of denser metal.

The disadvantages of a Type IV vessel compared to a Type III include higher permeation rates (~2 times) (Ref. 110). Excessive leakage limits the life of the RFC system and increases the mass of excess reactant required, so the reactant management and storage subsystems have a requirement to limit the overall external leakage rates. Type IV vessels exhibit the same liner failure issues due to debonding. Without heating, RFC reactant tanks could be exposed to a temperature as low as $-177\text{ }^{\circ}\text{C}$, and Type IV vessels become brittle and, thus, structurally compromised at low temperatures.

Type V vessels have an all-composite construction with no liner, where the composite material handles all of the stresses of the pressurized fluid as well as containment (Ref. 106). This allows Type V to be the lightest vessel of all types, to better handle cyclic loading with no liner delamination concern and to not have the corrosion concerns as metal liners.

Type V vessels are the newest of all the tank types and few vendors currently exist. There is a lack of design standards available for these vessels. While some aerospace companies have successfully developed Type V tanks, the majority are often small scale with low operating pressures, with most tanks being less than a foot in diameter and containing pressures of less than 7 MPa. Type V proposals for this project would most likely be fully custom new designs, potentially adding cost and lead time to test and qualify the units. Another disadvantage of having no liner means the H_2 molecules have an easier path to permeate through the vessel walls.

2.7.4 Identified Vendors and Feedback

A summary of the different pressure vessel advantages and disadvantages is shown in Table VIII.

In total, 20 manufacturers of storage vessels have been screened for the RFC project. Several could not provide a proposal or proposed solutions that did not meet all stated requirements. Most of the vessels are not rated for the full temperature range required, and the only one that barely meets the temperature range is a COPV Type V with a comparatively high price. One proposal received from a vendor met all of our most critical design requirements while also having a competitive price. The best choice to date seems to be a Type III COPV with an aluminum liner. With a wide range of available sizes and a pressure rating of 34 MPa, it appears optimum among the available vessels (Ref. 110).

2.8 Remote Pressure Control

RFC system performance is highly pressure sensitive and gases in these systems must be precisely pressure regulated to ensure successful performance and reliability. FCs frequently require small delivery pressure adjustments during operation. There are critical differential pressures to control for successful performance. The O_2 over H_2 differential pressure affects membrane integrity, long-term durability, and safety. The O_2 over product H_2O differential pressure directly impacts the effectiveness of passive H_2O removal from O_2 cavity. A high pressure differential results in O_2 gas bubbles in the product H_2O outlet, while a low or negative pressure differential causes flooding of the O_2 cavity. This flooding obstructs the reaction surface and dramatically reduces performance. For EZs, operating pressure is a critical factor in determining efficiency. Optimizing operational pressure over a RFC cycle can dramatically improve RTE.

TABLE VIII.—ADVANTAGES AND DISADVANTAGES OF AVAILABLE PRESSURE VESSEL TYPES

Type of vessel	Advantages ^a	Disadvantages
I	Readily available Designed to ASME standard Least expensive No permeation	Not a realistic flight option Heaviest of all vessels
II	Lighter than Type I Readily available Designed to ASME standard No permeation	Not a realistic flight option Heavier than Type III, IV, or V More expensive than Type I
III	More of a proven technology that is already used in industry (i.e., more available vendors) Design standards are more defined (DOT and AIAA) Lower cost Shorter lead times Lower permeation rate than Type IV	Heavier than Type V vessels (~2 to 2.5 times) Safety concerns Liner failure (liner and composite debonding or separating and liner collapse) Pressure cycling could be a cause Liner corrosion May be H ₂ O carryover entering the vessels
IV	More of a proven technology that is already used in industry (i.e., more available vendors) Design standards are more defined (DOT and AIAA) Lower cost Shorter lead times No liner corrosion Lighter than Type III	Heavier than Type V Higher permeation rate than Type III (~2 times) Safety concerns Becomes brittle and structurally compromised at low temperatures Liner failure (liner and composite debonding or separating and liner collapse) Pressure cycling could be a cause
V	Lightest vessel type More capable of handling pressure and temperature cycling (no liner delamination concern) No corrosion concerns	Higher permeation rate than Type III and IV Lack of design and certification standards Less proven technology Highest cost Longer lead times

^aAmerican Society of Mechanical Engineers (ASME). American Institute of Aeronautics and Astronautics (AIAA). Department of Transportation (DOT).

During testing in a TVAC or any other location where manual regulator adjustments are not possible, a remote pressure control device may be required. Existing commercially available products require too much input power, mass, cost, and remain incompatible with vacuum environments and violate electrical classification requirements as described in Section 1.2.1. A mass flow controller or an electronic regulator would be an option except for the high mass and power draw. For small-scale RFCs, the 10- to 30-W power consumption of these devices is too great. There are not any low-mass, low-power, inexpensive remote controlled pressure regulators. Even the most compact models double the mass compared to a single-stage regulator alone (Ref. 111). Commercial options tend to be at least 2.3 kg.

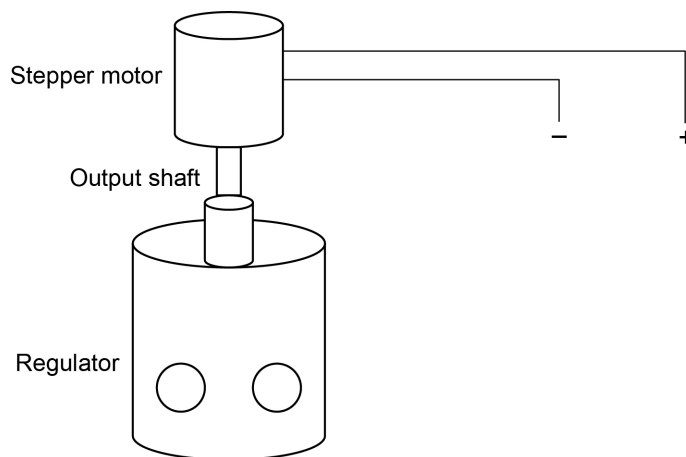


Figure 10.—Stepper motor connected to pressure regulator.

There is a need for a product that enables active adjustment of a pressure regulator in response to upstream and downstream pressure fluctuations, reduces mass and volume compared to commercially available products, is compatible with vacuum environment operation, is highly reliable, and is safe for use in hazardous locations. It would be a notable improvement to develop and demonstrate a remote, compact, lightweight, and inexpensive means of precisely regulating and controlling gas pressures in a dynamic system.

A vacuum-rated stepper motor attached to a manual regulator handle is a potential solution to the described pressure control issue. The plan is to compare connecting the motor and regulator by a belt and pulley system and a direct attachment of the motor shaft to the regulator handle. The basic concept is shown in Figure 10, where the motor output shaft is directly connected to the regulator adjuster.

There are several known challenges in developing a useful prototype. One is the successful physical connection of a stepper motor output shaft to the adjustment handle of a manual regulator. The connection must be strong enough to repeatedly translate motor movement to handle rotation. Any slippage would result in an inconsistent response. Another task is to develop and tune the electronic feedback loop for automating the pressure setpoint adjustment, maintaining differential pressure setpoints with operator input. The resulting product will be tested in a vacuum chamber and in a pressurized gas system to evaluate performance.

3.0 Safety and Reliability

For the lunar RFC, there are layered safety and reliability requirements for software, PMAD, and BOP components. As RFCs are expected to operate automatically, the temperature and pressure of the lunar surface, even a simulated one, pose additional challenges to the BOP components and subsystems. Important safety and reliability issues related to BOP are addressed in the subsequent sections.

3.1 Relief Devices

In RFC, H₂ and O₂ reactants are in gaseous states and stored at high pressure to reduce storage volume. The maximum operational pressure results from a complex and mission-specific trade between cost, pressure vessel volumes, acceptable reactant crossover rates in the EZ stack, and the total mass of the high-pressure components. Not all RFC subsystems are designed to contain the same maximum pressures. The H₂ and O₂ storage vessel pressures may be as high as 20 MPa, whereas nominal FC operating pressure is <0.5 MPa with a design sealing pressure of ~1 MPa. A pressure regulator is used to

control FC operating pressure, but failure of a regulator could overpressurize the FC stack. In the high-pressure sections, risk of overpressurization comes from large environmental temperature variations and potential component-level malfunctions such as uncontrolled heaters, pumps, or electrochemical stack reactions. Therefore, safety devices are needed to prevent overpressure conditions in both high- and low-pressure sections of both reactants for a RFC. For certain mission scenarios, it may be possible to justify a lack of overpressure relief devices, but that is not standard practice nor applicable to this RFC ground demonstration. It is probable that not all of the safety measures implemented by this ground demonstration will be utilized in a spaceflight mission given the substantial difference in requirements and constraints.

Burst disks (BDs) and pressure relief valves (PRVs) are the two main types of pressure safety devices used by this project. A BD, also known as a rupture disk, is designed to burst at a certain pressure and release gas from the system. These devices are simple mechanical components. Once the disk breaks, the openings do not close, and a failed rupture disk must be manually replaced. Besides simplicity, these are preferred in applications where a spring-loaded PRV is inappropriate due to the operating conditions, leak rates, or environment. For a RFC used on the lunar surface, replacing the disk is not feasible and a majority, if not all, of the gaseous contents will be lost in case the disk breaks, rendering the RFC useless. Both H₂ and O₂ are indispensable to RFC operation so loss of either reactant will immediately reduce RFC energy storage capacity. Therefore, BDs alone are potentially risky options for RFCs.

A PRV is a spring-loaded valve that opens when the pressure exceeds the pressure setting of the spring to discharge contents. Once the pressure decreases to the rated range, the valve will reclose. Therefore, it releases the excessive pressure without liquidating all system contents. PRVs are more complicated than BDs, and there are concerns that PRVs are prone to leak, especially for H₂ gas. The leak rates of BDs are lower, but H₂ is especially difficult to seal in all circumstances and will leak at some rate through any relief device. Additionally, the typical 2- to 3-year terrestrial RV recertification intervals are incompatible with long-duration space missions.

A further consideration is that pressure safety device failure in conjunction with H₂ service has been reported (Ref. 112). For steels and other alloys, exposure to H₂ has resulted in the reduction of mechanical strength, as a result of HEE. This can lead to drift in setpoint and ultimately mechanical failure. For BDs, HEE of the BD material has caused activation of BDs below the designated relief pressure (Refs. 112 to 114). PRVs are prone to internal leaks as well, especially for H₂ service. H₂ can get into the bonnet of a PRV and potentially reach the spring. Upon exposure to H₂, the strength of the spring reduces over time because of HEE. Even when selecting internal materials that are compatible with H₂, relief set pressure drift has been observed, whereas O₂ PRV operation is much more consistent. Unintentional set pressure changes could result in inadequate system protection (if the valve does not open at the desired pressure) or loss of reactant (if the valve opens or additionally leaks during normal operation). Despite many efforts to use materials resistant to HEE effects at expected RFC operating conditions, HEE can still cause serious issues in long-term operation.

In oil, chemical, and petrochemical plants (Ref. 115), BDs and PRVs are occasionally used in combination to minimize leaks and maintain the reclosing capability. A BD may be installed in series with a PRV, typically with the BD upstream of the PRV. This method is applicable to RFCs, but it adds complication and mass. Since pressure relief devices function based on differential pressure across a unit, if the first device in the series leaks over time, pressure will build up in between the two relief devices. This could prevent the device from opening and protecting the system from an overpressure event. Thus, an excess flow valve should be incorporated in parallel to vent the middle section during normal operation. This valve is designed to close automatically when significant flow is sensed. Utilizing three components in place of one reduces risk slightly, at the penalty of additional mass and complexity.

3.2 Flow Switch Interlock Overview and Requirements

Since RFCs are relatively complex systems, it is desirable to design in automated protection limits and shutdowns where possible to minimize reliance on software response. Flow switches installed in the coolant loop and the EZ recirculation loop will act as safety devices preventing localized overheating resulting from a loss of thermal fluid recirculation. If a flow switch detects that the flow rate drops below a setpoint, it will disconnect the heater supply power. The requirements are similar for the flow switches in the coolant loop and the EZ recirculation loop, with the main differences being flow rate, media, and operating pressure specifications.

An ideal flow switch for a RFC system would be tailored for low flow and high pressure. It would also have low mass, SS wetted components, minimal flow restriction, a wide operating temperature range, VCR fittings, and high reliability with a long lifetime that does not require service.

Compared to more unique RFC components, flow switch system integration is simpler. For a flight test, vibration and reliability testing should still be completed, but for the RFC demonstration, only minor verification testing is necessary. Therefore, no subsystem test plan is detailed in this section. The following sections will address the specific requirements of each loop.

3.2.1 Coolant Loop

Table IX lists the key requirements for the flow switch in the coolant loop and the specifications for two of the best commercially available options for the operating conditions, denoted as Options A and B (Refs. 116 and 117). The key requirements for the RFC are the ability to operate inside of a TVAC, the operating temperature range, maximum operating pressure, flow rate, hazardous location certification, compatibility with the fluid media, mass, and inlet and outlet port type and size, with size being secondary to type. In addition to these requirements, a long lifetime without the need for service is also required. The lifetime requirement is challenging for vendors to quantify, as it largely depends on how often the switch will cycle. Flow switches can operate in the field for multiple years without requiring service.

Except for inlet and outlet port type, both models meet the requirements, however, Option A is significantly lower in mass, which is important for future flight projects, therefore, it was selected for the coolant loop flow switch. The maximum pressure drop is estimated to be 6.9 kPa over the flow range. Additionally, the manufacturer recommends the use a 50- μ m filter upstream of the unit.

3.2.2 Electrolyzer Recirculation Loop

Table X lists the key requirements for the flow switch in the EZ recirculation loop and the specifications for two of the best commercially available options for the operating conditions, named here as Options C (Ref. 118) and D (Ref. 119). It is challenging to find flow switches that operate at low flow rates and high pressure. Many of the flow switches that are compatible with pressures above 17.2 MPa, have minimum flow rates of 1,900 cm³/min or higher and inlet and outlet ports of 1-in. National Pipe Thread Taper (NPT) or larger, adding unnecessary weight and the need for additional fitting adapters.

Except for the inlet and outlet port type, both models meet the requirements, however, Option C is significantly lower in mass, which is important for future flight projects. Therefore, it was selected for the EZ recirculation loop flow switch. It is Explosive Atmospheres (ATEX) zone 1 certified, which is similar to the CI/DivII/GB hazardous location rating. The estimated maximum pressure drop across the flow switch is 20 kPa.

TABLE IX.—SELECTION CRITERIA FOR COOLANT LOOP FLOW SWITCH

Selection criteria	Coolant loop requirement	Select flow switch model	
		Option A	Option B
Vacuum chamber operation	Yes	Yes	Yes
Operating temperature range, °C	4 to 85	–29 to 148	–268 to 148
Maximum operating pressure, MPa	0.345	6.89	4.14
Flow rate, cm ³ /min	567	379 to 3,785	Made to specifications
Certified for hazardous location	Yes	Yes: Class I Division 2 Group B	Yes: Class I Division 2 Group B
Compatible with propylene glycol-H ₂ O mixture	Yes	Yes	Yes
Weight, kg	Minimum	0.88	4.1
Inlet and outlet port type	Vacuum coupling radiation preferred	National Pipe Thread Taper (NPT)	NPT
Inlet and outlet port size	1/4 in. preferred	1/4 in.	1/4 in.

TABLE X.—SELECTION CRITERIA FOR ELECTROLYZER (EZ) RECIRCULATION LOOP FLOW SWITCH

Selection criteria	EZ recirculation loop requirement	Select flow switch model	
		Option C	Option D
Vacuum chamber operation	Yes	Yes	Yes
Operating temperature range, °C	4 to 85	–10 to 100	–268 to 148
Maximum operating pressure, MPa	17.24	35	68.9
Flow rate, cm ³ /min	390	200 to 3,000	Made to specifications
Certified for hazardous location	Yes	Yes: Explosive Atmospheres (ATEX) zone 1	Yes: Class I Division 2 Group B
Compatible with H ₂ O	Yes	Yes	Yes
Weight, kg	Minimum	1	4.1
Inlet and outlet port type	Vacuum coupling radiation preferred	National Pipe Thread Taper (NPT)	NPT
Inlet and outlet port size	1/4 in. preferred	1/4 in.	1/4 in.

3.3 Catalytic Recombiner for Reactant Purity

Gas crossover (unwanted permeation through membranes) is a known issue for high-pressure EZs and results in O₂ in the product H₂ stream and H₂ in the product O₂ stream (Ref. 120). In a previous RFC demonstration, test operation had to be shut down when the H₂ concentration in O₂ exceeded 1 percent and was rising (Ref. 6). It has also been noted in ISS OGA operation that a low but measurable H₂ in O₂ concentration (up to 0.5 percent) can exist during stack startup (Ref. 12). The driving force for the transfer of dissolved gases from one side to the other is the gradient of chemical potential (chemical species gradient) across the membrane during operation, which results from the pressure gradient (Ref. 121). The mass transport mechanism is mostly diffusion controlled and follows Fick’s first law of diffusion (Refs. 121 to 123). Additionally, more recent investigations identify a minor convective transport process along with the major diffusive transport process (Refs. 121 to 123). Since the gases are dissolved in liquid H₂O in a liquid feed EZ, the electrode recombination kinetics may be slowed, increasing gas crossover. Leakage and

accumulation of H₂ in air or O₂ can lead to fire and explosion. This poses a safety risk because there is a non-zero potential for combining fuel (H₂) and oxidizer (O₂) at dangerous mixtures in various places in the RFC system.

At normal temperature and pressure conditions, the lower explosion limit (LEL) of H₂-O₂ mixtures is 4.0 mol% H₂, and the upper explosion limit (UEL) is 93.9 mol% H₂ (Refs. 124 and 125). The explosion limits expand with temperature (Refs. 125 and 126). The relationship with pressure is more complex. At 80 °C and 15 MPa (2,176 psi), which is similar to the operating conditions of the EZ stack, the LEL of H₂-O₂ mixtures is 5.3 mol% H₂, and the UEL is 95.5 mol% H₂ (Refs. 124 and 125). Since the RFC is a closed system, it is possible that gas crossover concentrations build up over time and repeated operating cycles until reaching or exceeding the LEL. To provide a safety margin at the LEL, the H₂ concentration should never exceed 2 mol% H₂ in the O₂ EZ outlet stream. For a similar buffer at the UEL, the H₂ EZ outlet concentration should not be less than 98 mol% H₂ with an O₂ remainder. Especially during preliminary testing, it is essential to have instruments to measure these concentrations.

H₂-in-O₂ and O₂-in-H₂ sensors are available for flowthrough and low-pressure applications, but these sensors do not exist for high-pressure applications. Detection technologies based on thermal conductivity, optical, and combined methods have been reported to be able to cover 0.1 to 100 percent of H₂ in air (Refs. 127 and 128). However, most commercial sensors are designed for pressure ranging only from 70 to 130 kPa. In a laboratory setting, H₂ in mixed gases is typically measured using mass spectrometry or gas chromatograph techniques with excellent sensitivity and selectivity. Like typical room concentration monitors, these are all generally expensive, prohibitively massive, use too much electrical power, and waste reactant with continuous sampling through slipstreams or periodic grab samples to analyze. These sampling processes each present a severe limitation for aerospace applications (Ref. 129). Such sensors are also known to exhibit calibration drift issues over time intervals too short for long-term RFC use (Ref. 15). For ISS OGA, this results in keeping three spares on station at all times and 14 more on the ground ready for rotation. This incurs severe costs in astronaut hours to perform regular maintenance tasks, not to mention the significant 4.7-kg mass of each unit.

There are eight general types of H₂ detection technologies (Ref. 127). In a previous survey of commercially available H₂ sensors for NASA aerospace applications, four of these sensor types (catalytic combustion, electrochemical, oxide semiconductor, and thermal conductivity) have been evaluated (Ref. 129). The authors noted a difference in requirements between aerospace applications and traditional applications. There is a growing demand for smaller and inexpensive sensors that can be used in a wider array of environments, since detection and accurate measurement of H₂ has profound industrial, technological, and medical importance. In 2007, the U.S. Department of Energy (DOE) published a list of target specifications, as presented in Table XI and compared against RFC project specifications. The DOE performance target is very stringent, and it remains challenging to meet the target metrics, so these goals were reaffirmed in 2015 (Ref. 130).

All COTS sensors fall short of the response time goal, although chemiresistors are considered a promising sensing system for fast sensing. In combination with other sensing systems and nanotech fabrication, an experimental sensor with a response time of less than 1 s has been reported (Ref. 131). This type of sensor appears most likely to meet the challenge of rapidly and reliably detecting H₂ in air to ensure safety (Refs. 131 and 132). Despite the strict requirements of the DOE performance target, it does not address all issues of RFC gas sensors. While most H₂ sensors are designed for monitoring H₂ only in ambient air, detection of H₂ in O₂ is needed for RFCs, where the O₂ flows through a tube and is pressurized up to 17.2 MPa. Similar to terrestrial objectives, low cost, miniaturization, and high power efficiency are also desirable.

TABLE XI.—DEPARTMENT OF ENERGY (DOE) AND REGENERATIVE FUEL CELL (RFC) TARGETS OF GAS SENSORS FOR H₂-O₂ BINARY MIXTURES

Parameter	DOE	ISS OGA ^a	RFC
Measurement range (full scale), percent	0.1 to 10	0.01 to 4.00	0.1 to 5.0 and/or 95.0 to 99.9 (% of H ₂)
Flow rate, SLPM	NA	1 to 12	0.1 to 31
Operating temperature, °C	-30 to 80	18 to 55	4 to 85
Response time, s	<1	<6	No requirement defined
Pressure, MPa	none	Up to 0.2	Up to 17.2
Accuracy, percent of full scale	5	-----	5
Gas environment	Ambient air, 10 to 98 percent relative humidity range	H ₂ -O ₂ mixture, 10 to 98 percent relative humidity range	H ₂ -O ₂ mixture, 10 to 98 percent relative humidity range
Lifetime	10 years	>201 days	5 years
Operating environment	Atmospheric pressure	Atmospheric pressure	Vacuum
Interference resistant to noted expected impurities	For example: hydrocarbons	Nitrogen, H ₂ O	Nitrogen, H ₂ O

^aInternational Space Station (ISS). Oxygen Generation Assembly (OGA).

It is much beyond the scope of the RFC project to develop improved gas sensors and will likely be identified as an area for future development. Judging by the difficulties of other groups to create or improve such devices, this is not a trivial challenge. A reliable, enduring technology of some sort is needed to ensure pure O₂ and H₂ process streams. This device could proactively prevent hazardous concentrations, thus removing the need for continuous measurement, or could provide alternative means of concentration monitoring.

3.3.1 Applicable Mitigations

There are several mitigation strategies that can be used to limit the amount of gas crossover, though none are ideal or completely effective as decreased crossover reduces ionic conductivity thereby decreasing efficiency (Ref. 133). One strategy is to increase the thickness of the membranes in the EZ. A thicker membrane reduces the gas crossover; however, it also results in higher ohmic voltage losses, which decrease efficiency (Refs. 133 and 134). Afshari et al. showed that at 80 °C and a balanced pressure of 0.1 MPa (much lower pressure than expected for lunar RFC operation) there is not much of an improvement in gas crossover once the membrane thickness reaches 200 μm or more over a current density range of 0 to 1,000 mA/cm² (Ref. 133). Furthermore, the consequences of gas crossover are reduced at higher current densities, though this trend follows an exponential decay, and at membrane thicknesses of about 200 μm or more, there is minimal improvement above 300 mA/cm².

Membrane type also plays a role in the amount of gas crossover. There are novel membranes that promote conductivity over permeability better than traditional commercial options, but long-term durability becomes less known (Ref. 135). Gas permeability also tends to rise over time because of membrane degradation in the forms of loss of thickness and development of pinholes. To mitigate the diffusion coefficient or the solubility of the gas, inorganic fillers can be dissolved into the membrane, such as silica or zirconium oxide (Ref. 121). In a previous study, Grigoriev et al. showed that the diffusion coefficient and the solubility coefficient could be reduced by a factor of up to 10 depending on the concentration of the zirconium dioxide filler that was used. The negatives to this method are a

reduction in the ionic conductivity, increased resistance losses during electrolysis, and a lower cell voltage efficiency (Ref. 121).

The solubility and mobility of gases in hydrated perfluorinated solid polymer electrolytes are such that an increase in gas crossover occurs with increasing temperature, pressure, and current densities (Refs. 121 and 136). Another mitigation strategy is to avoid operation at high pressures, as gas crossover increases linearly with operational pressure, up to 20 MPa (3,000 psi) (Refs. 122 and 137). However, from a system level, it is advantageous to operate the EZ at high pressure (up to 17.2 MPa for this project) to eliminate the need to further compress gases, decreasing costs and system complexity (Refs. 121 and 134). Additionally, there is an increase in gas crossover when there is unbalanced pressure between the cathode and anode sides of the membrane (Ref. 133). This RFC system will be operating with balanced pressure because both product gases need to be stored at high pressure to maintain a reasonable system volume.

Permeated gases can be recombined internally to the EZ stack at the counter electrodes to form H₂O. This is not a trivial challenge and many developments are considered proprietary material. Precious metal catalysts are often used in the electrodes of PEM EZ and can be H₂-O₂ recombination catalysts. The best O₂ evolution catalyst is iridium, so it is often used as an anode catalyst for RFC EZs. Unfortunately, iridium is not a good catalyst for recombination (Refs. 123, 138, and 139). On the other side, platinum is used as a cathode catalyst for H₂ evolution and is also a good catalyst for recombination. Addition of a Pt alloy catalyst on the anode side can help reduce the H₂ concentration in O₂ below the explosion limit in some circumstances (Refs. 138 and 139).

Experiments at atmospheric pressure were done by Takenaka et al. where MEAs were prepared in which one side of the membrane was plated with a Pt electrode and the other side was not treated (Ref. 139). When the Pt electrode was plated only on the cathode, the impurity concentration of O₂ at the cathode remained low, while the H₂ concentration at the anode increased. When the Pt electrode was plated on the anode, the O₂ concentration at the cathode increased significantly, while the H₂ concentration at the anode remained low. These results indicate that the gases that permeated through the membrane were consumed at the counter electrode and that the plated electrode played a critical role in producing high-purity gases (Ref. 140). In another study, when H₂ was fed at 4 vol% in the O₂ stream in a packed bed catalytic reactor, which utilized a PtCo alloy as the catalyst at 80 °C and ambient pressure, 99.5 vol% of the H₂ was immediately converted to H₂O with the residual H₂ concentration below 0.02 vol% (Ref. 139). However, when the same catalyst was used in the anode compartment of a single PEM electrolysis cell, at 2 MPa and 55 °C with a current density of 25 to 300 mA/cm², the residual H₂ in O₂ was still above 1 vol% (Ref. 139). Additionally, when a packed bed reactor was tested with the PtCo alloy catalyst in the wet state, a much lower recombination conversion was observed (Ref. 139).

Grigoriev et al. evaluated the gas crossover at elevated pressure using a cell in which the backside surface of the current collector was platinized to promote recombination reactions (Ref. 120). It was reported that the H₂ concentration in the anode decreased significantly and that low levels (<2 vol%) could be maintained. However, it was also concluded that a pressure of 3 MPa is the upper limit and beyond that other treatment is required to maintain the impurity concentration below 2 vol% (Ref. 120). This is still a lower pressure compared to the RFC system. Grigoriev et al. also described that reduction of H₂ content by using a gas recombiner connected in series with an anodic liquid-gas separator is promising treatment for high-pressure applications (Ref. 120). This research indicates that recombination catalysts in the electrodes of high-pressure PEM EZs are insufficient at reducing the gas crossover to safe limits at high pressures. The RFC system is closed, so even if the concentration of gas crossover was not at the explosion limit, it could continue to build up until that limit is reached. Therefore, additional pieces of equipment, such as in-line catalytic recombiners, may be required.

Accounting for RFC system design requirements and tradeoffs, the EZ will have a membrane without fillers, a thickness of about 250 μm (0.010 in.), operate at balanced pressure of at least 12.4 MPa and up to 17 MPa, in a temperature range of 4 to 85 $^{\circ}\text{C}$. The average current density will be about 420 mA/cm^2 with a maximum of 600 mA/cm^2 , though the technology could operate above 1,000 mA/cm^2 . The membrane will also feature an internal catalyst to promote recombination. As previously noted, these mitigation strategies may not be sufficient, so additional recombiners will be developed and added downstream of the vapor-liquid separators to reduce the concentration of containment gases to safe concentrations.

3.3.2 Catalytic Recombiner Design

Catalytic recombiners are primarily used in the nuclear power industry (Refs. 141 to 143). They are passive pieces of equipment where gas flows into the bottom of a convective case. Close to the bottom of the case is a high surface area catalytic element, which promotes the recombination reaction. As the reaction occurs, the temperature increases, and the gas continues to rise, eventually exiting through the top. Two protective inlet and outlet flame-arresting grids are usually positioned on either end of the convective case to prevent ignition of the ambient atmosphere during operation (Ref. 120). These commercial recombiners are significantly larger than required for the designed RFC system. The units are also optimized for ambient to low pressures and a much wider temperature range, up to several hundred degrees higher, than the RFC operating parameters (Refs. 141 and 144). Therefore, a custom recombiner design is needed for high-pressure EZ use.

In an initial study by Grigoriev et al., it was recommended that recombiners should be located as close as possible to the electrolysis cell, where the hazardous $\text{H}_2\text{-O}_2$ mixtures are formed, however, this is not possible when liquid H_2O is circulated through the EZ and optimal operation requires dry gases (Ref. 120). When wet gases were used, the recombination process was delayed by up to 10 min after production started and the conversion efficiency of the recombiner was significantly altered, yielding lower gas purities (Ref. 120). When dry gases were used, the start time was reduced to 1 to 2 min, and the conversion efficiency was improved. Additionally, to increase the conversion efficiency, a longer residence time is often needed, resulting in a large increase in volume of the recombiner, which is not always practical (Ref. 120).

A COTS laboratory scale recombiner system is not available, so recombiner designs and catalysts were investigated. The requirements for the recombination catalyst are that it has to have a high activity level so that it functions at low temperature ($<85^{\circ}\text{C}$), low H_2 concentration ($<1.5\text{ mol}\% \text{H}_2$ in O_2) and/or low O_2 concentrations ($<1.5\text{ mol}\% \text{O}_2$ in H_2), and high pressure (up to 17.2 MPa), as well as be minimally affected by the presence of H_2O . The identified catalyst, shown in Figure 11, is a metal-based catalyst plug (a mixture of activated Pt and Pd) that is formed from knitted wire, does not absorb H_2O , is self-drying, has a 1.3-cm diameter, is about 1 cm tall, and is expected to have at a minimum 99.9 percent conversion with up to 99.99 percent possible.

Using kinetic data and catalyst bed sizing with a safety factor of at least 4 times, the bed size was calculated based on worst-case conditions using vendor recommendations. For the product O_2 stream at 0.14 MPa (20 psia), 60 $^{\circ}\text{C}$, constant temperature, 200 g/h, and 2 mol% H_2 in O_2 , the required bed size was initially calculated to be 1.2-cm diameter and 27 cm long. This diameter does not account for potential channeling effects (i.e., gas flowing through the bed without adequate catalyst contact), which may be prevented by making the vessel at least 6 times the diameter of the catalyst particle. This would expand the vessel to have a 7.6-cm diameter and be 10.2 cm long. The kinetics of the O_2 in H_2 reaction are slightly slower than the H_2 in O_2 reaction, but as the vessel is already oversized, and the oxygen stream



Figure 11.—Recombiner catalyst.

has a lower mass flow rate, the same vessel dimensions will work for both product streams. Additionally, as pressure and temperature increase, the reaction kinetics increase as well. At 12.4 MPa, 60 °C, constant temperature, 200 g/h, and 2 mol% H₂ in O₂, the vessel would need to be 7.6 cm in diameter and only 0.05 cm long. Therefore, with the vessel designed for the slowest kinetics and over a 4 times safety factor, there should be a sufficient amount of catalyst for recombination.

3.3.3 Planned Catalytic Recombiner Testing

A test plan is created to verify the effectiveness of the catalytic recombiner for the EZ product O₂ and H₂ streams. To minimize risk and because higher temperature and pressure should only improve the reaction rate, the maximum test pressure will be 0.86 MPa (125 psia) and, the temperature range will be 4 to 80 °C. The product O₂ stream flow rate will vary from 100 to 200 g/h. The concentrations to be tested range from 0.01 to 1.5 mol% H₂ in air and 0.01 to 1.5 mol% H₂ in O₂, using premixed gases to simplify the design and avoid accidentally forming a flammable mixture. The product H₂ stream flow rate will vary from 13 to 26 g/h. The concentrations to be tested range from 0.01 to 1.5 mol% O₂ in 95 percent N₂ with the balance being H₂ and 0.01 to 1.5 mol% O₂ in H₂. The pressure will be controlled by back- and forward-pressure regulators. The gas will be heated by heating tape wrapped around the tubing. For testing at the minimum temperature, a chiller will be used to cool the recombiner to the setpoint. N₂ will be used as a purge gas in between tests and as a quench, if needed.

Figure 12 shows the piping and instrumentation diagram (P&ID) for the product O₂ stream recombiner test. The gas mixture will flow from the cylinder (XC001) to the back-pressure regulator (XR001), which will reduce the pressure. The gas will then be heated to its setpoint by the heating tape wrapped around the tubing. After the heater, the gas will flow through a mass flow controller (XMC001) and proceed to the catalytic recombiner (XCR001). The temperature of the recombiner will be monitored by several thermocouples (XTC003 to XTC005) regulated by a PCL (CP001) and chiller (CL001). The recombination reaction is exothermic and may be observed as a temperature rise during operation. If the H₂O produced from the reaction condenses, it will drop down into the oversized condensed H₂O collector (WC001), while the gas, along with any H₂O vapor from the reaction, will continue to flow up to the forward-pressure regulator (XR002). This regulator will maintain the pressure in the recombiner and further reduce the pressure downstream. Finally, the gas will flow through the flammable gas sensor (XGS001), which will measure the residual H₂ concentration before venting. Additionally, the gas composition can be measured by a residual gas analyzer that would utilize the sample port. The P&ID for the product H₂ subsystem test is similar.

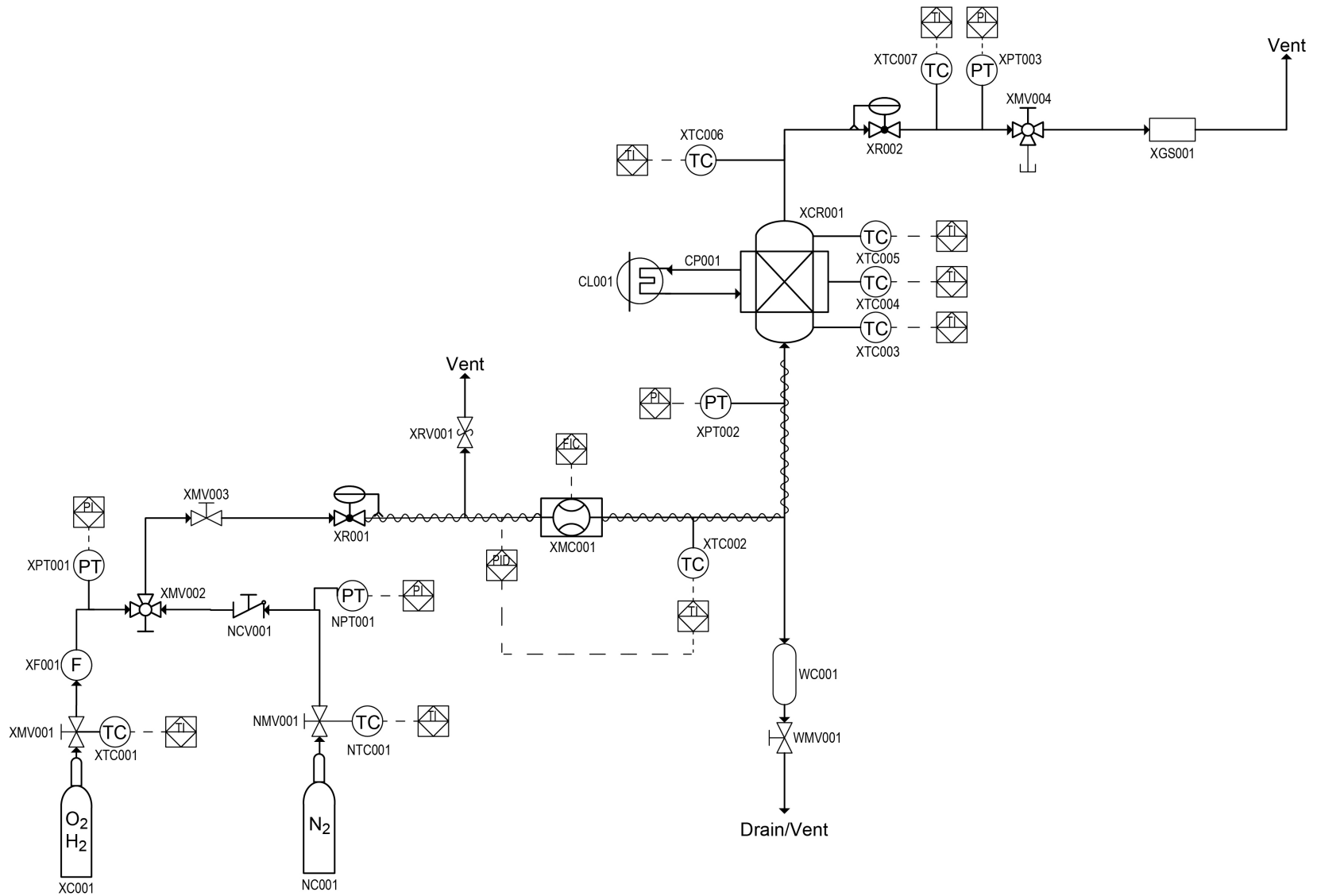


Figure 12.—Piping and instrumentation diagram for product O₂ subsystem test. Container (C). Chiller (CL). Coolant pump (CP). Check valve (CV). Filter (F). Flow indicator and controller (FIC). Gas sensor (GS). Mass flow controller (MC). Manual valve (MV). Nitrogen (N). Pressure indicator (PI). Proportional-integral-derivative (PID). Pressure transducer (PT). Regulator (R). Temperature indicator (TI). Water (W). Oxygen (X).

A flame arrestor was considered for installation on either end of the recombiner or to be incorporated into the catalyst support in the vessel, but after consulting with experts at the NASA White Sands Test Facility, it was determined that during subsystem testing, there is not a likely failure mechanism that could result in a flame or detonation. Consideration of a flame arrestor or a procedure for a N₂ quench should be considered in the overall RFC system. In the event of a flight project, the catalyst should undergo vibrational testing.

3.4 Material Compatibility

When it comes to safely and reliably controlling and containing H₂, O₂, and DI H₂O at high pressures and concentrations for long time periods, there are many potential concerns regarding the adverse interactions of the process fluids with RFC components. The following sections summarize some of the known issues.

3.4.1 Regenerative Fuel Cell Corrosion Considerations

Corrosion in RFCs is promoted by impurities introduced into the system and fluids by the electrochemical stacks and BOP components. To moderate or prevent the corrosion, a designer must first evaluate the impurity sources. Electrochemical conversion of H₂ and O₂ to and from H₂O in RFC relies on PEMs. Currently, perfluorinated sulfonic acids (PFSA) are the standard material for PEM, which serves as the conductor for protons between electrodes, as a gas separator, and as an electrical insulator. PFSA are a subcategory of PFASs, but not all PFASs are PFSA. PFSA is inert to H₂, O₂, and H₂O, however, membrane degradation manifests as reduced thickness, pinhole formation, and reduction of protonic conductivity, etc., and has been widely observed in both FCs and EZs (Refs. 75 and 145 to 152). Gradual breakdown of PEMs degrade electrochemical cell performance and will ultimately cause the failure of the FC and/or EZ stacks. The loss of thickness and pinhole formation increase gas crossover permeation of H₂ and O₂ across PEMs, which reduces FC cell voltages and decreases efficiency and quality of H₂ and O₂ produced by EZ.

It is generally accepted that one degradation mechanism is caused by radicals generated in the electrochemical process that separate C-F chemical bonds and release HF from the PEM. HF in product H₂O effluent can be detected and used to estimate degradation rates. Besides the C-F bond, attack of the C-S bonds of sulfonic acid releases sulfuric acid (H₂SO₄), resulting in the reduced protonic conductivity. Furthermore, C-O and C-C bond attacks lead to breakdown of the PFSA polymer structure and releases sulfonic acidic compounds. Another consequence is the contamination of product H₂O exiting the stacks. In RFCs, the H₂O will be recycled instead of disposed. Degradation products of HF and other acids corrode exposed 316 SS wetted surfaces and leach the ions of Fe, Cr, and Ni from these wetted surfaces. The Fe ion exacerbates the degradation of PFSA membrane in both of PEM FC and EZ (Refs. 75, 148, and 150 to 152). This is one reason that some terrestrial H₂ and air FC vendors use titanium alloy bipolar plates instead of 316 SS (Ref. 153). Due to materials compatibility concerns, titanium cannot be used in any O₂ wetted areas of a RFC without formal approval from the NASA White Sands Test Facility upon completion of an O₂ compatibility assessment and a hazards evaluation that includes destructive testing. Fe, Cr, and Ni cations may deposit on the electrodes of the FC or EZ. They can block the catalyst active sites and deactivate the electrochemical process on the electrodes for FC and EZ (Refs. 150 to 152). The multivalent ions have stronger affinity for sulfonic acid groups in PFSA than the targeted transiting protons and could partially block or slowdown the protonic transportation in PEM. Also, the cationic impurities provide a pathway for stray currents and impair the Coulombic efficiency during charge and discharge of RFC.

There are indications that short-side-chain (SSC) PFSA shows better chemical durability than long-side chain (LSC) membranes (Ref. 154). SSC PEM also exhibits better protonic conductivity than LSC membranes. Chemical modification, crosslinking, and forming composites can improve PEM chemical stability further. Better durability of PEM means longer service life and reduced contamination of H₂O effluent.

SS has been used in the treatment, storage, and distribution of drinking H₂O for over 50 years. Passivated SS is not prone to corrosion or leaching when used with DI or pure H₂O at ambient temperature. It is often chosen as the material of construction for processing equipment in the pharmaceutical industry because of its inherent corrosion resistance and ease of use. Under some environments, SS is not inert and degradation of SS may occur (Refs. 155 to 157). The corrosion increases with impurity in H₂O and temperature. However, the corrosion and leaching tend to decrease with time as passivated surface layers form. Almost all of the wetted RFC system is to be passivated 316 SS including tubing and valves. Hot (typically above 65 °C) pure H₂O can be aggressive to the ferrite content of SS, causing 316 SS to rouge. It is a fine rust that produces a red-brown discoloration on the surfaces of SS. For rouging to occur, either the protective chromium oxide layer has yet to be established or it may be disrupted (Ref. 155). This rouging has been observed in NASA FC test systems. Impurities such as acids or halides help to break the protective chromium oxide layer and accelerate the corrosion of SS. Additional protective coatings may be applied to prevent this. CrN or glass by physical vapor deposition, gold by arc discharge deposition, and PTFE coating by electrostatic spray methods of applying coating on SS are limited by line of sight. The protective coating can be applied on the surface of a bipolar plate, for example, but not on the surface of the inner side of SS tubing without difficulty.

Corrosion of 316 SS caused by acidic PEM degradation products is well reported (Refs. 148, 153, 158, and 159), but other forms of SS also induced concern. Taking one particular component type, solenoid valves, as an example, even though most valve bodies are made of 316 SS, the plunger (or armature) is often made of 400 series SS (typically 430F grade), which is more susceptible to corrosion (Ref. 160). The plunger must be ferromagnetic that is more prone to corrosion by HF, H₂SO₄, and other acids. The 300 series SS (such as 316) is nonmagnetic and more corrosion resistant.

3.4.1.1 Planned Corrosion Testing

It is beyond the scope of the RFC project to make internal changes to electrochemical stacks that produce the acid products. The primary issue for this task is to identify and empirically evaluate the potential life-limiting corrosion issues and minimize the resulting effects. The H₂O purification and deionization efforts are described in Section 2.1. Additionally, there will be tests to quantify the effect of high-purity H₂O storage inside of metal vessels. This will involve H₂O quality measurements and corrosion characterization of H₂O effects over time on PTFE or glass-lined 316 SS, 316 SS, and C-276 and 600 nickel alloy tubing.

Due to the differences of materials and design of the electrochemical stacks, operation condition, sampling, methods of testing, etc., variation of testing results is anticipated. The corrosion of SS by product H₂O can be ex situ evaluated by measurement of Fe, Cr, and Ni dissolution in product H₂O, as well as electrochemical characterization such as cyclic voltammetry, amperometry, galvanic coupling, AC impedance, etc., but none are likely to be a part of the current project (Refs. 158, 159, and 161). A previous investigation revealed 14-ppm fluorine ion and pH of 3.7 in the product H₂O, as well as contamination of Fe, Cr, and Ni (Ref. 148). Two different studies both identified 11-ppm fluorine ion in product H₂O (Refs. 158 and 159). The other product H₂O samples with higher fluorine ion concentrations were collected after 500 or 1,000 h of operation (Refs. 158 and 159). Product H₂O with higher fluorine ion concentrations are more acidic. Fluorine release rates tend to start high, establish a constant rate after a few hundred hours

to single-digit thousands of hours, then increase prior to failure. Tracking values and comparing to previously recorded measurements may enable future performance prediction.

Besides the corrosion of metal surfaces caused by product H₂O, the electrical potential in FC and/or EZ can electrochemically corrode wetted metal surfaces. The rate of corrosion is measured by shunt current that depends on conductivity of the H₂O and the applied electrical voltage (Ref. 161). Based on the ionic conduction of H₂O, the corrosion of the wetted metal can occur if the potential is beyond the passivation range of a few volts. DI H₂O has some conductivity, and acidic impurities in product H₂O enhances its conductivity. It can be a serious problem if the shunt current is not mitigated in a FC or EZ.

The first step of testing will collect the H₂O leaving the FC and EZ stacks during stack and subsystem acceptance and verification testing. In addition to pH and fluorine concentration, H₂SO₄ concentration should also be measured as the acid contributes to the acidity of the product H₂O (Refs. 75, 158, and 159). Concentrations of cations such as Fe, Cr, and Ni in product H₂O are usually measured by atomic absorption spectroscopy, inductively coupled plasma atomic emission spectroscopy, etc. (Refs. 148 and 160). Testing of pH and concentrations of fluoride, sulfate, and cations of the product H₂O can reveal the corrosion of PEM-based stacks. These measurements characterize the degradation of the membranes within FC and EZ stacks. A recent publication reveals the correlation between releasing of fluorine ion and the degradation of PEM in EZ (Ref. 162). The accumulation of HF within the EZ for ISS OGA was the cause of the EZ stack premature failure in 2010 (Refs. 13 and 75).

3.4.2 Hydrogen Design Considerations

Gas diffusion rate is inversely proportional to the square root of molecular weight. With the lowest molecular weight, H₂ has the highest diffusion rate. The high diffusion rate predicts high rate of permeation or leak during its production, transportation, and storage. H₂ leakage through seals and at pipe fittings can be an issue especially when the RFC is operated under vacuum and a wide temperature range. Certain fitting types leak more than others, so fitting selection or elimination can be important decisions to reduce H₂ leakage.

HEE is a more relevant issue for H₂ material compatibility. It is a process resulting in a decrease in the fracture toughness or ductility of a metal due to the presence of atomic hydrogen (Refs. 163 and 164). The decrease of the fracture toughness includes both static loading and cyclic (fatigue) stress modes. HEE is also known as hydrogen-assisted fracture. It usually manifests as cracking of metal at loading levels well below the yield strength of the material. Prior to the crack, the material may exhibit the reduction of mechanical strength (Ref. 112). Since the RFC system relies on metals as structure materials and some metals are in contact with high-pressure H₂, the risk of HEE should be addressed and remediated through appropriate material selection.

Temperature also influences HEE. For austenitic SS, embrittlement is most severe as temperatures decrease toward -150 °C (Ref. 163). At lower temperature, the solubility and diffusivity of atomic hydrogen in steels are too low to fill sufficient trapping sites. At higher temperature, atomic hydrogen diffuses too fast to be trapped (Refs. 163 and 164). An index between 1 and 0 has been used for qualitative rating of severity of HEE, with 1 for no HEE at all and 0 for most severe. For 316 SS, the HEE is most sensitive around -50 °C with HEE index of 0.7, a category of high HEE. At that low temperature, the material should be cautiously used only for limited applications with detailed fracture mechanics and crack growth analysis in H₂ (Ref. 163).

Further investigation reveals that Ni content plays an important role in HEE index. When Ni contents are above 12.5 wt%, the HEE index exceeds 0.96, a category of negligible HEE (Ref. 163). Per American Iron and Steel Institute (AISI) specification, the Ni content in 316 SS is 10.00 to 13.00 wt%. At 10.5 wt% of Ni, the HEE index descends to 0.48, indicating extreme HEE (Ref. 163). Within the normal range of Ni

content for 316 SS, there is some risk of HEE at low temperature (Ref. 165). The 316 SS is impervious to HEE at typical room temperature even with pressure approaching 70 MPa, but even 1 MPa H₂ is a problem at -50 °C. Within the austenitic SS family, 309, 310, and 314 have high Ni contents and are less prone to HEE at low temperature and high pressure. This is yet one more reason (in addition to reactant storage vessel design limitations and H₂O and O₂ phase change concerns) to include heating of components outside the thermal enclosure.

Strain-induced martensitic transformation may affect HEE of austenitic SS as well. Plastic deformation involving elongation, compression, etc., is necessary for the metal forming processing. This processing converts some of austenitic phase in austenitic SS to martensitic phase and hardens the material. The martensitic phase has high solubility of atomic hydrogen and enhances its diffusivity (Ref. 166). Strain-induced martensitic transformation enhances HEE susceptibility of austenitic SS. An annealing process is sufficient to restore the original austenitic structure and its HEE resistance.

Regarding aluminum alloy COPV liners, dry H₂ has negligible effects on those materials, and no HEE occurs (Ref. 163). Humidified H₂ and O₂ corrode aluminum alloys and may cause stress corrosion cracking of high-strength aluminum alloys (Refs. 104 and 163).

3.4.3 Oxygen Design Considerations

Although O₂ permeation or leakage is lower than that of H₂, gas leak rate is still considerably higher than that of liquids. Low-leak fittings are important for O₂ production, transportation, and storage. High-pressure O₂ is a much stronger oxidizer than air at ambient pressure. The combined effects of high pressure and O₂ concentration enhance the likelihood of ignition and its combustion rate. Substances that do not combust in ambient air, such as grease, oil film, metal or elastomer powder, and thin plastics may react energetically in high-pressure O₂. Therefore, any surfaces that may come into contact with O₂ in the RFC must be carefully examined for combustible materials. Residual lubricating oil and grease, fingerprints, fine particulate metals and polymers, etc., shall be removed per ASTM-G93, Standard Guide for Cleanliness Levels and Cleaning Methods for Materials and Equipment Used in Oxygen-Enriched Environments (Ref. 167). Oxygen cleaning is a method of preparing equipment intended for use with either liquid or gaseous O₂ because contaminants in an O₂-rich system pose serious risks. For the RFC, oxygen cleaning eliminates fire or explosion danger due to flammable contaminants in the forms of inorganic, organic, particulate, film, or fluid. It is critical to follow the design guidelines listed in the ASTM MNL 36 "Safe Use of Oxygen and Oxygen Systems" to minimize ignition hazards associated with material selection, adiabatic ignition, component design, system design, cleaning processes, and operational procedures (Ref. 168).

4.0 Conclusions

As described herein, there are numerous balance of plant (BOP) component design challenges that exist for an aerospace regenerative fuel cell (RFC) system. From high-pressure gaseous reactant storage, fluid management, thermal regulation to safety assurance, the BOP performs essential functions to combine fuel cell (FC) and electrolyzer (EZ) technologies into a feasible RFC system. Component availability, performance, and long-term reliability issues remain major challenges constraining BOP development. Addressing these issues may accelerate development of new technologies and will be important for the advancement of RFC energy storage technology.

With the advantage of low cost and ease of certification and availability, commercial-off-the-shelf (COTS) products are preferred for BOP components and subsystems selection, if feasible. Most COTS components and subsystems for BOP were designed and manufactured for normal terrestrial applications

operated under ambient conditions. Some meet the design requirements of operational temperature range, vacuum, and material compatibility for the RFC system. The others only partially meet the RFC specifications. For some components, no standard commercial options satisfy the required specifications. These components are procured following customized design to meet the RFC performance requirements. Composite overwrapped pressure vessels (COPVs) and variable conductance heat pipes (VCHPs) are examples of components that follow this procurement path.

Testing is important in evaluating parameters of operation so that they are ready for key functions of BOP for integrating FC and EZ stacks into an integral RFC system. FC and EZ testing will be conducted along with the component and subsystem testing. Upon completion of laboratory component and subsystem assessments, prototype testing will be performed prior to the integration of the RFC system. The goal of the prototype spiral development cycle is to iterate on component, subsystem, and power management and distribution (PMAD) evaluation for continuous improvement before the final system assembly. It will identify system-level issues and areas of enhancement early so the necessary changes can be made prior to the final verification test of the integrated RFC system. BOP components and subsystems perform specialized tasks in the RFC and should have longer service lives than those of FC and EZ stacks. While the FC and EZ stack configurations have been determined, the selection of some BOP components will be finalized upon completion of the identified testing.

Appendix A.—Nomenclature

AC	alternating current
AEM	anion exchange membranes
AIAA	American Institute of Aeronautics and Astronautics
AISI	American Iron and Steel Institute
ASME	American Society of Mechanical Engineers
ATEX	Explosive Atmospheres
BD	burst disks
BOP	balance of plant
C	container
CFU/ml	colony forming units per milliliter
CHP	conventional heat pipe
CI/DivII/GB	Class I Division 2 Group B
CL	chiller
COPV	composite overwrap pressure vessel
COTS	commercial off the shelf
CP	coolant pump
CTE	coefficient of thermal expansion
CV	check valve
DC	direct current
DI	deionized, deionizing
DOE	Department of Energy
DOT	Department of Transportation
DSNE	NASA Cross-Program Design Specification for Natural Environments
EPA	Environmental Protection Agency
EPL	external pumped loop
ESM	European Service Module
EZ	electrolyzer
F	filter
FC	fuel cell
FFR	force-to-friction ratio
FIC	flow indicator and controller
FT-EPL	freeze-tolerant external pumped loop
GN ₂	gaseous nitrogen
GS	gas sensor
HEE	hydrogen environment embrittlement
IR	infrared radiation
ISO	International Organization for Standardization
ISS	International Space Station
IX	ion exchange
LEL	lower explosion limit
LEO	low Earth orbit
LN ₂	liquid nitrogen
LSC	long side chain
MC	mass flow controller

MEA	membrane electrode assembly
MLI	multilayer insulation
MTBF	mean time between failure
MV	manual valve
N	nitrogen
NCG	noncondensable gas
NEC	National Electric Code
NFPA	National Fire Protection Association
NPT	National Pipe Thread Taper
OGA	Oxygen Generation Assembly
P&ID	pipng and instrumentation diagram
PCL	primary cooling loop
PEM	proton exchange membrane
PFAS	per- and polyfluoroalkyl substances
PFSA	perfluorinated sulfonic acids
PI	pressure indicator
PID	proportional-integral-derivative
PMAD	power management and distribution
PRVs	pressure relief valves
PSM	Pressure Safety Manager
PT	pressure transducer
PTL	passive thermal louver
PV	photovoltaic
PVS	pressure vessels and pressurized systems
PWM	pulse width modulation
$Q_{\text{absorbed}} = Q_{\text{emitted}}$	adiabatic surface with no heat load
Q_{ELE}	electrical flow
Q_{TH}	thermal flow
q_{emitted}	energy radiated by surface
q_{IR}	absorbed IR
$q_{\text{refl},IR}$	reflected IR
$q_{\text{refl},solar}$	reflected solar radiation
q_{solar}	absorbed solar radiation
R	regulator
RFC	regenerative fuel cell
RTE	round-trip efficiency
SAC	strong acid cation
SBA	strong base anion
SBIR	Small Business Innovation Research
SMARTS	Shape Memory Alloys for Regulating Thermal Control Systems in Space
SS	stainless steel
SSC	short side chain
STD	NASA Technical Standards
STS	Space Transportation System
TI	temperature indicator
TOC	total organic carbon

TRL	technology readiness level
T_s	effective sink temperature
TVAC	thermal vacuum chamber
UEL	upper explosion limit
URFC	unitized reversible fuel cell
UV	ultraviolet
VCHP	variable conductance heat pipe
VCR	vacuum coupling radiation
VLPS	vapor-liquid phase separator
W	water
WAC	weak acid cation
WBA	weak base anion
WF	working fluid
X	oxygen
ΔP	pressure change

Appendix B.—Lunar Surface and Regenerative Fuel Cell Information

B.1 Lunar Surface Thermal Environment for Regenerative Fuel Cell and Simulation of This Environment in Thermal Vacuum Chamber

This is a brief summary of results to clarify regenerative fuel cell (RFC) project thermal design choices and how a best estimate of the actual lunar surface thermal environment that the RFC hardware would experience will be simulated in the Johnson Space Center thermal vacuum chamber (TVAC) facility. Details of the thermal modeling and discussion of the complete set of results will be documented in more detail in a future publication. The lunar surface thermal environment for the RFC needs to be accurately simulated in a TVAC to demonstrate this technology at a technology readiness level (TRL) of 5 or greater, that is, tested in a relevant environment. This appendix will describe the best estimate of the lunar surface environment and the capabilities and limitations to simulating this environment in a TVAC. It will also clarify some of the thermal radiation terminology, such as the differences between lunar surface temperature and effective sink temperature.

For the lunar surface thermal environment, the location of the RFC is assumed to be at the lunar equator. The thermal environments for RFC during launch, low Earth orbit (LEO), transit to the Moon, and landing on the lunar surface are not being considered. The lunar surface environment is defined in the NASA Cross-Program Design Specification for Natural Environments (DSNE) standard (SLS–SPEC–159) (Ref. 169). The lunar surface environment is defined in Reference 169 Section 3.4.6 with space sink temperature and solar flux defined in Section 3.3.9.1.

B.2 Lunar Surface Temperature

The full lunar surface temperature is not specified by DSNE in detail, although some data is provided for a few specific lunar latitudes. Instead, the values for lunar surface temperature for RFC were derived utilizing a lunar surface thermal model developed in Thermal Desktop® (C&R Technologies, Inc.) thermal analysis software utilizing solar flux, space sink temperature, and regolith thermal properties provided in DSNE. Figure 13 displays the variation in the lunar surface temperature from this model over a complete lunar day at a latitude of 0°. The lunar surface temperature results from this model have undergone some initial comparison with Diviner instrument data (Ref. 170). Specific guidance on development of the thermal model was obtained from the NASA Human Landing Systems Lunar Thermal Analysis Guidebook (Ref. 171).

B.3 Effective Sink Temperature

The lunar surface temperature is often the temperature value reported in various tables and handbooks as a sort of representative temperature that hardware would be exposed to on the lunar surface. While lunar surface temperature does have a large thermal effect on any type of hardware close to or on the lunar surface, for thermal design purposes, an effective sink temperature is a more appropriate value. The definition for effective sink temperature is described in the following sentences and shown in Figure 14. Effective sink temperature is T_s , which is the temperature reached by an adiabatic surface with no heat load (i.e., $Q_{\text{absorbed}} = Q_{\text{emitted}}$). Sources of energy include infrared radiation (IR) and solar radiation, either direct solar radiation or reflected (albedo). Absorbed energy from the lunar surface (or other planets) is q_{IR} and solar radiation is q_{solar} . Emitted energy for the reflected solar radiation is $q_{\text{refl,solar}}$, lunar IR is $q_{\text{refl,IR}}$, and energy radiated by the surface is q_{emitted} , which is due to its temperature. The T_s is highly dependent on (1) the orientation of the hardware; (2) the hardware view factor to the lunar surface, space, and solar flux direction; and (3) surface optical properties, namely absorptivity and emissivity.

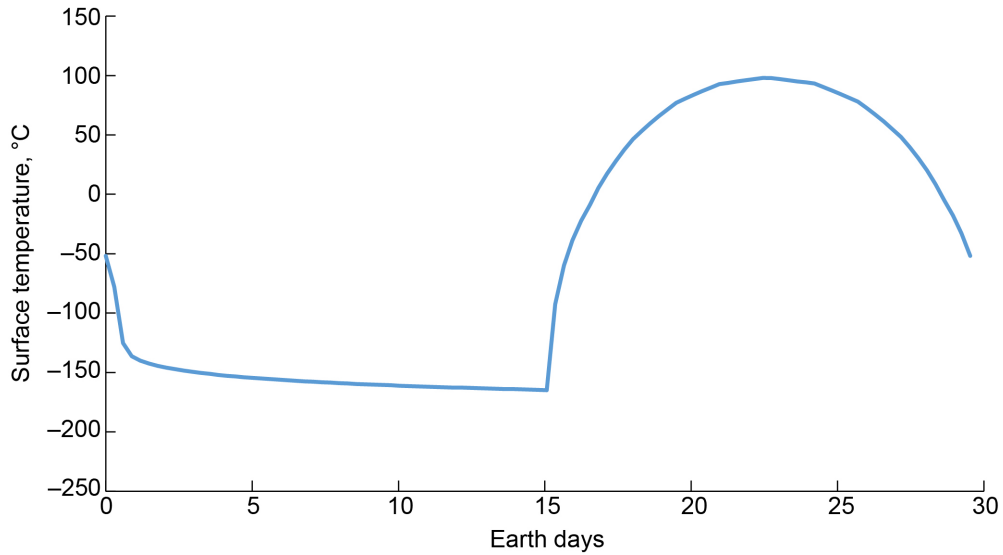


Figure 13.—Variation in lunar surface temperature over complete lunar day cycle (~28 days). Peak temperature near solar noon is 118 °C, and low temperature near end of lunar night is -177 °C.

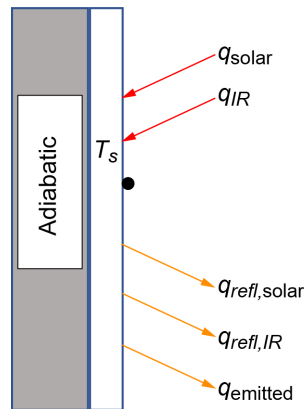


Figure 14.—Infrared radiation (IR) and solar radiation on adiabatic surface. Effective sink temperature (T_s). Absorbed IR (q_{IR}). Absorbed solar radiation (q_{solar}). Reflected solar radiation ($q_{refl,solar}$). Reflected IR ($q_{refl,IR}$). Energy radiated by surface ($q_{emitted}$).

The passive thermal design approach for RFC was to simulate via this lunar surface thermal model the lunar surface environment using relatively simple RFC thermal model geometries with surface optical properties achievable with several selected multilayer insulation (MLI) outer layer materials or coatings. The T_s was calculated for each of three RFC subsystems, the thermal enclosure, the storage tanks, and the radiator.

B.3.1 Design Choice for Multilayer Insulation Outer Layer on Regenerative Fuel Cell Thermal Enclosure

For the RFC thermal enclosure, a simple cube (1 m on a side) was used as the thermal geometry in the lunar surface thermal environment model. Figure 15 displays the T_s results over a lunar day cycle for three MLI outer layer choices that span α/ϵ ratios of <1 , ≈ 1 , and >1 . The maximum and minimum temperatures are provided in Table XII.

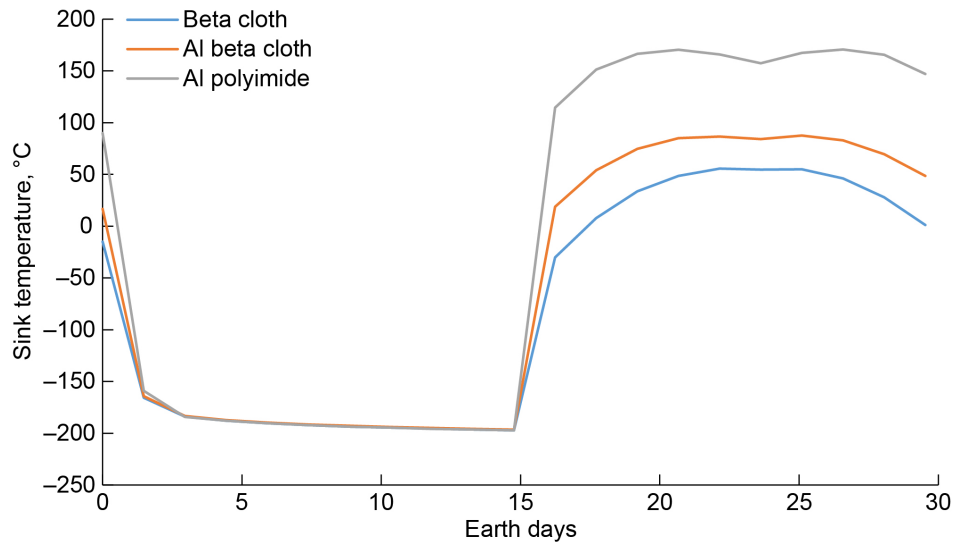


Figure 15.—Variation of effective sink temperature over lunar day for regenerative fuel cell thermal enclosure and tanks for several multilayer insulation outer layer choices.

TABLE XII.—MAXIMUM AND MINIMUM TEMPERATURES FOR REGENERATIVE FUEL CELL THERMAL ENCLOSURE AND TANKS FOR SEVERAL MULTILAYER INSULATION (MLI) OUTER LAYER CHOICES

MLI outer layer	Effective sink temperatures, T_s , °C		Tank heater power, W
	Day	Night	
Beta cloth enclosure	56	-197	119.1
Aluminized beta cloth enclosure	88	-197	112.4
Aluminized polyimide enclosure	171	-197	64.2

The requirement for the thermal enclosure is to maintain the RFC components within a temperature range of 4 to 85 °C, so the beta cloth was chosen as the MLI outer layer for the thermal enclosure to maintain enclosure surface temperatures below 85 °C during the lunar day. The lunar night thermal enclosure surface temperatures are estimated to reach -197 °C regardless of MLI outer layer choice, but the MLI internal layers, active heaters on RFC components (if needed), and the primary cooling loop (PCL), will maintain the RFC components above this minimum temperature.

B.4 Design Choice for Multilayer Insulation Outer Layer on Regenerative Fuel Cell Storage Tanks

For the RFC storage tanks, the same RFC thermal enclosure thermal geometry and analysis results were utilized to select the MLI layer. The maximum temperature for exposure of these tanks recommended by the vendor is 121 °C, so the aluminized beta cloth, as shown in Table XII, is selected to limit this upper temperature to 88 °C. Note that the temperature range for these tanks, given in Table VII, is given as -177 to 188 °C. In use, the lower temperature will likely be limited to 4 °C via heaters to avoid freezing of any H₂O content in the stored O₂ and H₂ gases. The heater power estimates were also calculated (in a separate RFC system thermal model) to maintain this lower temperature bound and are also provided in Table XII. Note that choosing aluminized poly (4,4'-oxydiphenylene-pyromellitimide) as the outer layer material would

provide the lowest heater power requirements but this choice would violate the upper tank temperature limit during the lunar day.

B.5 Radiator

The radiator is a unique thermal challenge on the lunar surface, in that the RFC will need to reject 400 W during the lunar day when the T_s will be the highest. The RFC will generate 600 W of waste heat during the lunar night, but this is not the worst thermal heat rejection case since the radiator would be rejecting this heat to a lower T_s . In addition, this waste heat may be useful to maintain component temperatures inside the RFC thermal enclosure and could also be utilized to keep the lander systems (or other customer) warm. Using the same lunar surface thermal model, but with a 1- by 1-m two-dimensional sheet serving as the radiator model geometry, an analysis was performed with the radiator in a vertical orientation (perpendicular to lunar surface). A vertical orientation was chosen for the radiator panel for two design reasons: (1) the variable conductance heat pipes (VCHPs) have the best performance if the condenser sections (mounted to radiator panel) are in a vertical orientation and (2) a vertical orientation minimizes lunar dust collection on panel surfaces, which would degrade the heat rejection capability over time. A horizontal orientation would have lower lunar day T_s due to having no view factor to the lunar surface, assuming the radiator surface facing the lunar surface is insulated with MLI, to minimize lunar surface infrared radiation (IR).

The optical properties of Aeroglaze[®] Z93 white paint (Parker Hannifin Corporation) were assumed for the radiator surface coating but note that there are a number of good choices for radiator coatings that have low absorptance to emittance ratios (Ref. 34). Figure 16 shows the variation in T_s results for the vertical orientation. Note that this analysis also assumes the radiator is edge-on to the Sun during the entire lunar day, by orientation being parallel to the lunar equatorial plane.

The thermal model of the radiator predicts a worst-case T_s of 48 °C near noon during the lunar day. This makes heat rejection challenging if the operating temperature of the RFC PCL is in the range of 50 to 60 °C. To lower the T_s , a parabolic reflector is proposed in the design to achieve a lower T_s by shielding the radiator surfaces from the lunar surface IR. An initial thermal analysis with this parabolic reflector predicted a reduced T_s of -37 °C for the worst case (near solar noon).

B.6 Simulation of Lunar Surface Thermal Environment in Thermal Vacuum Chamber

The previous sections describe the results of thermal modeling of the lunar surface environment and the passive thermal design choices for the RFC per the worst-case lunar thermal hot and cold conditions. This section briefly discusses the simulation capabilities of the TVAC and limitations between the TVAC simulation and the actual lunar surface thermal environment.

The thermal shrouds in the Johnson Space Center TVAC can presently reach 150 °C (hot extreme) and -184 °C (cold extreme). This temperature range does not quite bound the maximum and minimum T_s predicated by the lunar thermal environment modeling discussed. From the thermal modeling results discussed, the radiator will see a T_s of -194 °C, and the thermal enclosure and tanks will see a T_s of -197 °C during the lunar night. This adds just a small error of ~4 percent in terms of heat loss. In our best understanding of the lunar surface environment, a flight RFC system operating on the lunar surface would likely see the worst temperature extremes or temperature gradients when other environmental factors are taken into account, that is, solar flux, view to space in eclipse, view to lunar surface terrain, etc. For example, the TVAC facility does not include a solar simulator, so the lunar day thermal environment will be simulated by setting the TVAC shroud temperature to the T_s predicted by the lunar surface environment modeling. This relatively uniform sink temperature will not simulate the potential thermal gradients between the surface of the RFC thermal enclosure and tanks, which have different view factors to the lunar surface and sky (space).

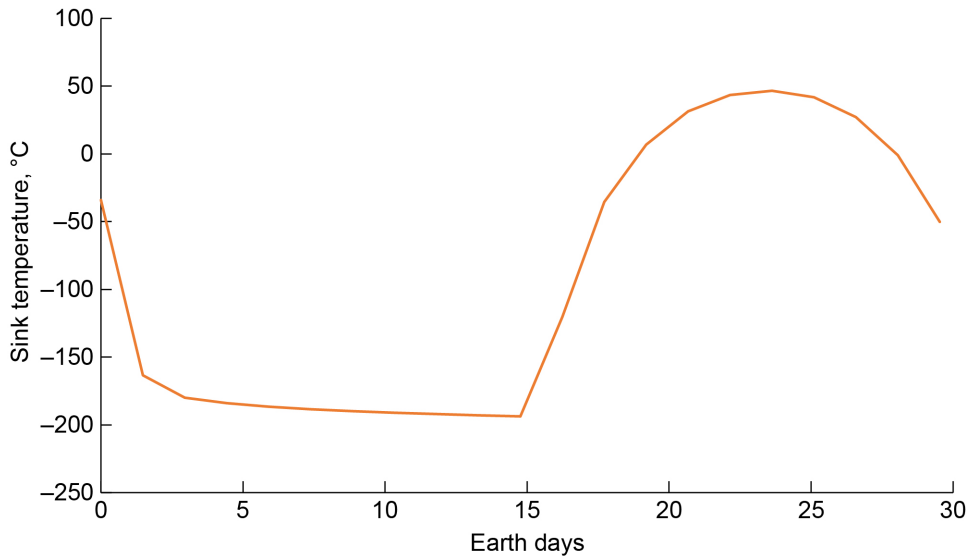


Figure 16.—Variation of effective sink temperature over lunar day cycle for regenerative fuel cell radiator in vertical orientation. Peak temperature near solar noon is 48 °C and low temperature during the lunar night is -194 °C.

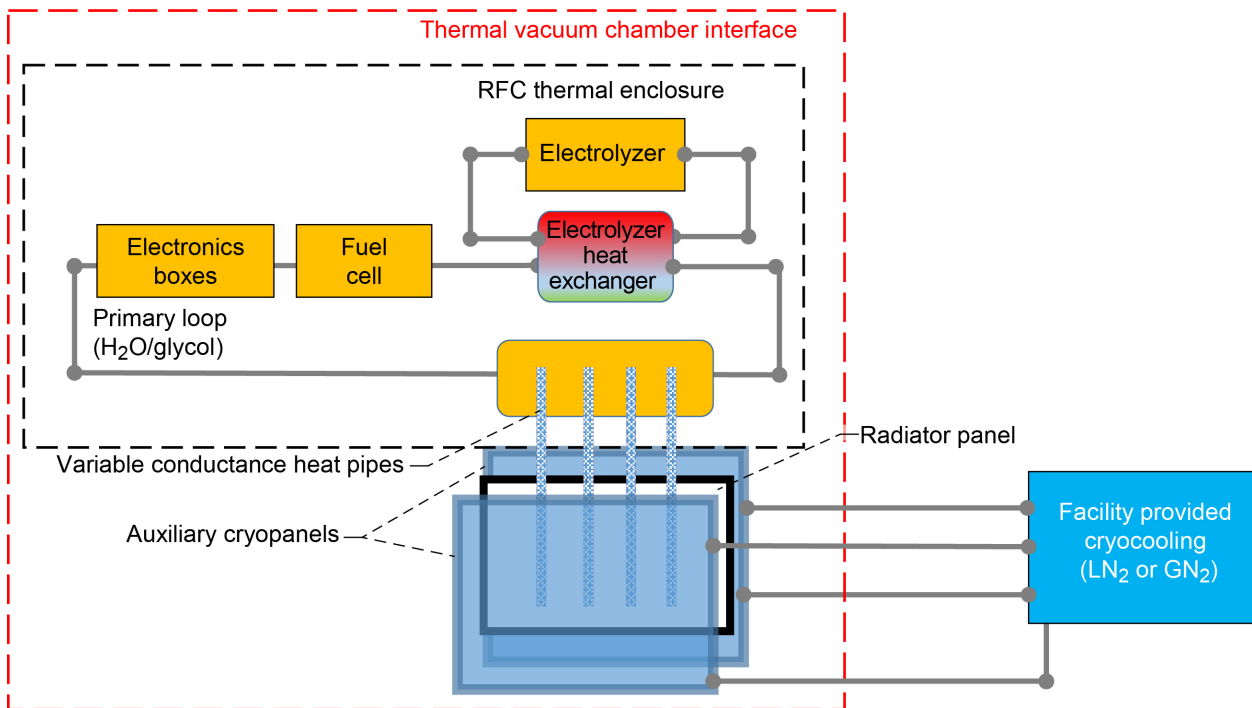


Figure 17.—Schematic showing proposed thermal vacuum chamber simulation of lunar surface environment. Liquid nitrogen (LN₂). Gaseous nitrogen (GN₂). Regenerative fuel cell (RFC).

In order to provide the T_s environment for the RFC radiator during the lunar day, a separate means of providing this temperature is needed. Figure 17 shows a simple schematic of the proposed TVAC configuration to achieve these two separate environments. The RFC thermal enclosure (black dotted line) and RFC storage tanks (not shown) are exposed to the main shroud of the TVAC facility to simulate temperatures in Figure 14. The RFC radiator is sandwiched between two separate auxiliary panels, cooled and heated by a separate facility system, to simulate the temperatures in Figure 16. An alternative option

being considered, is to replace the radiator panel with a cold plate mounted to the condenser sections of the VCHPs, with the cold plate cooled to the predicted radiator panel temperature that will need to be predicted via thermal modeling. Note that the parabolic reflector mentioned in the previous radiator section would not be fabricated; it is a proposed design solution for a RFC flight system. This would be simulated in the TVAC test by adjusting the operating temperature of the auxiliary panels to simulate the T_s based on lunar surface thermal environment analyses.

References

1. Smith, P.J., et al.: Lunar Equator Regenerative Fuel Cell System Efficiency Analysis. NASA Technical Memorandum, to be published, 2022.
2. Guzik, Monica C., et al.: Regenerative Fuel Cell Power Systems for Lunar and Martian Surface Exploration. AIAA 2017–5368, 2017.
3. Titterington, W.A.: Regenerative Fuel Cell System. Technical Report, Dec 1968–Jun 1970. [200 W]. AFAPL–TR–70–53, 1970.
4. Barbir, F.; Molter, T.; and Dalton, L.: Efficiency and Weight Trade-Off Analysis of Regenerative Fuel Cells as Energy Storage for Aerospace. *Int. J. Hydrog. Energy*, vol. 30, no. 4, 2005, pp. 351–357.
5. Garcia, Christopher P., et al.: Round Trip Energy Efficiency of NASA Glenn Regenerative Fuel Cell System. NASA/TM—2006-214054, 2006. <https://ntrs.nasa.gov>
6. Bennett, William R.; Smith, Phillip J.; and Jakupca, Ian J.: Analysis of 100-W Regenerative Fuel Cell Demonstration. NASA/TM-20205000357, 2020. <https://ntrs.nasa.gov>
7. Pu, Zonghua, et al.: Regenerative Fuel Cells: Recent Progress, Challenges, Perspectives and Their Applications for Space Energy System. *Appl. Energy*, vol. 283, no. 116376, 2021.
8. National Aeronautics and Space Administration: Fuel Cells: A Better Energy Source for Earth and Space. 2005. https://www.nasa.gov/centers/glenn/technology/fuel_cells.html Accessed Mar. 1, 2022.
9. Cohn, Ernest M.: Terrestrial Applications of Electrochemical Space Power Research. Presented at the AIAA 3rd Annual Meeting, Boston, MA, 1966. <https://arc.aiaa.org/doi/pdf/10.2514/6.1966-1012> Accessed Mar. 1, 2022.
10. Cohn, Ernest M.: NASA's Fuel Cell Program. *Fuel Cell Systems*. G.J. Young and H.R. Linden, eds., *Advances in Chemistry*, Vol. 47, Ch. 1, American Chemical Society, Washington, DC, 1969, pp. 1–8.
11. Warshay, Marvin; and Prokopius, Paul R.: *The Fuel Cell in Space: Yesterday, Today and Tomorrow*. NASA TM–102366, 1990. <https://ntrs.nasa.gov>
12. Takada, Kevin C.; Ghariani, Ahmed E.; and Van Keuren, Steven: Advancing the Oxygen Generation Assembly Design to Increase Reliability and Reduce Costs for a Future Long Duration Mission. ICES–2015–115, 2015.
13. Takada, Kevin, et al.: Oxygen Generation Assembly Design for Exploration Missions. ICES–2018–113, 2018.
14. Takada, Kevin, et al.: Advanced Oxygen Generation Assembly for Exploration Missions. ICES–2019–107, 2019.
15. Takada, Kevin, et al.: Status of the Advanced Oxygen Generation Assembly Design. ICES–2020–190, 2020.
16. Giacoppo, Giosue; Hovland, Scott; and Barbera, Orazio: 2 kW Modular PEM Fuel Cell Stack for Space Applications: Development and Test for Operation Under Relevant Conditions. *Appl. Energy*, vol. 242, 2019, pp. 1683–1696.
17. Ganjehsarabi, Hadi: Performance Assessment of Solar-Powered High Pressure Proton Exchange Membrane Electrolyzer: A Case Study for Erzincan. *Int. J. Hydrog. Energy*, vol. 44, no. 20, 2019, pp. 9701–9707.
18. Espinosa-Lopez, Manuel, et al.: Modelling and Experimental Validation of a 46 kW PEM High Pressure Water Electrolyzer. *Renew. Energy*, vol. 119, 2018, pp. 160–173.
19. Kuleshov, N.V., et al.: Development and Performances of a 0.5 kW High-Pressure Alkaline Water Electrolyser. *Int. J. Hydrog. Energy*, vol. 44, no. 56, 2019, pp. 29441–29449.

20. Siemens AG: Green Ammonia and Hydrogen at Scale. 2019. <https://www.ammoniaenergy.org/wp-content/uploads/2021/06/1.3-Siemens-ammonia-and-hydrogen-Martin-Hablutzet-publish.pdf> Accessed Mar. 1, 2022.
21. Williams, J.-P., et al.: The Global Surface Temperatures of the Moon as Measured by the Diviner Lunar Radiometer Experiment. *Icarus*, vol. 283, 2017, pp. 300–325.
22. Broeren, Robert L.; and Duschatko, R. John: International Space Station Design-to-Freeze Radiators. SAE Technical Paper 972345, 1997. <https://doi.org/10.4271/972345> Accessed Mar. 8, 2022.
23. Ungar, Eugene K.: Spacecraft Radiator Freeze Protection Using a Regenerative Heat Exchanger With Bypass Setpoint Temperature Control. SAE Technical Paper 2008–01–2170, 2008. <https://saemobilus.sae.org/content/2008-01-2170/> Accessed Mar. 8, 2022.
24. Exxon Mobil Corporation: COOLANOL. 2022. <https://www.mobil.com/en-us/aviation/pds/gl-xx-coolanol?p=2&p> Accessed Mar. 8, 2022.
25. Kurt J. Lesker Company: Galden HT—PFPE Heat Transfer Fluid. 2022. <https://www.lesker.com/newweb/fluids/pdf/11-012-fl-ds-galdenpfpe-heattransferfluiddatasheet.pdf> Accessed Mar. 8, 2022.
26. Dynalene, Inc.: Dynalene MV—Ultra-Low Temperature Heat Transfer Fluid. 2020. <https://www.dynalene.com/wp-content/uploads/2020/07/Dynalene-MV-Tech-Data-Sheet-Rev1.pdf> Accessed Mar. 8, 2022.
27. 3M Company: 3M Novec 7000 Engineered Fluid. 2021. <https://multimedia.3m.com/mws/media/121372O/3m-novec-7000-engineered-fluid-tds.pdf> Accessed Mar. 8, 2022.
28. 3M Company: 3M Novec 7100 Engineered Fluid. 2009. <https://multimedia.3m.com/mws/media/199818O/3m-novec-7100-engineered-fluid.pdf> Accessed Mar. 8, 2022.
29. 3M Company: 3M Novec 7200 Engineered Fluid. 2009. <https://multimedia.3m.com/mws/media/199819O/3m-novec-7200-engineered-fluid-en.pdf> Accessed Mar. 8, 2022.
30. 3M Company: 3M Novec 7300 Engineered Fluid. 2009. <https://multimedia.3m.com/mws/media/338713O/3m-novec-7300-engineered-fluid.pdf> Accessed Mar. 8, 2022.
31. MultiTherm: Ultra-Low Temperature Heat Transfer Fluid MultiTherm ULT-170. <https://web.archive.org/web/20060714060853/https://www.multitherm.com/multitherm-ult-170.html> Accessed May 10, 2022.
32. van Gerner, H.J.; van Benthem, R.C.; and van Es, J.: Fluid Selection for Space Thermal Control Systems. ICES–2014–136, 2014.
33. NASA Research Announcement: Topic 4 Novel Heat Transfer Fluids. Space Technology—Research, Development, Demonstration, and Infusion 2021, Appendix 80HQTR21NOA01–21LUSTR–B5, 2021.
34. Gilmore, David G., ed.: Spacecraft Thermal Control Handbook. Vol. I, Second ed., The Aerospace Press, El Segundo, CA, 2002.
35. Smith, Phillip J.; and Colozza, Anthony J.: Characterization of Flat-Plate Heat Pipe Functionality for Fuel Cell Application. NASA/TM—2019-219974, 2019. <https://ntrs.nasa.gov>
36. Chen, W., et al.: A Multi-Environment Thermal Control System With Freeze-Tolerant Radiator. AIAA 2013–3354, 2013.

37. Anderson, William; Ellis, Michael C.; and Walker, Kara L.: Variable Conductance Heat Pipe Radiators for Lunar and Martian Environments. AIP Conf. Proc., vol. 1103, no. 1, 2009, pp. 57–66.
38. Sierra Nevada Corporation: SNC Space Systems Product Catalog. 2020, pp. 135–140. <https://www.sncorp.com/media/3189/space-systems-product-catalog-2020.pdf> Accessed Apr. 27, 2022.
39. Chang, B.J., et al.: Engineering Model System Study for a Regenerative Fuel Cell. NASA CR–174801, 1984. <https://ntrs.nasa.gov>
40. Elston, Levi J., et al.: Qualitative Evaluation of a Liquid-Vapor Separator Concept in Micro-Gravity Conditions. AIP Conf. Proc., vol. 1103, no. 1, 2009, pp. 3–13.
41. Guo, Q., et al.: Gas/Water and Heat Management of PEM-Based Fuel Cell and Electrolyzer Systems for Space Applications. Microgravity Sci. Technol., vol. 29, 2017, pp. 49–63.
42. Best, Frederick; and Ellis, Michael: Experimental and Analytical Results of a Liquid-Gas Separator in Microgravity. AIP Conf. Proc., vol. 458, no. 1, 1999, pp. 779–784.
43. TeGrotenhuis, Ward E.; and Stenkamp, Victoria S.: Normal Gravity Testing of a Microchannel Phase Separator for Insitu Resource Utilization. NASA/CR—2001-210955, 2001. <https://ntrs.nasa.gov>
44. Finodeyev, Filip; Ghrist, Melissa; and Best, Frederick: Development of a Passive Flow Coalescence Device for Two-Phase Separation Under Microgravity. AIP Conf. Proc., vol. 746, no. 1, 2005, p. 141.
45. McQuillen, John; Sankovic, John; and Hall, Nancy Rabel: Multiphase Flow Separators in Reduced Gravity. Proceedings of the ASME 2005 International Mechanical Engineering Congress and Exposition, Orlando, FL, 2005, pp. 737–743.
46. Weislogel, M.M.; Thomas, E.A.; and Graf, J.C.: A Novel Device Addressing Design Challenges for Passive Fluid Phase Separations Aboard Spacecraft. Microgravity Sci. Technol., vol. 21, no. 257, 2009.
47. Wu, Xiongjun, et al.: Development of a Passive Phase Separator for Space and Earth Applications. Sep. Purif. Technol., vol. 189, 2017, pp. 229–237.
48. Bahadori, Alireza; and Vuthaluru, Hari B.: Rapid Estimation of Equilibrium Water Dew Point of Natural Gas in TEG Dehydration Systems. J. Nat. Gas Sci. Eng., vol. 1, no. 3, 2009, pp. 68–71.
49. Bahadori, Alireza; and Vuthaluru, Hari B.: Simple Methodology for Sizing of Absorbers for TEG (Triethylene Glycol) Gas Dehydration Systems. Energy, vol. 34, no. 11, 2009, pp. 1910–1916.
50. Ghiasi, Mohammad M., et al.: Rigorous Models to Optimise Stripping Gas Rate in Natural Gas Dehydration Units. Fuel, vol. 140, 2015, pp. 421–428.
51. Rincón, Marcelo Diaz; Jiménez-Junca, Carlos; and Duarte, Carlos Roa: A Novel Absorption Process for Small-Scale Natural Gas Dew Point Control and Dehydration, J. Nat. Gas Sci. Eng., vol. 29, 2016, pp. 264–274.
52. Han, Jingli, et al.: Gas Drying With Ionic Liquids. AIChE J., vol. 64, no. 2, 2018, pp. 606–619.
53. Kohl, Arthur L.; and Nielsen, Richard B.: Gas Dehydration and Purification by Adsorption. Gas Purification, Fifth ed., Gulf Professional Publishing, Houston, TX, 1997, pp. 1022–1135.
54. Wang, Xiuli; and Economides, Michael: Natural Gas Processing. Advanced Natural Gas Engineering, First ed., Gulf Publishing Company, Houston, TX, 2009, pp. 115–169.
55. Gandhidasan, P.; Al-Farayedhi, Abdulghani A.; and Al-Mubarak, Ali A.: Dehydration of Natural Gas Using Solid Desiccants. Energy, vol. 26, no. 9, 2001, pp. 855–868.
56. Farag, Hassan A.A., et al.: Natural Gas Dehydration by Desiccant Materials. Alexandria Eng. J., vol. 50, no. 4, 2011, pp. 431–439.

57. Tanchuck, Brenden, et al.: Adsorptive Drying of CO₂ Using Low Grade Heat and Humid, Ambient Air. *Sep. Purif. Technol.*, vol. 120, 2013, pp. 354–361.
58. Morishige, Kunimitsu; and Iwasaki, Hiroshi: X-ray Study of Freezing and Melting of Water Confined Within SBA-15. *Langmuir*, vol. 19, no. 7, 2003, pp. 2808–2811.
59. Mead-Hunter, Ryan; King, Andrew J.C.; and Mullins, Benjamin J.: Aerosol-Mist Coalescing Filters—A Review. *Sep. Purif. Technol.*, vol. 133, 2014, pp. 484–506.
60. Sokolović, Dunja, et al.: Novel Coalescer With Bed of Waste Polymer Fibers for Liquid Aerosol Separation. *Sep. Purif. Technol.*, vol. 263, no. 118187, 2022.
61. Acor, Lori G.; and Mirdadian, David: Benefits of Using Deliquescent Desiccants for Gas Dehydration. *SPE-82139-MS*, 2003.
62. Wang, Karen L., et al.: Hollow Fiber Air Drying. *J. Membrane Sci.*, vol. 72, no. 3, 1992, pp. 231–244.
63. Ye, Xinhuai; and LeVan, M. Douglas: Water Transport Properties of Nafion Membranes Part I. Single-Tube Membrane Module for Air Drying. *J. Membrane Sci.*, vol. 221, 2003, pp. 147–161.
64. Laguntsov, N.I., et al.: Natural Gas Drying and Cleaning of Carbon Dioxide by Membrane Gas Separation. *Petrol. Chem.*, vol. 57, 2017, pp. 132–138.
65. Kurchatov, I.M., et al.: Hybrid Solutions of Compressed Gas Drying. *J. Phys. Conf. Ser.*, vol. 1099, no. 012033, 2018.
66. Riangvilaikul, B.; and Kumar, S.: An Experimental Study of a Novel Dew Point Evaporative Cooling System. *Energ. Buildings*, vol. 42, no. 5, 2010, pp. 637–644.
67. Nada, S.A.: Air Cooling-Dehumidification/Desiccant Regeneration Processes by a Falling Liquid Desiccant Film on Finned-Tubes for Different Flow Arrangements. *Int. J. Therm. Sci.*, vol. 113, 2017, pp. 10–19.
68. Lin, Jie, et al.: Thermodynamic Analysis of a Hybrid Membrane Liquid Desiccant Dehumidification and Dew Point Evaporative Cooling System. *Energ. Convers. Manage.*, vol. 156, 2018, pp. 440–458.
69. Burke, Kenneth A.; and Jakupca, Ian: Unitized Regenerative Fuel Cell System Gas Dryer/Humidifier Analytical Model Development. NASA/TM—2004-213355 (AIAA 2004-5700), 2004. <https://ntrs.nasa.gov>
70. Light, Truman S., et al.: The Fundamental Conductivity and Resistivity of Water. *Electrochem. Solid-State Lett.*, vol. 8, no. 1, 2005, p. E16.
71. Maryatt, Brandon W.: Lessons Learned for the International Space Station Potable Water Dispenser. *ICES-2018-114*, 2018.
72. National Research Council: *Methods for Developing Spacecraft Water Exposure Guidelines*. National Academy Press, Washington, DC, 2000.
73. National Aeronautics and Space Administration: *NASA Engineering Design Challenges—Environmental Control and Life Support Systems Water Filtration Challenge*. 2008. https://www.nasa.gov/pdf/280748main_Water_Filtration_Guide.pdf Accessed Mar. 3, 2022.
74. Carter, Layne, et al.: Status of ISS Water Management and Recovery. Presented at the 47th International Conference on Environmental Systems, Charleston, SC, 2017. <https://ntrs.nasa.gov/citations/20170008984> Accessed Mar. 3, 2022.
75. Carpenter, Joyce, et al.: Investigation Into the High-Voltage Shutdown of the Oxygen Generation System Aboard the International Space Station. *AIAA 2012-3613*, 2012.
76. Bents, David J.: Hydrogen-Oxygen PEM Regenerative Fuel Cell Energy Storage System. NASA/TM—2005-213381, 2005. <https://ntrs.nasa.gov>

77. Bowman, Elizabeth M., et al.: Investigation of the Makeup, Source, and Removal Strategies for Total Organic Carbon in the Oxygen Generation System Recirculation Loop. Submitted to the 45th International Conference on Environmental Systems, Bellevue, WA, 2015.
78. Bowman, Elizabeth M., et al.: Analysis of Chemical and Microbial Components Adsorbed on the Ion Exchange Bed in the Oxygen Generation System Recirculation Loop. ICES–2017–253, 2017.
79. Bennett, William R.; Smith, Phillip J.; and Jakupca, Ian J.: Analysis of 100-W Regenerative Fuel Cell Demonstration. NASA/TM-20205000357, 2020. <https://ntrs.nasa.gov>
80. SUEZ: Handbook of Industrial Water Treatment. Chapter 08—Ion Exchange, Water Demineralization & Resin Testing, 2022. <https://www.suezwatertechnologies.com/handbook/chapter-08-ion-exchange> Accessed Mar. 7, 2022.
81. Hoffman, B.; and Aspden, J. Denis: Critical Aspects of Ion Exchange Resin Performance in High Temperature Condensate Polishing Applications. Power Plant Chemistry, vol. 8, no. 8, 2006, pp. 460–468. <https://www.osti.gov/etdeweb/biblio/20789576> Accessed Mar. 7, 2022.
82. DuPont: Amberlite MB20 H/OH Ion Exchange Resin. Product Data Sheet, 2019.
83. Tulsion: Thermax Ion Exchange Resins SDS Brochure. Summarized Data Sheet, 2020.
84. DYNALENE: IC–093–01 Ion Exchange Resin Cartridge. 2022. <https://www.dynalene.com/product/ic-093-04-ion-exchange-resin-cartridge/> Accessed Mar. 7, 2022.
85. Steele, John, et al.: Redesign of the Extravehicular Mobility Unit Airlock Cooling Loop Recovery Assembly. ICES–2016–[221], 2016.
86. Steele, John, et al.: Design of an On-Orbit Point-of-Use Adsorbent Filter for the Extravehicular Mobility Unit Influent Feed-Water. ICES–2018–103, 2018.
87. Volpin, Federico, et al.: Urine Treatment on the International Space Station: Current Practice and Novel Approaches. Membranes, vol. 10, no. 11, 2020, p. 327.
88. Steele, John, et al.: Antimicrobials for Water Systems in Manned Spaceflight—Past, Present, and Future Applications and Challenges. ICES–2018–104, 2018.
89. Lim, XiaoZhi: Can Microbes Save Us From PFAS? Chem. Eng. News, vol. 99, no. 10, 2021.
90. U.S. Environmental Protection Agency: Ultraviolet Disinfection Guidance Manual for the Final Long Term 2 Enhanced Surface Water Treatment Rule. EPA 815–R–06–007, 2006.
91. Watts: SmartStream UV. Product Specifications, 2022. <https://www.watts.com/dfsmedia/0533dbba17714b1ab581ab07a4cbb521/14402-source/es-wq-smartstream-a-pdf> Accessed Mar. 7, 2022.
92. Gonzalez, Yenifer; Salgado, Pablo; and Vidal, Gladys: Disinfection Behavior of a UV-Treated Wastewater System Using Constructed Wetlands and the Rate of Reactivation of Pathogenic Microorganisms. Water Sci. Technol., vol. 80, no. 10, 2019, pp. 1870–1879.
93. Watts: SmartStream. 2022. <https://www.watts.com/our-story/brands/smartstream> Accessed Mar. 7, 2022.
94. Mercer, J.R.: Paper 12: Reliability of Solenoid Valves. Proceedings of the Institution of Mechanical Eng., vol. 184, no. 2, 1969.
95. Angadi, S.V., et al.: Reliability and Life Study of Hydraulic Solenoid Valve. Part 2: Experimental Study. Eng. Fail. Anal., vol. 16, no. 3, 2009, pp. 944–963.
96. Okada, Fabio; Haller, Jack; and Arceo, Manny: Technology Update: Low-Power Solenoid Valves. Control Engineering, 2011. <https://www.controleng.com/articles/technology-update-low-power-solenoid-valves/> Accessed Mar. 7, 2022.
97. Skufka, Collin: Solenoid Valve Reliability in Lower Power Operations. 2019. <https://www.processingmagazine.com/valves-actuators/article/15587707/solenoid-valve-reliability-in-lower-power-operations> Accessed Mar. 7, 2022.

98. Stewart, Loren L.; Bukowski, Julia V.; and Goble, William M.: Improving Reliability & Safety Performance of Solenoid Valves by Stroke Testing. 2017. <https://www.exida.com.sg/wp-content/uploads/2017/12/Improving-Reliability-and-Safety-Performance-of-Solenoid-Valves.pdf> Accessed Mar. 7, 2022.
99. Stewart, Loren L.: How to Improve Reliability and Safety of Solenoid Valves. 2017. <https://www.valvemagazine.com/articles/how-to-improve-reliability-and-safety-of-solenoid-valves> Accessed Mar. 7, 2022.
100. Parker Hannifin Corporation: Parker O-Ring Handbook. ORD 5700. https://www.parker.com/literature/Parker_O-Ring_Handbook.pdf Accessed Mar. 7, 2022.
101. Gems Sensors, Inc.: D Series Valve Coil Self Heating. 2021. <https://www.gemssensors.com/blog/blog-details/d-series-valve-coil-self-heating> Accessed Apr. 27, 2022.
102. Connelly, Elizabeth: Current Status of Hydrogen Liquefaction Costs. DOE Hydrogen and Fuel Cells Program Record. U.S. Department of Energy Record 19001, 2019.
103. Barbir, F.; Molter, T.; and Dalton, L.: Efficiency and Weight Trade-Off Analysis of Regenerative Fuel Cells as Energy Storage for Aerospace Applications. *Int. J. Hydrog. Energy*, vol. 30, no. 4, 2005, pp. 351–357.
104. San Marchi, C.: Technical Reference on Hydrogen Compatibility of Materials: Aluminum Alloys, Non-Heat Treatable Alloys: Pure Aluminum (code 3101). Sandia National Laboratories, Livermore, CA, 2015.
105. NASA Technical Standards System: NASA Requirements for Ground-Based Pressure Vessels and Pressurized Systems (PVS). NASA-STD-8719.17, version C, 2017.
106. Meyer, K.J., et al.: Lightweighting Matters in Energy Storage. *Reinf. Plast.*, vol. 58, no. 4, 2014, pp. 20–23. [https://doi.org/10.1016/S0034-3617\(14\)70176-6](https://doi.org/10.1016/S0034-3617(14)70176-6) Accessed May 10, 2022.
107. Legault, Michael: Pressure Vessel Tank Types. *Composites World*, 2012. <https://www.compositesworld.com/articles/pressure-vessel-tank-types> Accessed Mar. 7, 2022.
108. Gardiner, Ginger: SpaceX Announces COPV’s Role in September Rocket Explosion. *Composites World*, 2017. <https://www.compositesworld.com/articles/spacex-announces-copvs-role-in-sept-rocket-explosion> Accessed Mar. 7, 2022.
109. Pradere, C.; and Sauder, C.: Transverse and Longitudinal Coefficient of Thermal Expansion of Carbon Fibers at High Temperatures (300–2500 K). *Carbon*, vol. 46, no. 14, 2008, pp. 1874–1884.
110. Steelhead Composites, Inc.: Lightweight Hydrogen Storage. 2020. <https://steelheadcomposites.com/hydrogen-storage/> Accessed Mar. 7, 2022.
111. Emerson: Electropneumatic Controller/Motors. TESCOM 70–2000 Series Product Catalog, 2022, pp. 635–636.
112. Burgess, Robert M., et al.: High Pressure Hydrogen Pressure Relief Devices: Accelerated Life Testing and Application Best Practices. NREL/TP-5400-67381, 2017.
113. U.S. Department of Energy: H2 Hydrogen Tools Tube Trailer Leak Through Over-Pressure-Protection Rupture Disk Lessons Learned. 2017. <https://h2tools.org/lessons/tube-trailer-leak-through-over-pressure-protection-rupture-disk> Accessed Mar. 7, 2022.
114. U.S. Department of Energy: H2 Hydrogen Tools High-Pressure Burst Disk Failure Lessons Learned. 2009. <https://h2tools.org/lessons/high-pressure-burst-disk-failure> Accessed Mar. 7, 2022.
115. BS&B Innovations, Ltd.: Rupture Disk (Bursting Disc) and Safety Relief Valve Combination. 2002. http://www.bsbsystems.com/Rupture_Disks/Reverse_Buckling_Disks/Safety_relief_valves-77-1006.html Accessed Mar. 7, 2022.

116. Gems Sensors and Controls: FS-930 Series—Oil Flow Switch, Compensates for Viscosity Change in Fluids. 2014.
117. Northeast Controls, Inc.: PEECO E Series Flow Switch. 2020. <https://peecoflowswitch.com/peeco-e-series-flow-switch/> Accessed Mar. 7, 2022.
118. Kobold: Flowmeters and Switches. Model SMW/SMO, 2018. [smw-smo-gb-flow.pdf \(kobold.com\)](http://www.kobold.com/smw-smo-gb-flow.pdf) Accessed Mar. 7, 2022.
119. Northeast Controls, Inc.: PEECO H Series Flow Switch. 2002. <https://peecoflowswitch.com/peeco-h-series-flow-switch/> Accessed Mar. 7, 2022.
120. Grigoriev, S.A., et al.: Hydrogen Safety Aspects Related to High-Pressure Polymer Electrolyte Membrane Water Electrolysis. *Int. J. Hydrog. Energy*, vol. 34, no. 14, 2009, pp. 5986–5991. <https://www.sciencedirect.com/science/article/pii/S0360319909001219> Accessed Mar. 7, 2022.
121. Grigoriev, S.A., et al.: High-Pressure PEM Water Electrolysis and Corresponding Safety Issue. *Int. J. Hydrog. Energy*, vol. 36, no. 3, 2011, pp. 2721–2728.
122. Trinke, P.; Bensmann, B.; and Hanke-Rauschenbach, R.: Current Density Effect on Hydrogen Permeation in PEM Water Electrolyzers. *Int. J. Hydrog. Energy*, vol. 42, no. 21, 2017, pp. 14355–14366.
123. Bernt, M., et al.: Analysis of Gas Permeation Phenomena in a PEM Water Electrolyzer Operated at High Pressure and High Current Density. *J. Electrochem. Soc.*, vol. 167, no. 124502, 2020.
124. Schröder, V., et al.: Explosion Limits of Hydrogen/Oxygen Mixtures at Initial Pressures Up to 200 Bar. *Chem. Eng. Technol.*, vol. 27, no. 8, 2004, pp. 847–851.
125. Schroeder, V.; and Holtappels, K.: Explosion Characteristics of Hydrogen-Air and Hydrogen-Oxygen Mixtures at Elevated Pressures. *Proceedings of 2005 International Conference of Hydrogen Safety, Pisa, Italy, 2005.*
126. Wang, Xianming; and Law, Chung K.: An Analysis of the Explosion Limits of Hydrogen-Oxygen Mixtures. *J. Chem. Phys.*, vol. 138, no. 134305, 2013.
127. Hubert, T., et al.: Hydrogen Sensors—A Review. *Sens. Actuators B Chem.*, vol. 157, no. 2, 2011, pp. 329–352.
128. Boon-Brett, L., et al.: Identifying Performance Gaps in Hydrogen Safety Sensor Technology for Automotive and Stationary Applications. *Int. J. Hydrog. Energy*, vol. 35, no. 1, 2010, pp. 373–384.
129. Hunter, Gary W.: A Survey and Analysis on Commercially Available Hydrogen Sensors. NASA TM-105878, 1992. <https://ntrs.nasa.gov>
130. U.S. Department of Energy: Hydrogen and Fuel Cell Technologies Office Multi-Year Research, Development, and Demonstration Plan. Section 3.7 Hydrogen Safety, Codes and Standards, Washington, DC, 2015.
131. Koo, Won-Tae, et al.: Chemiresistive Hydrogen Sensors: Fundamentals, Recent Advances, and Challenges. *ACS Nano*, vol. 14, no. 11, 2020, pp. 14284–14322.
132. Alenezy, Ebstam K., et al.: Low-Temperature Hydrogen Sensor: Enhanced Performance Enabled Through Photoactive Pd-Decorated TiO₂ Colloidal Crystals. *ACS Sens.*, vol. 5, no. 12, 2020, pp. 3902–3914.
133. Afshari, E., et al.: Performance Assessment of Gas Crossover Phenomenon and Water Transport Mechanism in High Pressure PEM Electrolyzer. *Int. J. Hydrog. Energy*, vol. 46, no. 19, 2021, pp. 11029–11040.
134. Scheepers, Fabian, et al.: Improving the Efficiency of PEM Electrolyzers Through Membrane-Specific Pressure Optimization. *MDPI Energies*, vol. 13, no. 3, 2020, p. 612.
135. Mittelsteadt-Giner, Inc.: High Temperature, High Pressure Electrolysis. DOE Hydrogen and Fuel Cells Program—FY 2015 Annual Progress Report. 2015, pp. II-31—II-34.

- https://www.hydrogen.energy.gov/pdfs/progress15/ii_b_4_mittelsteadt_2015.pdf Accessed May 10, 2022.
136. Omrani, Reza; and Shabani, Bahman: An Analytical Model for Hydrogen and Nitrogen Crossover Rates in Proton Exchange Membrane Fuel Cells. *Int. J. Hydrog. Energy*, vol. 45, no. 55, 2020, pp. 31041–31055. <https://doi.org/10.1016/j.ijhydene.2020.08.089> Accessed May 10, 2022.
 137. Barbir, Frano: PEM Electrolysis for Production of Hydrogen From Renewable Energy Sources. *Sol. Energy*, vol. 78, no. 5, 2005, pp. 661–669.
 138. Hiroshi, Ito, et al.: Cross-Permeation and Consumption of Hydrogen During Proton Exchange Membrane Electrolysis. *Int. J. Hydrogen Energy*, vol. 41, no. 45, 2016, pp. 20439–20446.
 139. Briguglio, Nicola, et al.: Flammability Reduction in a Pressurised Water Electrolyser Based on a Thin Polymer Electrolyte Membrane Through a Pt-Alloy Catalytic Approach. *Appl. Cat. B: Environ.*, vol. 246, 2019, pp. 254–265.
 140. Ito, Hiroshi, et al.: Properties of Nafion Membranes Under PEM Water Electrolysis Conditions. *Int. J. Hydrog. Energy*, vol. 36, no. 17, 2011, pp. 10527–10540.
 141. Snoeck, J.; Solaro, C.; and Moeyaert, P.: First Experience With the Installation of Passive Autocatalytic Recombiners. AECL–11762, NEA/CSNIR9(96)8, 1996, pp. 281–294.
 142. Reinecke, E.A., et al.: Design of Catalytic Recombiners for Safe Removal of Hydrogen From Flammable Gas Mixtures. *Proceedings of 2007 International Conference of Hydrogen Safety*, San Sebastian, Spain, 2007.
 143. Gardner, Lee, et al.: Humidity Tolerant Hydrogen-Oxygen Recombination Catalysts for Hydrogen Safety Applications. *Proceedings of 2017 International Conference on Hydrogen Safety*, San Sebastian, Spain, 2017.
 144. Koroll, G.W., et al.: Catalytic Hydrogen Recombination for Nuclear Containments. AECL Research. <https://www.osti.gov/etdeweb/servlets/purl/612635> Accessed Mar. 7, 2022.
 145. Yu, Ted H., et al.: Mechanism for Degradation of Nafion in PEM Fuel Cells From Quantum Mechanics Calculations. *J. Am. Chem. Soc.*, vol. 133, no. 49, 2011, pp. 19857–19863.
 146. de Bruijn, Frank A.; Dam, V.A.T.; and Janssen, Gaby: Review: Durability and Degradation Issues of PEM Fuel Cell Components. *Fuel Cells*, vol. 8, no. 1, 2008, pp. 3–22.
 147. Christ, Jason M., et al.: Concentration Effects of Polymer Electrolyte Membrane Degradation Products on Oxygen Reduction Activity for Three Platinum Catalysts. *J. Electrochem. Soc.*, vol. 161, no. 14, 2014, pp. F1360–F1365.
 148. Pozio, A., et al.: Nafion Degradation in PEFCs From End Plate Iron Contamination. *Electrochim. Acta*, vol. 48, no. 11, 2003, pp. 1543–1549.
 149. Yuan, Xiao-Zi, et al.: Degradation of a PEM Fuel Cell Stack With Nafion Membranes of Different Thicknesses. *J. Power Sources*, vol. 205, 2012, pp. 324–334.
 150. Li, Na, et al.: Long-Term Contamination Effect of Iron Ions on Cell Performance Degradation of Proton Exchange Membrane Water Electrolyser. *J. Power Sources*, vol. 434, no. 226755, 2019.
 151. Li, Na; Araya, Samuel Simon; and Kaer, Soren Knudsen: The Effect of Fe³⁺ Contamination in Feed Water on Proton Exchange Membrane Electrolyzer Performance. *Int. J. Hydrog. Energy*, vol. 44, no. 26, 2019, pp. 12952–12957.
 152. Li, Na, et al.: The Effects of Cationic Impurities on the Performance of Proton Exchange Membrane Water Electrolyzer. *J. Power Sources*, vol. 473, no. 228617, 2020.
 153. Yoshida, Toshihiko; and Kojima, Koichi: Toyota MIRAI Fuel Cell Vehicle and Progress Toward a Future Hydrogen Society. *Electrochem. Soc. Interface*, vol. 24, no. 2, 2015, pp. 45–49.
 154. Jones, Deborah: Perfluorosulfonic Acid Membranes for Fuel Cell and Electrolyser Applications. Merck KGaA, Darmstadt, Germany, 2022. <https://www.sigmaaldrich.com/US/en/technical->

[documents/technical-article/materials-science-and-engineering/batteries-supercapacitors-and-fuel-cells/perfluorosulfonic-acid-membranes](#) Accessed May 10, 2022.

155. Cramer, Stephen D.; and Covino, B.S., Jr.: *Rouging of Stainless Steel in High-Purity Water*. ASM Handbook, Volume 13C: Corrosion: Environments and Industries, ASM International, Cleveland, OH, 2006.
156. Dong, Xia, et al.: Investigation of Stainless Steel Corrosion in Ultrahigh-Purity Water and Steam Systems by Surface Analytical Techniques. *J. Mater. Eng. Perform.*, vol. 19, no. 1, 2010, pp. 135–141.
157. Bernardi, Elena, et al.: Corrosion of AISI 316L in Ultrahigh-Purity Water: Surface Analyses and Metal Release. *Pharm. Eng.*, vol. 35, no. 2, 2015, pp. 71–77.
158. Agneaux, A., et al.: Corrosion Behaviour of Stainless Steel Plates in PEMFC Working Conditions. *Fuel Cells*, vol. 6, no. 1, 2006, pp. 47–53.
159. Andre, Johan; Antoni, Laurent; and Petit, Jean-Pierre: Corrosion Resistance of Stainless Steel Bipolar Plates in a PEFC Environment: A Comprehensive Study. *Int. J. Hydrog. Energy*, vol. 35, no. 8, 2010, pp. 3684–3697.
160. Auvinen, Sonja, et al.: Cost Effective In-Situ Characterization of Coatings for PEFC Bipolar Plates Demonstrated With PVD Deposited CrN. *J. Electrochem. Soc.*, vol. 158, no. 5, 2011, B550.
161. Bennett, William R.; Hoberecht, Mark A.; and Lvovich, Vadim F.: Analysis of Shunt Currents and Associated Corrosion of Bipolar Plates in PEM Fuel Cells. *J. Electroanal. Chem.*, vol. 737, 2015, pp. 162–173.
162. Marocco, Paolo, et al.: Online Measurements of Fluoride Ions in Proton Exchange Membrane Water Electrolysis Through Ion Chromatography. *J. Power Sources*, vol. 483, no. 229179, 2021.
163. Lee, Jonathan A.: Hydrogen Embrittlement. NASA/TM-2016–218602, 2016. <https://ntrs.nasa.gov>
164. Martin, May L., et al.: Hydrogen Embrittlement in Ferritic Steels. *Appl. Phys. Rev.*, vol. 7, no. 041301, 2020.
165. Michler, Thorsten; Yukhimchuk, Arkadiy A.; and Naumann, Joerg: Hydrogen Environment Embrittlement Testing at Low Temperatures and High Pressures. *Corros. Sci.*, vol. 50, no. 12, 2008, pp. 3519–3526.
166. San Marchi, C.; and Somerday, B.P.: *Technical Reference on Hydrogen Compatibility of Materials*. SAND2008–1163, 2008.
167. ASTM G93: *Standard Practice for Cleaning Methods and Cleanliness Levels for Material and Equipment Used in Oxygen-Enriched Environments*. 2003. (This is a free version.)
168. 168 ASTM MNL36: *Safe Use of Oxygen and Oxygen Systems: Handbook for Design, Operation, and Maintenance: Second Edition*. ASTM International, West Conshohocken, PA, 2007.
169. National Aeronautics and Space Administration: *Cross-Program Design Specifications for Natural Environments (DSNE)*. SLS–SPEC–159, Rev. G, 2019.
170. Hurley, Dana M., et al.: An Analytic Function of Lunar Surface Temperature for Exospheric Modeling. *Icarus*, vol. 255, 2015, pp. 159–163.
171. National Aeronautics and Space Administration: *Human Landing System Lunar Thermal Analysis Guidebook*. HLS–UG–001, 2021.

